MICROWAVE SINTERING AND CHARACTERIZATON OF SOFT MAGNETIC POWDER METALLURGICAL Ni-Fe ALLOYS

A THESIS SUBMITTED TO
THE GRADUATE SCHOOL OF NATURAL AND APPLIED SCIENCES
OF
MIDDLE EAST TECHNICAL UNIVERSITY

BY

DERYA ERDEM

IN PARTIAL FULFILLMENT OF THE REQUIREMENTS
FOR
THE DEGREE OF MASTER OF SCIENCE
IN
METALLURGICAL AND MATERIALS ENGINEERING

JUNE 2011

Approval of the thesis:

MICROWAVE SINTERING AND CHARACTERIZATION OF SOFT MAGNETIC POWDER METALLURGICAL Ni-Fe ALLOYS

submitted by **Derya ERDEM** in partial fulfillment of the requirements for the degree of **Master of Science in Metallurgical and Materials Engineering Department, Middle East Technical University** by,

Prof. Dr. Canan ÖZGEN _____
Dean, Graduate School of **Natural and Applied Sciences**

Prof. Dr. Tayfur ÖZTÜRK _____
Head of Department, **Metallurgical and Materials Engineering**

Assoc. Prof. Dr. Arcan F. DERİCİOĞLU _____
Supervisor, **Metallurgical and Materials Engineering Dept., METU**

Examining Committee Members:

Prof. Dr. Ali KALKANLI _____
Metallurgical and Materials Engineering Dept., METU

Assoc. Prof. Dr. Arcan F. DERİCİOĞLU _____
Metallurgical and Materials Engineering Dept., METU

Prof. Dr. Vedat M. AKDENİZ _____
Metallurgical and Materials Engineering Dept., METU

Prof. Dr. Adem KURT _____
Welding Education Dept, Gazi University

Assist. Prof. Dr. Y. Eren KALAY _____
Metallurgical and Materials Engineering Dept., METU

Date: 27.06.2011

I hereby declare that all information in this document has been obtained and presented in accordance with academic rules and ethical conduct. I also declare that, as required by these rules and conduct, I have fully cited and referenced all material and results that are not original to this work.

Name, Last name: Derya ERDEM

Signature :

ABSTRACT

MICROWAVE SINTERING AND CHARACTERIZATION OF SOFT MAGNETIC POWDER METALLURGICAL Ni-Fe ALLOYS

Erdem, Derya
M.Sc., Department of Metallurgical and Materials Engineering
Supervisor: Assoc. Prof. Dr. Arcan F. Dericioğlu

June 2011, 127 pages

In this study, prealloyed austenitic stainless steel and premixed soft magnetic Ni-Fe permalloy compacts were consolidated through microwave and conventional sintering routes at combinations of various sintering temperatures and compaction pressures. Sintered alloys were characterized in terms of their densification, microstructural evolution as well as mechanical and magnetic properties. The effect of sintering method in terms of the applied sintering parameters on the final properties of the compacts were investigated in a comparative manner. It was determined that microwave sintered permalloys are superior compared to their conventionally sintered counterparts in densification response, microstructural characteristics such as pore shape and distribution as well as mechanical properties for both austenitic stainless steel and permalloy compacts. However, permeability of the microwave sintered permalloys was inferior to their conventionally sintered counterparts in some cases due to microstructural refinement associated with microwave sintering route.

Keywords: Microwave sintering, permalloy, soft magnetic properties, mechanical properties, densification

ÖZ

YUMUŞAK MANYETİK Ni-Fe TOZ METALURJİK ALAŞIMLARIN MİKRODALGA İLE SİNTERLENMESİ VE KARAKTERİZASYONU

Erdem, Derya
Yüksek Lisans, Metalurji ve Malzeme Mühendisliği Bölümü
Tez Yöneticisi: Doç. Dr. Arcan F. Dericioğlu

Haziran 2011, 127 sayfa

Bu çalışmada, ön alaşımlı östenitik paslanmaz çeliklerin yanısıra manyetik özelliklere sahip toz metalurjik Ni-Fe (Nikel-Demir) alaşımları hem mikrodalga sinterleme yöntemiyle hem de konvansiyonel yöntemle üretilmiş ve üretilen alaşımlar yüzde yoğunlaşım, mikroyapısal, mekanik ve manyetik özellikler bakımından karakterize edilerek konvansiyonel yönteme kıyasla incelenmiştir. Hem östenitik paslanmaz çelikler, hem de yumuşak manyetik Ni-Fe alaşımları, mikrodalga sinterleme yöntemi ile konvansiyonel karşıtlarına kıyasla azalan işlem sürelerinde daha yüksek sinterlenmiş yoğunluklarda, azalan tane boyutu ve gözeneklilik yüzdesi ile iyileştirilmiş mekanik özelliklerde üretilebilmiştir. Ancak, yumuşak manyetik özellikler gösteren Ni-Fe alaşımları, kimi koşullarda mikrodalga sinterleme yöntemi ile üretildiklerinde konvansiyonel karşıtlarından daha az manyetik geçirgenlik göstermektedir. Bu durumun, mikrodalga sinterleme yönteminin karakteristiği olan kısalan işlem sürecinin getirdiği tane boyutu azalması ile ilişkili olduğu düşünülmektedir.

Anahtar Kelimeler: Mikrodalga sinterleme, nikel-demir alaşımları, mekanik özellikler, manyetik özellikler.

To my mom

ACKNOWLEDGEMENTS

I would like to express my sincere appreciation to Assoc. Prof. Dr. Arcan Dericioğlu for his supervision, guidance, support and encouragement throughout the study.

I also would like to present my gratefulness to PhD student Derya Kapusuz for her guidance and tutorials throughout my SEM trainings and her kind friendship. I am also grateful to my labmates Gökçe Şen, Selen Gürbüz Güner, Ayşegül Afal and Eda Aydoğan.

I want to express my special gratefulness to Göksu Gürer, Murat Tolga Ertürk and Bulutay Güneş for their support and invaluable friendships.

I would also like to thank to my precious diving buddies Ahmet Fatih Koç, Beybin İlhan, Cemre Artan, Gökçe Aköz, Oğuzhan Temel, Tayfun Asker and Elif Yılmaz for sharing such a great experience and their company. I would also like to thank to Itır Önal for her kind friendship and support.

I am grateful to Ahmet Arda Kozan for growing up with me, for being the best mentor and for always being there. Finally I owe a great debt to my family; my mother Nurten Erdem, my sister Deniz Erdem, my father Kenan Erdem for their continuous love and support throughout my life.

TABLE OF CONTENTS

LIST OF TABLES

TABLES

LIST OF FIGURES

FIGURES

CHAPTER 1

INTRODUCTION

Soft magnetic materials (SMM), which are characterized by low magnetic loss, high saturation magnetization and maximum permeability, are utilized in a wide range applications including transformer laminations, armature stampings, magnetic recording heads, AC cores in electrical machinery operating at frequencies from 50 Hz to several MHz etc., and they have a considerable importance in electronic and communication industries.

SMM(s) are generally classified in two material types, namely ferromagnetic and ferrimagnetic materials. Ferromagnetic materials mainly consist of Iron and Nickel alloys being used in applications operating at frequencies below 2 kHz in the bulk form and below 50 kHz in the powdered or laminated form. Ferrimagnetic materials composed of metal oxides and characterized by high electrical resistivity are generally utilized for applications well beyond 80 MHz.

Among ferromagnetic materials, iron rich alloys are preferred for applications requiring high saturation density; however, their low electrical resistivity constitutes an important drawback, which h leads to high eddy current losses at AC applications. On the other hand, nickel based alloys exhibit high initial and maximum permeability displaying improved loss characteristics.

Currently, three main types of Nickel-Iron alloys have extensive industrial use, which are 36% Ni alloys for maximum resistivity, 50% Ni alloys for maximum saturation magnetization and 80% Ni alloys for optimum permeability. In addition to the optimum permeability they provide, 80% Ni alloys are widely preferred for zero

magnetocrystalline anisotropy. For ferromagnetic SMMs, operation at higher frequencies requires special effort to minimize eddy current and hysteresis losses owing to the low electrical resistivity of the metallic systems. Therefore, for frequencies extending up to 50 kHz powdered form of SMMs is widely utilized.

Powder metallurgy approach offers many advantages in the manufacturing of soft magnetic materials such as minimal residual porosity, refined and homogenous microstructures, near net shaping and opportunity to produce complex geometries, which would otherwise require considerable machining, as well as minimization of eddy current losses due to the subdivision of the material. Typically, powder metallurgical (P/M) parts are usually heat treated in conventional (electrically heated) furnaces, where heating takes place by radiative heat transfer from the surface to the interior. To avoid thermal gradients during sintering, heating rate is kept low which causes microstructural coarsening and decrease in densification.

Microwave sintering surpasses many problems associated with conventional sintering because of the rapid, volumetric and uniform heating it provides, as a consequence of the fact that heating occurs as a result of the interaction with the incident electromagnetic radiation within the sample body. Until recent years, it was believed that metallic samples cannot be heated by microwaves, since they reflect most of the incident radiation in the monolithic state. However, during last decade, it has been shown by many researches that metals can too be heated and sintered through microwave radiation provided that they are in powder form, yet the exact mechanism of microwave heating of particulate metals remains to be unknown.

In this study, effect of microwave sintering on microstructural evolution, magnetic properties and densification response as well as mechanical characteristics of the Ni-Fe alloy of permalloy composition (80 wt% Ni) has been investigated. In a comparative manner, identical samples were processed through conventional sintering method and subsequently characterized to gain a deeper understanding on the effects of microwave sintering on the physical properties of metallic systems. Densification response, residual porosity, grain size, microhardness, permeability

and hysteresis behavior were investigated as the key properties of as-sintered alloys to compare the mechanical and magnetic performance of microwave and conventionally sintered products. In addition to these, diffusion couples prepared from elemental Nickel and Iron powders were sintered via conventional and microwave sintering routes and characterized by electron probe microanalysis (EPMA) to shed a light on the effect of microwave sintering on the diffusion behavior of the powder metallurgical compacts. Moreover, characterization of conventionally processed counterparts provided comparative aspect on the effect of microwave heating method on the diffusion behavior of the constituent atoms.

CHAPTER 2

THEORY

2.1. Microwave Fundamentals

Microwaves are electromagnetic (EM) waves with frequencies ranging from 300 MHz to 300 GHz of the electromagnetic spectrum with corresponding wavelengths of 300to 1mm (Figure 2.1.). Microwaves are generated by magnetrons which gives electrons from a cathode circular path in precision made circular cavities. The frequency of the generated waves are increased to GHz range from the 50 Hz AC by resonance, and the microwaves are carried from the magnetrons to the working cavity by a waveguide [2].

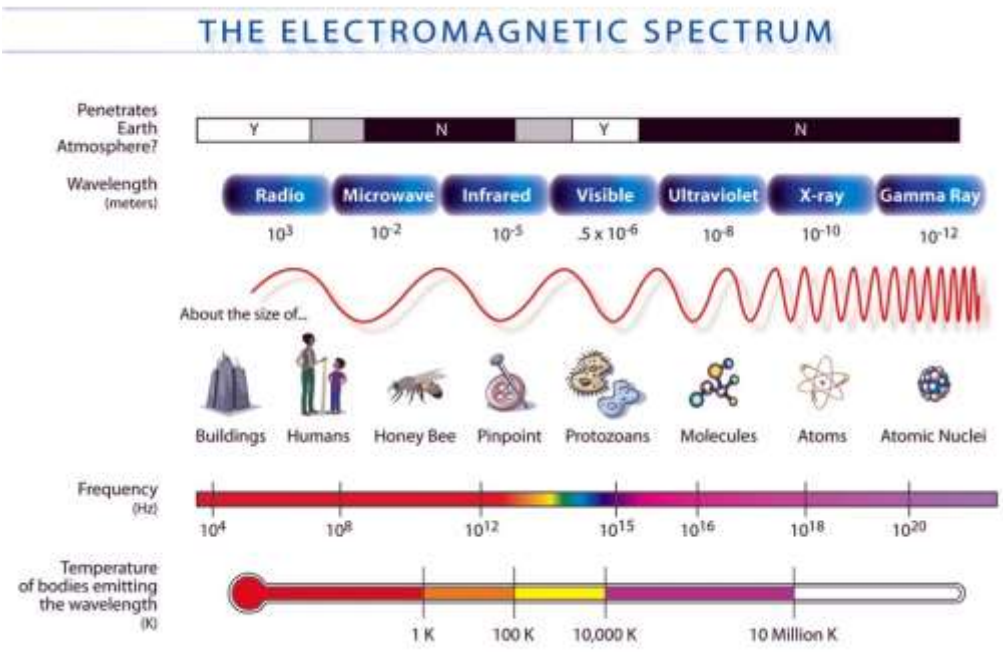

Figure 2.1. The electromagnetic spectrum [3].

As it can be inferred from the equations and discussions given in appendix I, knowledge and control of electromagnetic properties of a material such as permittivity and permeability are essential in determining the interaction between the incident microwave radiation and the material.

2.1.1. Permittivity

Permittivity, ε^*, is the measure of a dielectric material's polarization ability in response to an external electric field and in the ideal case, assumed to be lossless. However, permittivity of real dielectrics constitutes an imaginary component, in addition to its real component, to account for the losses:

$$\varepsilon^* = \varepsilon' - j\,\varepsilon'' \qquad 1.1$$

where ε' refers to relative permittivity of the material and ε'' is the dielectric loss factor.

At this point, it is necessary to define dielectric loss tangent, tanδ, to determine how efficient a dielectric can convert electromagnetic energy to heat.

$$\tan\delta = \varepsilon'' / \varepsilon' \qquad 1.2$$

Here δ represents the phase difference between the oscillating electric field and polarization response of the material.

2.1.2. Permeability

Permeability, μ^*, is used to determine the response of a material to an applied magnetic field, and as in the case of permittivity, it has both real and imaginary parts:

$$\mu^* = \mu' - j\,\mu'' \qquad 1.3$$

where μ' being the relative permeability and μ'' is the magnetic loss factor.

2.1.3. Power Dissipation and Penetration Depth

Since microwave sintering is mainly a process of conversion of incident electromagnetic energy to heat, it is essential to express the equations describing conversion of electromagnetic energy to heat. The power dissipated per unit volume of the material via electrical and magnetic losses are given as [4, 5]:

$$p= (\sigma + w\varepsilon'')E^2 + w\mu''H^2 \quad 1.4$$

The terms on the left hand side of the electric field represents losses due to the conductivity and polarization of the material, and magnetic losses are mainly taking place due to the imaginary component of magnetic permeability. For dielectrics, which are known to have negligible conductivity and permeability; microwave absorption and corresponding heat dissipation occurs through polarization (also known as displacement currents) of the material. In this respect, for conductors, magnetic induction and conduction losses play an important role in the heat dissipation process while hysteresis losses are also present for ferromagnetic material[6].

Above discussions lead to the misconception that efficient power absorption and heat dissipation are solely dependent on dielectric and magnetic loss factors. However, penetration of microwaves through the body of a material is required for volumetric coupling of the material and incident electromagnetic radiation. The ability of microwaves to penetrate material interiors is described by penetration and skin depth concepts which are defined as the depth from the material surface at which microwave power is reduced to its 1/e value (penetration depth), and the strength of the electric field is reduced to its 1/e value (skin depth). Penetration depth and skin depth are given by equations 17 and 18, respectively [7]:

$$\text{Penetration Depth= } D_p= \frac{\lambda\varepsilon'}{2\Pi\varepsilon''} \quad 1.5$$

1.6

$$\text{Skin Depth} = \delta = \frac{2\rho}{\omega\mu}$$

It can be inferred from the above equations that the real components of ε^* and μ^* are the main parameters governing penetration and skin depths. Consideration of power dissipation and penetration ability of microwaves implies that an optimum combination of real permittivity and permeability with their imaginary counterparts is required so that microwaves can penetrate and be volumetrically absorbed (Figure 2.2). These discussions lead to the conclusion that to control and exploit the microwave heating process, an understanding of the microwave-material interactions and the loss mechanisms participating in the microwave absorption is required.

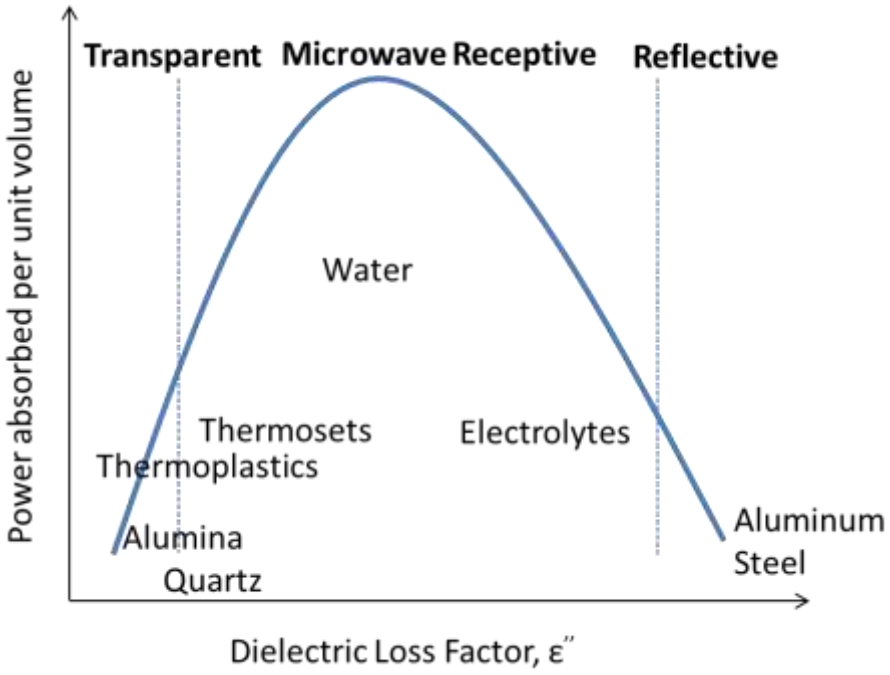

Figure 2.2. Microwave absorption capacity of various materials with respect to the dielectric loss factor [8].

2.2. Microwave- Material Interactions

The interaction of materials with the incident microwaves can be classified in three main categories in terms of the transmittance of the microwaves through the material:

2.2.1. Opaque Materials

Opaque materials neither transmit nor absorb the incident microwaves, and main portion of the electromagnetic radiation reflects from the material surfaces (Figure 2.3). Good electrical conductors with free electrons to generate superficial re-radiation fall into these category.

Figure 2.3. Schematic representation of reflection of electromagnetic waves from opaque materials' surface [6].

2.2.2 .Transparent Materials

Microwaves can pass through these materials with very little loss in their energy. Low loss dielectrics and insulators transmit microwaves without a significant attenuation (Figure 2.4); hence, these materials are exploited in furnace insulation and pressure window applications.

Figure 2.4. Schematic representation of transmittance of electromagnetic waves through transparent materials [6].

2.2.3. Absorber Materials

These materials couple efficiently with the electromagnetic waves and convert most of the microwave energy to heat (Figure 2.5). A wide range of materials from high loss dielectrics to powdered conductors are considered to be in this group.

Figure 2.5. Schematic representation of absorption of electromagnetic waves by lossy dielectrics [6].

2.3. Loss Mechanisms

Losses providing microwave absorption in materials are grouped as polarization, conduction and magnetic losses for all type of materials. Depending on the electromagnetic characteristics; one or more type of these mechanisms can be active and dominant on the coupling of the materials with incident microwave radiation. For dielectrics, coupling with the microwave radiation is generally occurs with the electric field component of the electromagnetic radiation, and microwave absorption resulting heat generation is due to the internally induced electric field by polarization of the material. For conductors, no internal induction of electric field is of concern, since free charges eliminate any potential difference within the conductor. Conductors usually interact with the magnetic component of the electromagnetic radiation; consequently, heat generation is the result of magnetic and/or eddy current losses which are described in the subsequent sections.

2.3.1. Polarization Losses

These types of losses are dominant in dielectrics where materials' response to the changing electric fields is formation of displacement currents via several polarization mechanisms being active depending on the frequency of the electromagnetic radiation.

2.3.1.1. Interfacial Polarization

This phenomenon is essentially accumulation of charges at free surfaces and interfaces of the material in presence of an external electric field. The phase difference between the switching electric field and the motion of the charges is the source of heat dissipation (Figure 2.6). Since this type of polarization occurs through the movement of charges across grain and/or second phase boundaries, the charges cannot keep up with the alternating field at higher frequencies; therefore, this mechanism is pronounced at lower frequencies.

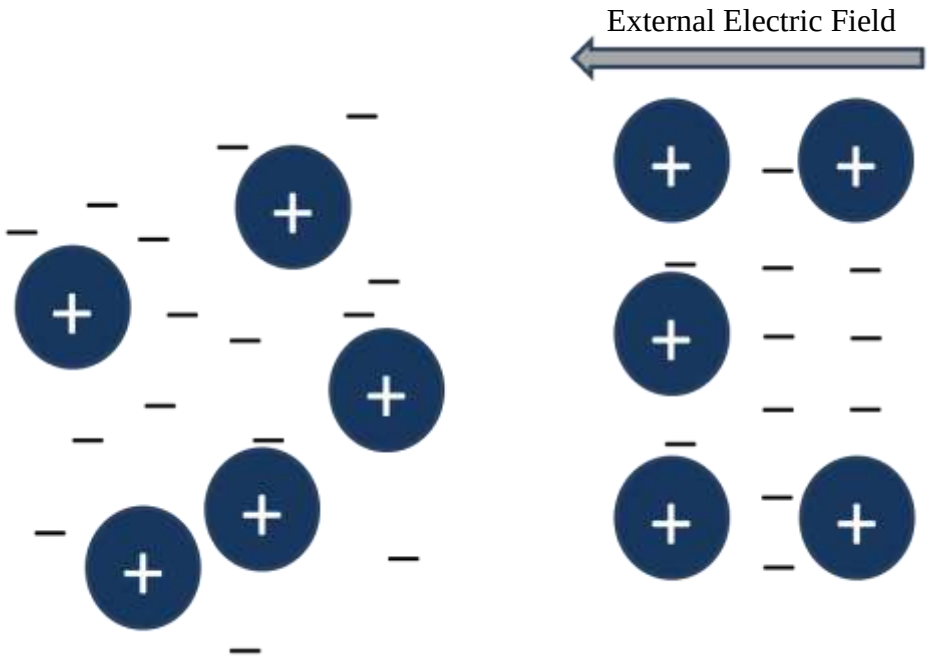

Figure 2.6. Interfacial polarization of charges around grain boundaries, pores, interparticle contacts etc.

2.3.1.2. Ionic Polarization

The displacement of inherently existing oppositely charged ions from their equilibrium lattice positions in response to the fluctuating external electrical field is responsible for the microwave absorption. Materials showing this type of polarization include alkali halides, salts and Group I-VII elements etc. (Figure 2.7). For efficient interaction between the material and incident electromagnetic radiation, the frequency of the incident radiation and the natural vibration frequency of the

atoms, which in general corresponds to high frequencies as far as infrared region of the electromagnetic spectrum, should be matching.

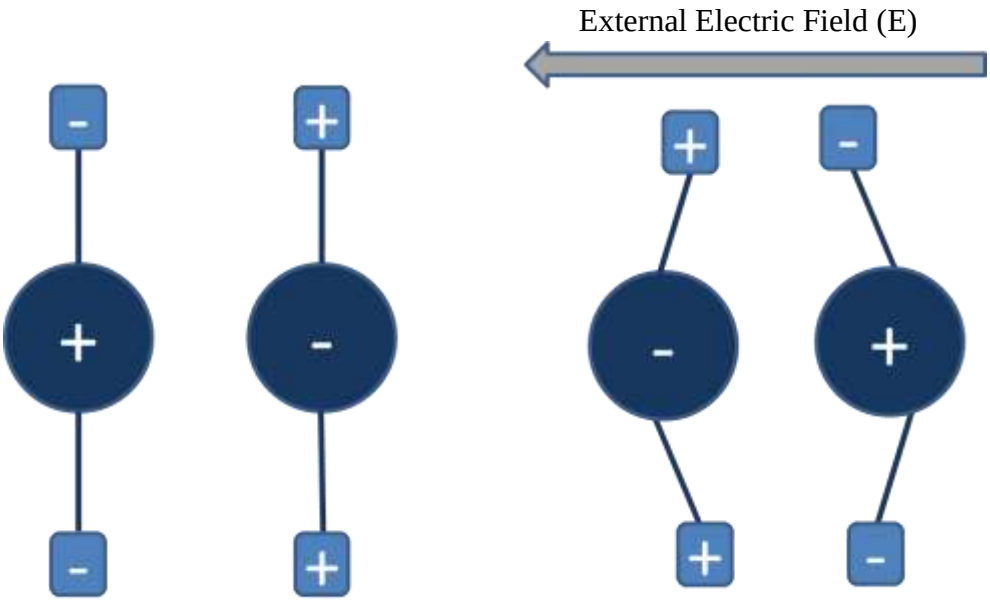

Figure 2.7. Schematic representation of ionic polarization.

2.3.1.3. Electronic Polarization

In covalent solids which have rigidly bound electrons, valence electrons align themselves more easily to the changing external electric field compared to the inertial core electrons (Figure 2.8). This mechanism is responsible for the high dielectric permittivity of such crystals as Si and Ge. Since electrons are relatively mobile, this polarization mechanism is responsible for the absorption of higher frequency electromagnetic radiation and said to be not contributing to heat dissipation at microwave frequencies.

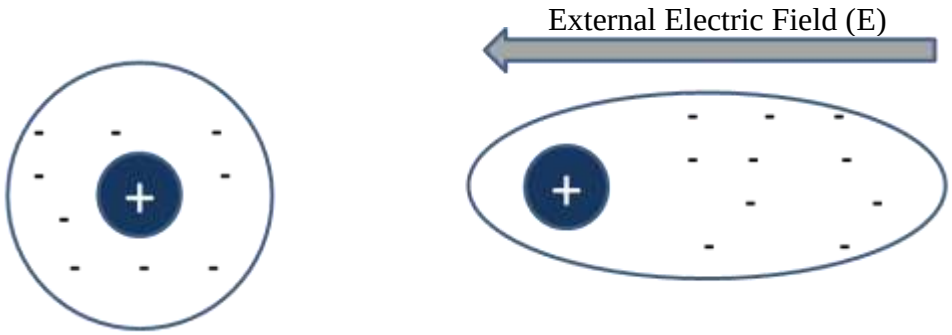

Figure 2.8. Schematic representation of electronic polarization pronounced in covalently bonded solids exposed to EM radiation at very high frequencies.

2.3.1.4. Orientation Polarization

This mechanism is pronounced for materials consisting of molecules with a nonzero dipole moment, i.e. in the case of combination of atoms having different electronegativity. In the presence of a changing electric field, the permanent dipoles in the material will try to align themselves with respect to the external field, and the resistance of the crystal against the movement of the dipoles will result in heat dissipation (Figure 2.9). Due to considerable mass of dipolar molecules, inertial resistance of the material is high to the displacement of the dipoles, and this mechanism is said to be the main mechanism of power absorption at microwave frequencies.

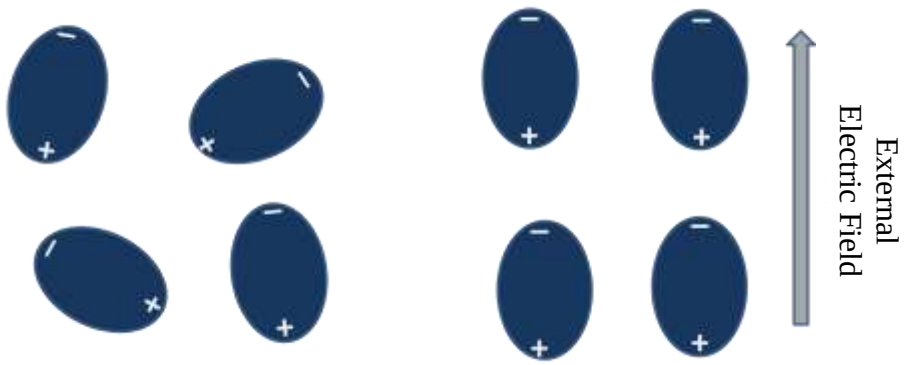

Figure 2.9. Schematic representation of dipolar polarization mechanism.

The frequency dependence of existing polarization mechanisms on the electromagnetic spectrum is schematically illustrated below in Figure 2.10:

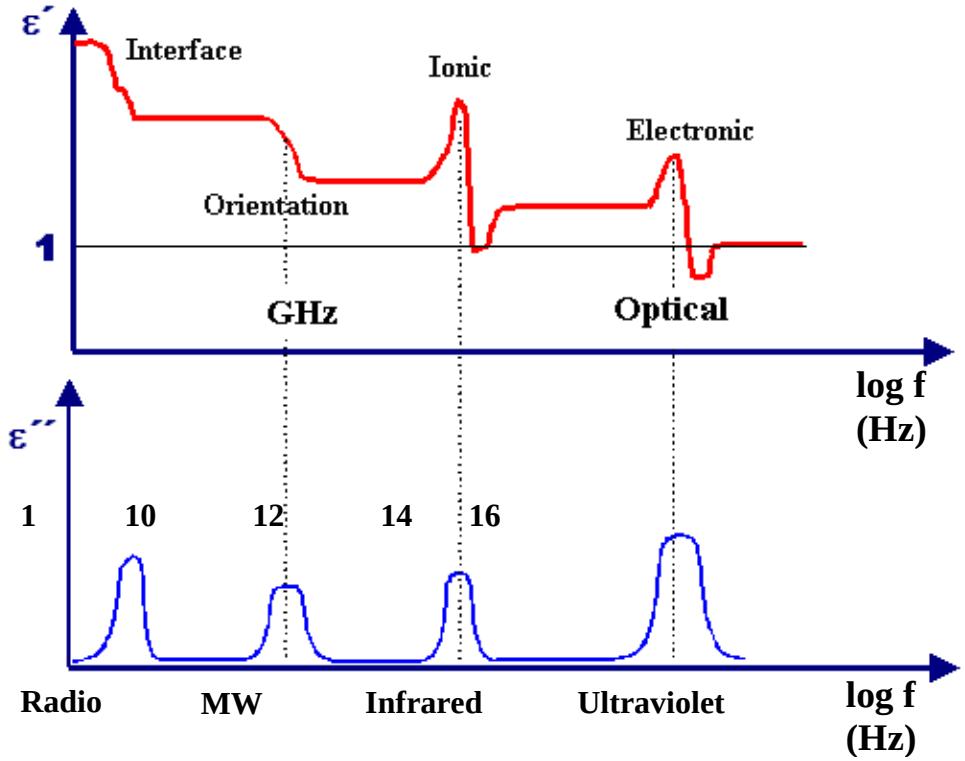

Figure 2.10. Polarization mechanisms of dielectric materials in response to changing electrical field with respect to frequency [9].

2.3.2. Conduction Losses

For insulating materials, as the temperature increases with the course of microwave heating, free charges can be created and electrical conductivity, leading to so called Joule heating, increases.

For conductors, eddy currents originated by magnetic induction cause resistive heating, however, the depth at which eddy currents are generated is determined by the penetration depth of microwaves, which is often limited to a few microns at room temperature. Hence, only superficial interaction and heating occurs in the case of bulk metals, and as a result bulk metals are generally known to reflect microwaves.

2.3.3. Hysteresis Losses

For ferromagnetic materials, losses are present due to hysteresis behavior at changing magnetic fields. Energy loss per cycle of the switching is represented by the area bounded by the B-H curve of the material (Figure 2.11).

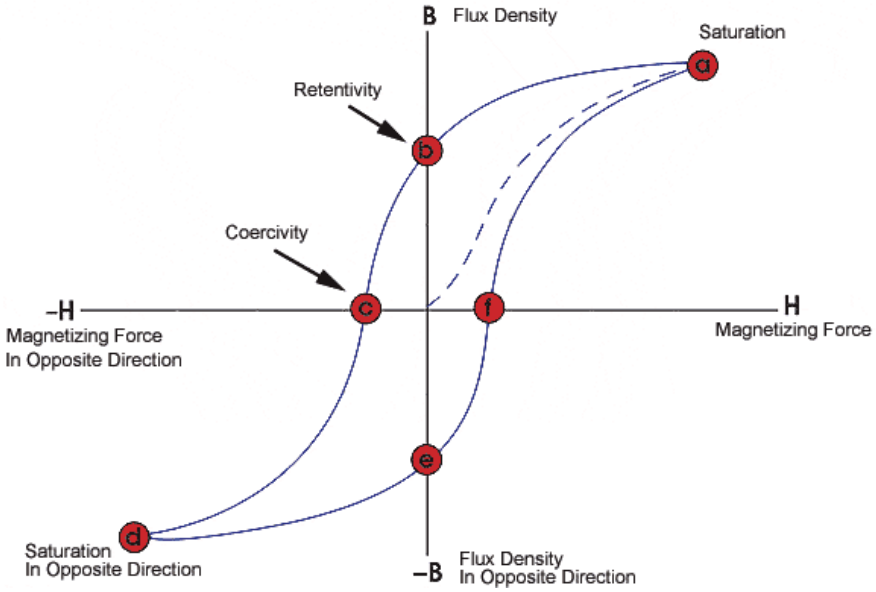

Figure 2.11. Hypothetical hysteresis curve for a ferromagnetic material [10].

To sum up, it has been reported that the main heating mechanism for ceramics and other insulators is the polarization response of the material owing to the dielectric permittivity and loss tangent. For electrical conductors, specifically, conduction losses arising from eddy currents and magnetic induction as well as hysteresis losses in case of ferromagnetic materials play an important role in microwave absorption and heat generation.

2.3.4. Magnetic Losses

Due to the unbalanced spin of electrons; there are magnetic dipoles inside the materials which create an inertia against the motion imposed by the external magnetic field. Magnetic losses account for the energy lost during the rotation of magnetic dipoles present in the paramagnetic materials to align themselves according to the external magnetic field, which is reversible. In diamagnetic materials, this

effect is reverse due to the balanced nature of electron spins causing the material to oppose the external magnetic field (Figure 2.12).

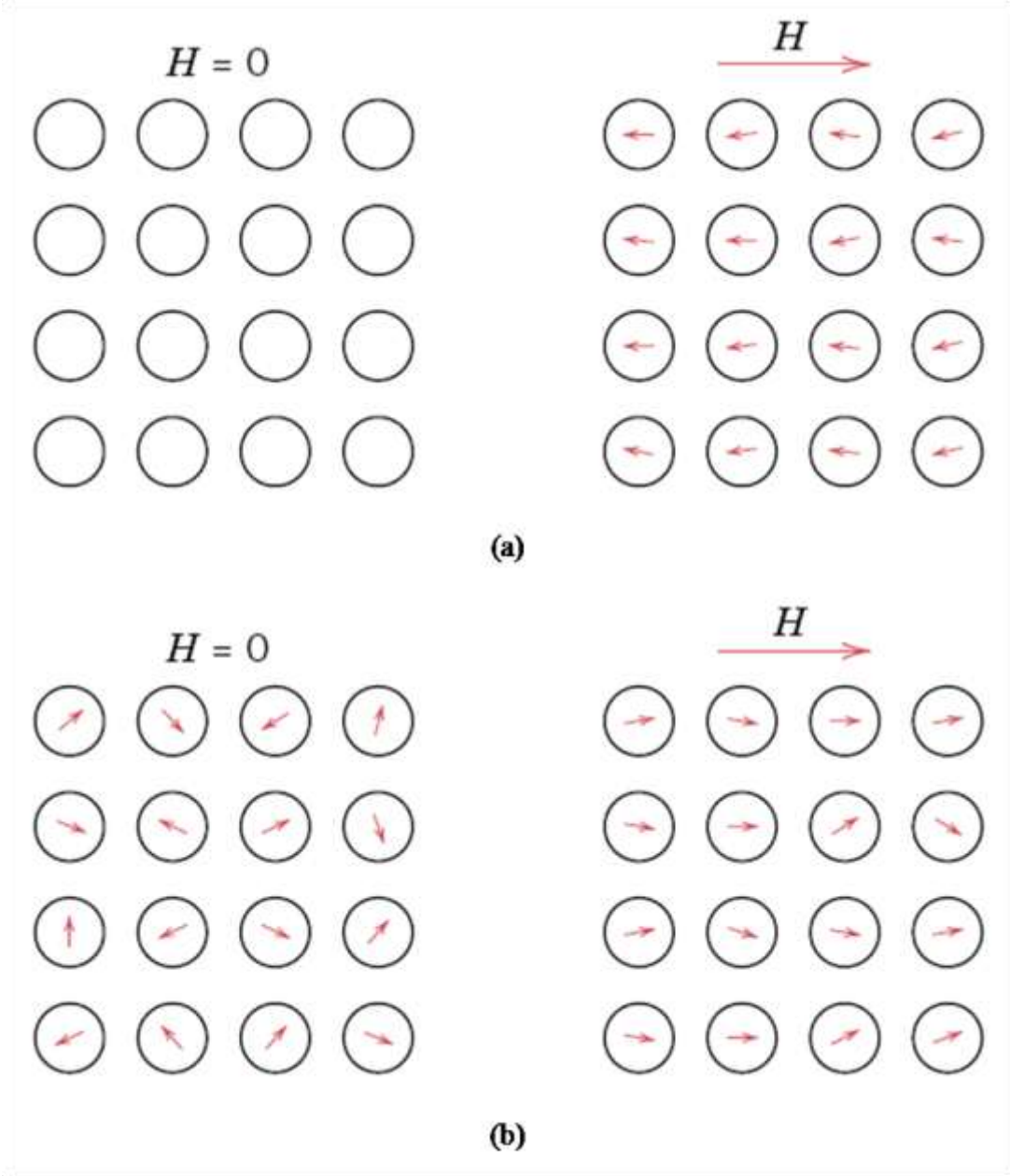

Figure 2.12. Magnetic dipole configuration in the absence / existence of applied magnetic field (H) for diamagnetic materials (a) and paramagnetic materials (b).

2.4. Microwave Heating

Microwave heating is an innovative and contemporary method exploited to process a wide range of materials including novel and conventional ones with several unique

advantages. As discussed earlier, microwave heating is dependent on materials' ability to absorb incident electromagnetic radiation and convert it to heat. Uniformity and efficiency of the microwave heating process is governed by one or more of the above-described loss mechanisms present in the material as well as the penetration depth of the microwave radiation.

In this chapter, the process-specific characteristics and application of microwave heating on several industrial processes and engineering materials will be presented.

2.4.1. Characteristics of Microwave Heating

Main characteristics of the microwave heating process include [2, 6];

- Volumetric heating and inverse temperature profile
- Controllable electric field distributions
- Rapid heating
- Selective heating of materials through differential absorption
- Self-limiting reactions
- Microwave effects

These effects provide benefits in terms of processing and superior properties in terms of material characteristics compared to conventional technique. Nevertheless, it simultaneously addresses new challenges and problems associated with the complex interaction mechanisms between materials and microwaves evoking above-mentioned characteristics. Thorough understanding of the interaction mechanisms together with the microwave heating characteristics is required to fully harness the advantages of the microwave heating process; therefore, following sections are dedicated to the detailed explanation of microwave heating characteristics.

2.4.1.1. Volumetric Heating and Inverse Temperature Profile

Difference in heat generation and corresponding temperature profiles are the key distinguishing feature of the microwave heating technique as compared to the conventional heating. In microwave heating, microwave radiation penetrates into the

sample and interacts with the it via dielectric polarization mechanisms or magnetic and/or eddy current interactions. As a result of these interactions, microwave energy gets absorbed and heat is generated within the sample body. Since heat is generated within the sample, the furnace insulators and elements are colder than the sample, so heat is lost to the surroundings from the sample surface. This situation lead to unique temperature distribution throughout the sample with surface being colder than the interiors (Figure 2.13) [5].

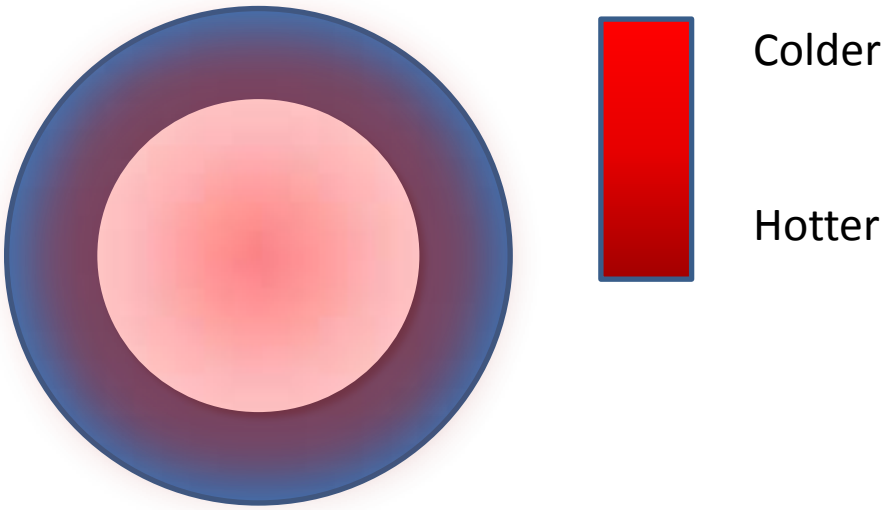

Figure 2.13 Temperature profile within the sample associated with microwave heating.

During conventional heating, heat energy is delivered to the surface of the material via radiation from the surfaces of heating elements where thermal energy is later transferred to the sample interiors by heat conduction mechanism. Consequently, sample surfaces are higher in temperature compared to sample interiors (Figure 2.14). Temperature differences and related thermal stresses are functions of the thermal conductivity of the sample and the heating rate of the furnace. Therefore, very slow heating rates and intermittent halts at intermediate temperatures are employed during conventional heating in order to establish thermal equilibrium within the sample and avoid thermal cracking [2].

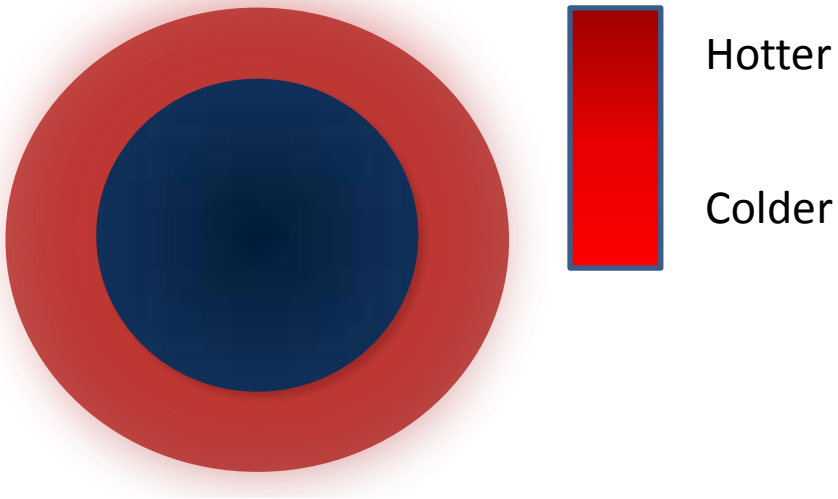

Figure 2.14. Temperarature profile of the sample sintered via conventional route.

The radiative heat transfer corresponds to the infrared region of the electromagnetic spectrum, and the penetration depth of infrared radiation is limited to superficial layers of the materials. Therefore, thermal energy is transferred from superficial layers to the material interiors through conduction from hotter to colder regions. Since heating is mainly dependent on the thermal diffusivity of the material, high heating rates cannot be achieved to avoid thermal gradients, distortions and cracking. In microwave heating case, volumetric interaction of materials with incident electromagnetic radiation occurs, so that heat is generated within the material body and conveyed to the exteriors from the surface creating an inverse temperature profile as compared to the conventional heating case. Hence, much higher heating rates can be employed, since temperature differences within the sample are minimized. However, it should be kept in mind that volumetric nature of the microwave heating is mainly dependent on the microwave absorption and

penetration properties of the material, which relies on many factors such as electromagnetic properties of the material, microwave frequency, densification, temperature etc.

Heat transfer mechanism relies on the heat conduction from material surfaces to the interiors, which implies that whole furnace insulators and heating elements needed to be heated to the desired temperature and the sample temperature approaches to the desired temperature asymptotically as the power of the conventional furnace is increased. In case of microwave heating, owing to the direct heat generation as a result of microwave absorption, average temperature of the sample increases linearly as the power of the microwave furnace increases. In this manner, temperature of the furnace components and atmosphere do not have primary influence on the heating of the sample. However, the temperature and humidity of the furnace atmosphere have secondary effects on the transmission of microwaves since the velocity of the electromagnetic radiation is dependent on permittivity and permeability of the medium (Equation 19) which are functions of composition and temperature.

$$c = (\varepsilon_0 \varepsilon_r \mu_0 \mu_r)^{-1/2} \qquad 1.7$$

c being the velocity of light in free space. The volumetric nature of the microwave heating can provide many benefits, such as products with minimized surface degradation originating from the heat loss from the surface, possibility of processing multiple samples and/or bulky samples with homogenized and refined microstructures owing to faster processing cycles, since the temperature distribution within the sample is uniform, together with energy savings. Microwave heating process utilizes as high as 95% of the input electrical energy while the efficiency of conventional heating route is usually around 85% of the input electrical energy [11].
The inverse temperature profile associated with volumetric heating exploited development of innovative materials as in the case of biocompatible materials with dense cores and porous surfaces to facilitate adhesion.

2.4.1.2. Controllable Field Distributions

In single mode microwave cavities, separation of electric and magnetic fields are possible, since only one wave mode is present inside the cavity. As the delivered power is constant, the cross product of electric field and magnetic field strengths are constants. Recalling that electric field lines decay on conductor surfaces, electric field strengths are minimized at the furnace walls while reaching to a maximum at the center of the cavity. In the same manner, magnetic field strength is maximum at the furnace walls and reaches to a minimum at the cavity center (Figure 2.15). By making use of different field distributions within the single mode cavity, selective heating of localized regions (for example for brazing or joining processes) can be achieved or interactions of materials with changing electric and magnetic fields can be studied separately.

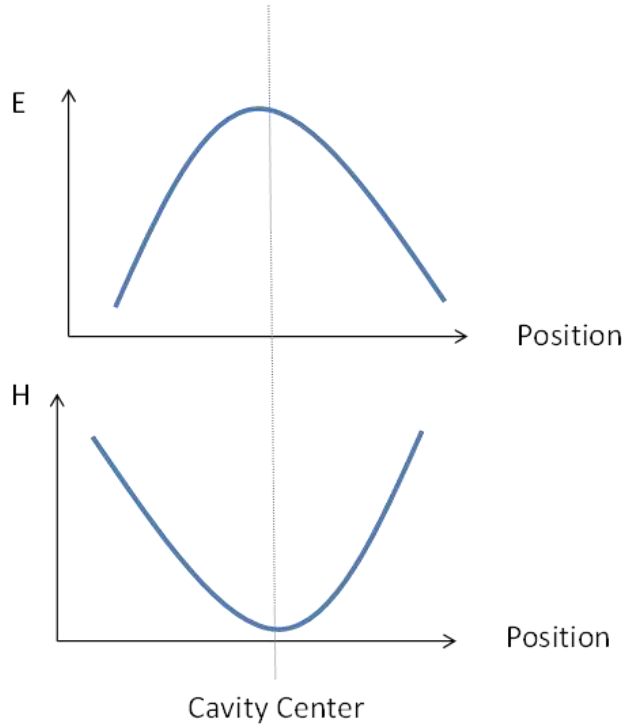

Figure 2.15. Schematic illustration of the distribution of electric and magnetic field strengths within a single mode cavity.

2.4.1.3. Selective Heating of Materials

Depending on the electromagnetic characteristics of the material selective heating of the materials can be achieved through microwave heating, since electromagnetic properties govern the coupling behavior with microwave radiation. For instance, microwave cookware and food packages are usually poor absorbers and good transmitters of microwaves to prevent overcooking and thermal runaway [12]. Another approach is to combine poor absorbers to good microwave absorbers, so that joining or bonding can be achieved. Furthermore, innovative chemical reactions and synthesis can be designed in a solvent and catalysis free environment by properly choosing the reactants [8, 11, 13, 14].

Good microwave absorbers can be utilized in initial heating of materials with low absorption properties. Materials such as SiC and graphite, termed as "susceptor"[15], are known to couple well with microwaves starting from room temperatures and used to aid initial heating of ceramics and powder metallurgical compacts to the temperatures where material itself begins to couple with microwaves as in the microwave sintering of ZrO_2. Suscepting SiC powders supply the initial heating of ZrO_2 powders to the critical temperatures. After reaching to critical temperatures, ZrO_2 powders start to couple with microwaves better than SiC powders and volumetric heating takes place. At this point, it is crucial to properly select the susceptor, which will provide the initial heating and loose its activity at the interaction temperatures of the sample [6].

2.4.1.4. Self-Limiting Characteristic

Due to a reaction, phase change or heating, certain materials lose their microwave absorption capability. As the microwave absorption decreases, heating rate also decays resulting in a self-limited heating profile. This feature associated with microwave heating harnessed mostly in microwave food packaging to avoid overcooking of the food and curing of epoxy, since cured epoxy couples less with incident microwave energy and microwave energy is concentrated around uncured regions [8].

2.4.1.5. Microwave Effects

The microwave effects or the so-called non-thermal effects are the anomalies encountered during microwave processing and cannot be explained by the inverse temperature profile compared to conventional heating. Accelerated kinetics and enhanced processing of materials including reduction in process time and temperatures, enhanced diffusion kinetics and reduced activation energies have been debated in the last decade. Some researchers denied the presence of such microwave effects and attributed observed acceleration and enhancement in the process to the inaccuracy in temperature measurements. However, studies comparing different temperature measurement techniques during microwave sintering have revealed that the temperature measurements are reliable, and results taken from the three most common temperature measurement tools, namely thermocouple, pyrometer and optical fiber probes are in good agreement with each other [5]. Another study indicated that there is at most 5% temperature difference between the interior and exterior regions of the powdered copper sample, which implies that such "microwave effects" do exist in many of the studied systems [16].

Observed reduction in activation energies for bulk diffusion in the third stage of sintering and enhanced densification at lower temperatures were mostly attributed to the local potential differences in the neighboring particles making up the bulk sample arising from the decrease in the electric field intensity due to the skin effect [17, 18]. The local electric field attracts more ions to the interparticle boundaries in ionic ceramics and claimed to cause local melting and plasma formations in the case of metallic samples, therefore promoting diffusion by creating easy paths for diffusion. Another reason may be originating from the fact that pore coalescence and grain growth is minimized owing to the fast heating rates to the sintering temperatures in the case of powdered samples. The inhibition of microstructural coarsening and suppression of stage II sintering enhances bulk diffusion where densification and pore rounding are facilitated which at the same time improves mechanical properties [19].

2.4.2. Limitations of Microwave Heating

Main problems encountered during microwave heating include thermal runaway, localized hot spots and complications related to heating atmospheres, which put a limit to increase the input microwave power resulting in an increase in the required field strength to further achieve higher heating rates and process temperatures.

2.4.2.1. Thermal Runaway

Thermal runaway is the sudden increase in temperature locally in the sample due to extensive microwave absorption exceeding the rate of heat loss to the surroundings. Occasionally this phenomenon turns into arcing and/or localized hot spots and melting of the sample. Samples with low thermal conductivities are prone to thermal runaway, since the heat losses from the sample depends mainly on heat conduction. Furthermore, certain dielectrics exhibiting an abrupt increase in the dielectric loss factor at elevated temperatures are especially subjected to thermal runaway. The electric field strength and input microwave energy should be elaborately selected to avoid overheating and thermal runaway [4].

2.4.2.2. Complications Related to Heating Atmospheres

As a consequence of the high electric field strength within the microwave cavities, the ionization and discharge of the furnace atmosphere may occur when the electric field strengths exceed the dielectric breakdown strength of the gases and create free charge carriers. The discharge phenomenon is generally creation of conductive paths between two points at different electrical potentials and can take place in arc, glow or plasma discharge forms according the continuity of the free charge carrier supplies [4]. The necessary electrical field strengths to surpass the dielectric strength of the gas is expressed by Paschen's curve (Figure 2.16) and is a function of the number of molecules present in the gas (can be expressed in terms of pressure and temperature) and composition; also known to be frequency dependent. It can be seen from Figure 2.16 that electric field strengths necessary to make the gas conductive decreases with decreasing gas pressure. This relation results from the fact that the mean free

path of the free charge carriers (may be electrons and/or ions generated by the external field) increase with decreasing gas pressure and reach to a minimum; so that the carriers can travel more distances along with the external field without being scattered. Nevertheless, it seems that after a certain point, the required electric field strengths seem to increase with a further decrease in gas pressure, which can be explained by a lack of continuous creation of free charges to sustain the continuity of the electrical discharge. Because of the above-mentioned facts care must be taken when working under vacuum, since a breakdown of the atmosphere can occur at lower operating electric field strengths, and a great deal of energy can be transferred to the sample through the arcs or glows resulting in burn damage, thermal runaway or local melting depending on the severity of breakdown [4].

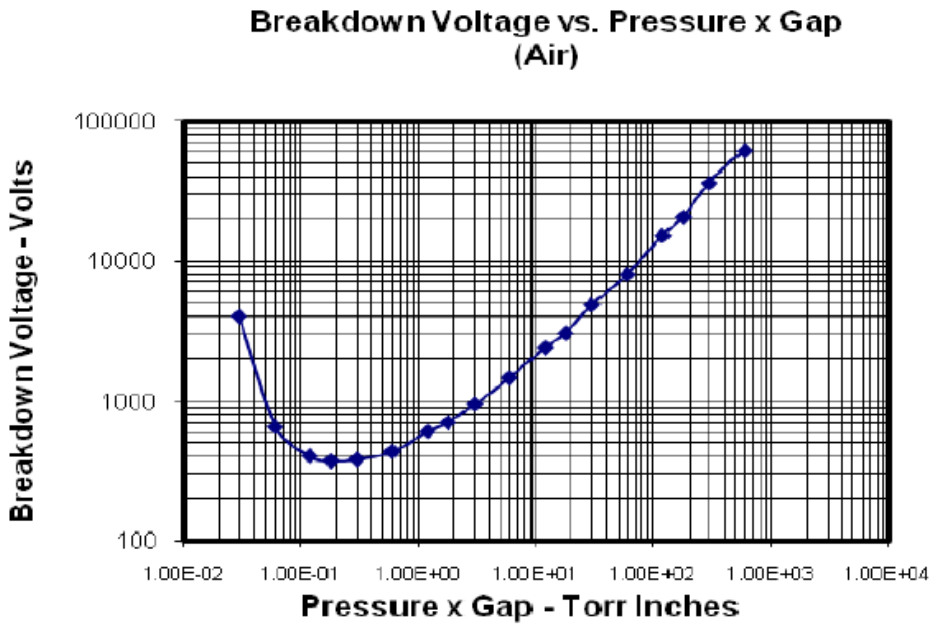

Figure 2.16. Paschen's curve depicting relation between breakdown strength and pressure of the gases [20].

A similar relationship between voltage and inter electrode separation exists as in the case of electric field strength and gas pressure. In this case, voltage decreases with decreasing separation distance, since the distance for the free charges to move from one electrode to the other becomes less; although, there is again a minimum in the necessary voltage, and the curve begins to rise steeply after a critical separation distance [4].

Another important factor determining the dielectric strength of the atmosphere is definitely the composition and molecular masses of the gases, since the work function of the gases is composition dependent, and the acceleration of formed ions along with the external field is controlled by the atomic inertia. For instance, argon and helium have high ionization potentials being noble gases in the upper portion of the VIIIA group of the periodic table. However, they have lower dielectric strengths than air implying that they are ionized via acceleration of ions (secondary ionization processes) owing to their small atomic masses. In addition to this, presence of impurities in the protective gas such as humidity or air can dramatically decrease the dielectric strength of gases by supplying extra free charges which further contributes to the ionization of the medium by secondary ionization processes. Therefore, the purity and the dryness of the protective gases are of special concern to avoid dielectric failure of the atmosphere. Furthermore, dielectric strengths of the gases are known to decrease with increasing temperature, which is caused by an initial decrease in density followed by an increase in the mean free paths of the charge carriers [20].

This situation may be pronounced and more frequently encountered in the case of microwave sintering of powder metallurgical compacts, since the work functions of the metals are smaller; hence, metals can donate more carriers to the surrounding which in turn contribute to the discharge process. Moreover, electrical field strength necessary to sustain a discharge is smaller than the strength necessary to initiate it, which in turn forces an immediate shut down in the power for a few seconds to redistribute free carriers to formed conductive path and restart [5].

2.4.3. Microwave Furnaces

Basically, two types of microwave cavities are available for industrial and research oriented applications, which are namely multimode and single mode applicators. The electric and magnetic field distributions and consequent temperature distributions are strongly linked to the cavity type, and each has its application specific advantages and disadvantages.

2.4.3.1. Single Mode Cavities

Only one mode of microwaves is supported in this type of furnaces, where the size of the cavity is modified on the order of the wavelength of microwave radiation to avoid multiple reflections and multiple wave modes. In this case, the microwave input is generally designed to have little variation in the frequency. Electric field strength is minimized near the edges of the cavity, since the electric field lines decay on the conducting furnace walls. As the input power of the furnace is constant, the magnetic field strengths are maximized at the furnace edges, where the power vector dictated by vector product of E and H is constant. Likewise, electric field is maximized at the center of the cavity, where magnetic field strengths are approaching to zero this time [5]. The distinct distribution of electromagnetic fields in single mode cavities offer several advantages such as [8];

- The numerical and analytical solutions to Maxwell's equations can be verified experimentally, since the field distributions and boundary conditions are simpler and determinate.
- The interaction of materials with varying separate electric and magnetic fields can be studied.
- Selective processing of materials can be possible by inserting the samples at proper positions of high electric/magnetic field strengths.
- Brazing and joining of ceramics can be possible without heating the remaining bulk of the ceramic by positioning the contact region in the center of the cavity (in other words at the point of maximum electric field strength).

However, despite these advantages the single mode applicators have a limited industrial use due to the non-uniformity of heating arising from the local fluctuations in electric/magnetic field strengths, and the relatively small size of the cavities and waveguides which do not allow processing of large scale products.

2.4.3.2. Multimode Cavities

In multimode cavities, a number of electromagnetic wave modes are simultaneously supported. Explicitly, the electric and magnetic field strength distributions are more

homogenous; consequently, the heating is more uniform. Unlike single mode cavities, multimode furnaces do not have size limitations, and even larger cavities provide better uniformity in heating by permitting multiple reflections. As a rule of thumb, the cavity size should be 100 times greater than the operation wavelength; however, for 2.45 GHz frequency this value corresponds to impractically large sizes. Because of this fact, other ways of improving uniformity are utilized:

- Number of magnetrons (electromagnetic wave generators) can be increased in a given cavity size. Wave distributions are expected to become more homogenous with increasing number of magnetrons
- Reflecting metal blades called “mode stirrers” can be employed to mix the electromagnetic waves.
- Samples can be placed into turntables which rotate and allow mixing of the electromagnetic waves.
- Susceptor materials either in powder or block forms can be placed near the sample to compensate for the heat losses and allow uniform temperature distribution within the sample. Hybrid heating route by means of susceptors are especially helpful for the initial stages of microwave heating of powder metallurgical parts, considering the fact that the skin depths, and hence the microwave absorption capacity of the conducting powders, increase with increasing temperature as depicted in the Figure 2.17.

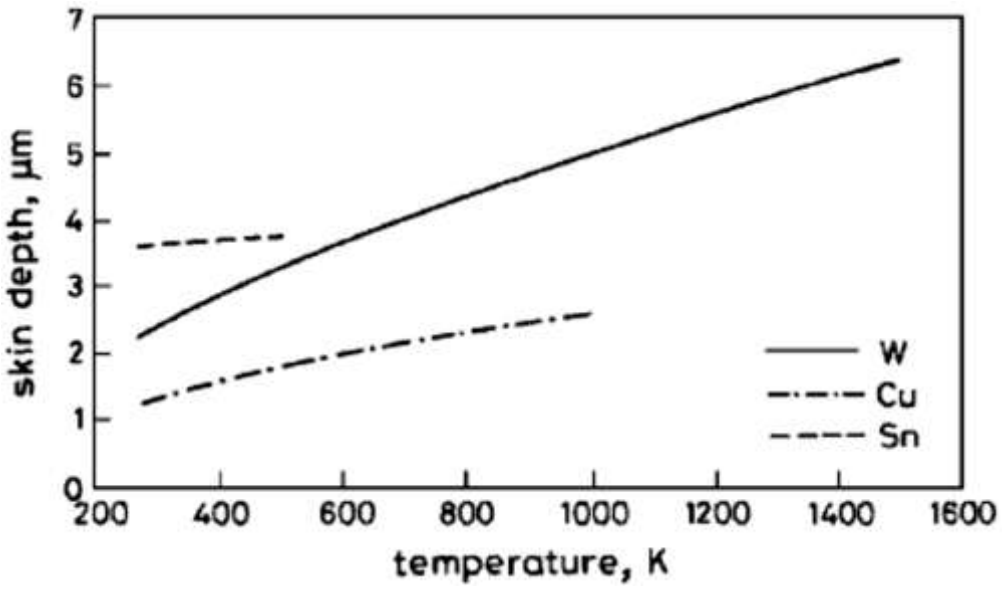

Figure 2.17. Skin depth values of various metals as a function of temperature [21].

Because of the homogenous electromagnetic wave distributions and flexible cavity size options, production of large scale and complex shaped samples is possible with multimode cavity usage. Therefore, multimode furnaces are preferred mostly for industrial applications [5, 8].

2.4.4. Microwave Heating of Metal Based Materials

Following the extensive research efforts on the radar applications during World War II, it was discovered that electromagnetic radiation in the GHz range can also be efficiently employed in industrial heating applications including food industry, manufacturing ceramic products, polymer curing and extractive metallurgical processes. Until recent decades, volumetric heating of metallic parts was thought to be inapplicable via microwave radiation, since monolithic metals are known to reflect a great portion of the incident electromagnetic radiation, and the extent of interaction is confined to the skin depths of the metallic parts, which in most cases is restricted to superficial layers of a few microns thick at room temperature.

However, recent studies indicated that unlike their monolithic counterparts, powder metallurgical parts consisting of conductive powders of dimensions on the order of the magnitude of the skin depth can couple efficiently with incident microwave

radiation and be heated volumetrically as well. Despite the fact that no exact mechanism can be proposed for this phenomenon, there are several attempts to explain the interaction of microwave radiation and powder metallurgical compacts, which often simultaneously consider Maxwell's equations and heat transfer relations along with penetration and skin depth concepts.

Recalling the general power equation representing the conversion of electromagnetic energy into heat energy through the loss mechanisms; power dissipated in the sample per unit volume is described by [4]:

$$P = (\sigma + w\epsilon'') \mathbf{E}^2 + w\mu'' \mathbf{H}^2 \qquad 1.8$$

where first term on the right hand side of the equation stands for conduction and displacement current losses while the second term indicates magnetic losses. For conductors, the displacement currents ($w\epsilon''$ term) are negligible owing to the low polarizability and dielectric loss factors. Hence, magnetic losses ($w\mu''$) and conduction losses (represented by σ, which is frequency independent from DC to microwave frequencies) originating from the induced eddy currents are responsible for microwave absorption of conductors [7, 16, 22]. Nevertheless, the dissipated power concept is insufficient, since it does not account for the penetration ability, i.e. the electric and magnetic field strengths, of E and H inside the material. At this point, it is obligatory to review penetration and skin depth concepts mentioned in section 2.1.3.

As can be inferred from aforementioned equations, the penetration ability of microwaves through the materials is governed by resistivity (ρ), dielectric permittivity (ϵ') and magnetic permeability (μ') of the material. For metals, which are electrical conductors, the dominating terms are resistivity (ρ) and magnetic permeability (μ') of the systems, since their dielectric permittivity is comparatively small. Approximate room temperature penetration depths of selected metals at 2.45 GHz microwave incidence are given in Table 2.1 calculated using the room temperature permeability and resistivity [11].

Table 2.1. Skin depth values of various metals at 2.45GHz

Element	Penetration Depth (μm)
V	11
Ni	8
Co	5
Fe	2
Al	2
Cu	1
Mg	<1

For bulk metals, interaction depths are limited to very superficial regions of the material as dictated by the penetration depths at microwave frequencies. However, one should keep in mind that both resistivity and permeability are dependent on the inherent properties of the material and sensitive to defects, temperature, grain and particle size etc. In this aspect, the resistivity and permeability of the powder metallurgical green compact should be considered instead of its bulk counterpart of theoretical density (TD). Owing to the high porosity and the insulating air gaps between the particles, powder metallurgical compacts have penetration depths on the order of millimeters, which corresponds to the order of magnitude of wavelength of the microwave radiation. Another fact to consider is the temperature sensitivity of resistivity and permeability, which implies an increase in the microwave absorption capability due to the tendency for increasing penetration depths at elevated temperatures. Due to high penetration depths in the green state, many metallic systems couple well with the microwave radiation and pure microwave heating can be possible [19, 21, 23]. For other systems, often hybrid heating with susceptor powders is of consideration to preheat the sample to interaction temperatures [24-27]. One other important contributing factor to the microwave heating of metal-based materials is the morphology of the starting powders. Pressability, hence, the green density is not the sole consequence of the particle morphology on microwave absorption, since microwave heating is reported to be more penetrating and volumetric in nature in less dense green parts [28]. However, the morphology of the

starting powders also influence the local concentrations of electrical field in the inter particle contact regions, where particles having more irregular shape create a more locally distorted electric field excessing the dielectric strength of the surrounding medium (air, binder etc.) leading to localized plasma ignition and consequent melt formation or rapid evaporation [7, 14, 28]. As a result, transport of atoms takes place in virtue of easier paths such as a plasma, liquid or evaporation-recondensation, therefore, often the densification response of the sintered products is better compared to conventional sintering under identical conditions [27, 29-34].

2.4.5. Effect of Separate Electric and Magnetic Fields

Studies concerning the effect of electric and magnetic field components of the microwaves on heating separately were conducted in single mode cavities. In these studies, the samples were positioned in the cavity center to obtain maximum electric field strength and placed at the cavity edges to obtain maximum magnetic fields [17, 35].

As explained earlier, heating takes places through absorption of electric and/or magnetic field components of the microwave radiation. Majority of the studies attribute volumetric heating of materials to the interaction of electric field and absorption of microwaves via dielectric loss mechanisms. Nevertheless, for a great deal of powder metallurgical compacts, interaction with the magnetic field component of the microwaves is thought to be the main contributor to the volumetric heating [6, 13, 21, 35, 36].

In a recently conducted study, effect of separate electric and magnetic fields on microwave heating of porous copper compacts has been investigated [16]. It was found that the initial heating rates achieved were higher in samples heated under pure magnetic field as compared to samples heated under pure electrical field. Both heating curves displayed a peak in temperature, with magnetically heated sample reaching to higher temperatures. It is worth mentioning that the abrupt peaks in temperatures disappeared at the subsequent heating cycles for both pure magnetic

and electrical heating, where the temperatures reached asymptotically to an equilibrium value. To check the reversibility of heating under pure electric and magnetic fields, samples that were first heated in pure electric field were subsequently exposed to magnetic field, and reverse has been done to samples that were initially heated in magnetic field. The spikes observed in temperature-time curves of the electrical heating followed by magnetic heating did not disappear for both heating cycles meaning that the effect of electrical heating is reversible. However, the spikes in the heating curves of the initially magnetically subsequently electrically heated samples vanished implying that the heating of magnetic field is irreversible. The findings of the results were explained by the more efficient coupling of conducting powders with the magnetic field component of the microwaves, and by the rapid neck formation and agglomeration of powders occurring shortly after exposure to magnetic fields leading to an increase in conductivity, and hence a decrease in the penetration depth of the microwave. The reversible effect of the electrical heating implies that there is a moderate interaction between the porous copper compact and electrical field, consequently, the neck formation is shifted to higher sintering temperatures and longer sintering times [16].

2.5. Microwave Sintering

In this section, fundamental phenomena underlying the improvement of the physical properties of powder metallurgical compacts by sintering will be briefly discussed, and then the effect of microwave sintering on various metallic systems is going to be dealt with in short in a comparative manner to conventional sintering.

2.5.1. Sintering

Due to excess energy associated with packed powders of green metal compacts, cohesion by neck growth takes place at elevated temperatures. Mass transport on an atomic scale towards neck region implies a decrease in surface area, which drives the sintering process. High temperatures are required to increase the average kinetic energies of atoms which results in accelerated diffusion [37].

Sintering starts with formation of point contacts between particles and observed to consist of three stages. In the Figure 2.18 showing an SEM micrograph, nickel particles of 33 microns in diameter are seen to form necks [37].

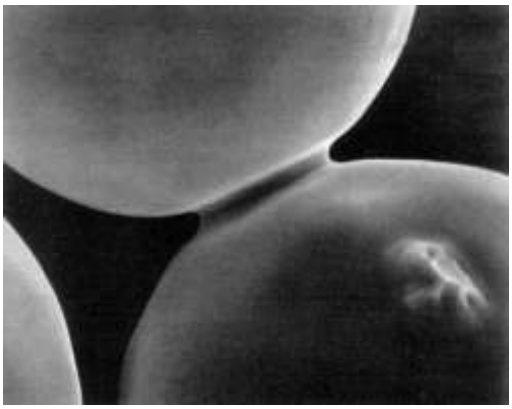

Figure 2.18. Neck formation during sintering[1].

In the initial stage, kinetics is driven by the curvature gradients in the neck region. Pores are open and fully interconnected with a rough morphology. In the intermediate stage, pore structure becomes much smoother with interconnected and cylindrical morphology. Driving force is the interfacial energy associated with grain boundaries and pore-solid interface. At the later period of intermediate stage sintering, pores start to have a smooth, spherical morphology being isolated from the grain boundaries which is very undesirable, since pores drag the grain boundaries suppressing grain growth resulting in remaining total interfacial area, i.e. residual driving force beneficial for densification kinetics. In the final stage, the kinetics is very slow and driven by the pore solid interface. The elimination of pores is extremely difficult, if there is a gas presence filling the pores [37].

After the sintering step, pronounced improvements [7, 19, 23, 29, 34, 37-47] occur at some of the physical properties of the compact which can be summarized as follows:

-Strength, elastic modulus (increase)
- Hardness, fracture toughness (increase)
- Electrical and thermal conductivity (decrease)
- Permeability to gases and liquids (decrease)

- Average grain number, size and shape (increase)
- Distribution of grain size and shape
- Average pore size and shape
- Distribution of pore size and shape
- Chemical composition and crystal structure.

2.5.2 Microwave Sintering of Powder Metallurgical (P/M) Compacts

After it has been discovered that P/M parts made up of powders with sizes in the order of penetration depths can effectively interact and get volumetrically heated by microwaves, several attempts have been made to adapt the microwave heating technology for sintering of P/M parts to exploit benefits of microwave sintering such as faster heating rates and processing cycles, energy efficiency as well as decreased processing temperatures. Reduction in the processing cycles and temperatures resulted in P/M products of higher sintered density, refined microstructures and improved mechanical performances as compared to their conventionally sintered counterparts for a great variety of metallic systems so far investigated [7, 27].
This section is dedicated to the specific applications of microwave sintering of various metallic systems with an emphasis on ferrous alloys and nickel to provide the theoretical background of this study.

2.5.2.1. Microwave Sintering of Cermets

One of the earliest applications of microwave sintering on P/M parts, this novel method has been adopted in the production of WC-Co cermets. Co-WC alloys are typically used in cutting tools owing to their high strength and wear resistance, where they contain a low fraction of Co (around 6-10wt%) as binder [48]. In studies regarding microwave sintering of WC-Co cermets, it has been shown that microwave sintered samples can obtained with lower porosity, refined microstructures, improved hardness and flank wear resistance along with higher coercivity at faster processing cycles compared to their conventionally sintered counterparts. One of the outstanding outcomes of these studies was the ability to produce WC-Co samples via microwave processing route with 8% higher densification compared to that of conventional route

at the same sintering temperature. Another benefit that came with microwave sintering of WC-Co samples was the inhibition of dissolution of W in Co with respect to conventionally sintered samples owing to the faster processing cycle of microwave sintering [48-51].

2.5.2.2. Microwave Sintering of Refractory Metals

Since the primary applications of refractory metals include elevated temperatures, sintering and processing temperatures of the refractory metals are high as well due to their high melting points. In the literature, microwave sintering of molybdenum (Mo) and tungsten (W) metal powders have been reported so far, where studies highlight the advantages of achieving near theoretical densities via microwave sintering route at comparatively low temperatures than conventional sintering temperatures. During microwave sintering of Mo powders, it was found that the sintered densities of the samples increase at a much faster rate with respect to sintering times as compared to the samples processed via conventional sintering route under identical conditions. Although the reasons behind this kinetic acceleration coming with the microwave sintering route are not clear, the enhancement in the sintering exploiting microwave energy has been stressed. It is generally accepted that samples with higher green densities exhibit higher sintered densities, which can be attributed mainly to the agglomerated powder morphology. At higher compaction pressures, the intra-agglomerate pores are filled via cold deformation of the powders, which in turn provide improved green and sintered densities [39]. Microwave sintering of W has been carried out for as received and high energy milled (activated) powders, and it was shown that activated powders having larger surface area and more amount of interparticle strain associated with high energy milling attained higher sintered densities due to more efficient absorption of microwave energy [52]. Moreover, it was found that W P/M compacts can be obtained with densification responses exceeding 95% TD in processing times less than 15 minutes, and microwave sintered W compacts have exhibited superior mechanical and microstructural properties than their conventional counterparts [48-51].

2.5.2.3. Microwave Sintering of Copper Alloys

Microwave and conventional sintering of bronzes belonging to the family of Cu alloys has been studied extensively. The effect of microwave sintering on densification, microstructure, hardness and homogenization has been investigated. Premixed and prealloyed bronze powders were employed in these experiments to study the influence of green density and powder conditions on microwave absorption. Compacts with prealloyed powders were observed to couple better with microwaves than their premixed counterparts, as characterized by the higher initial heating rates. This difference was thought to arise from the higher resistivity and higher corresponding penetration depths of the prealloyed powders. However, it was noted that premixed powders reached a higher sintered density than the prealloyed powders, both in microwave and conventional sintering case due to higher green strength of the premixed powdered samples [26]. To study the effect of green density on the sinterability of porous bronze compacts, samples with varying green densities have been both microwave and conventionally sintered. Samples having higher green densities showed a decrease in their sintered densities for both microwave and conventional sintering cases, since enhanced diffusion of Sn into Cu particles by the increased number of Cu-Sn contacts caused consequent melting and swelling. Surprisingly, samples with lower green strengths densified better via microwave sintering than their conventionally sintered counterparts implying that microwave sintering suppressed diffusion of Sn into Cu owing to faster processing cycles, and hence the melting and swelling of the compacts could have been avoided [26].

2.5.2.4. Microwave Sintering of Steels

Being one of the most widely used materials worldwide, microwave sintering of steels have been studied extensively. Among the worth noting benefits of microwave sintering of powder metallurgical steels are the enhancement of alloying element dissolution and consequent strengthening of the α phase, slightly improved densification and hardness at temperatures lower than conventional sintering, where the densification response of microwave sintered steels is a weaker function of the sintering response [23, 29]. It was also shown that complex and large geometries can

be successfully microwave sintered as well, though microwave sintering of simpler geometries is more convenient. Another interesting finding is the decline in the transition temperature from α to γ phase, which implies a lowering in the free energy and a stabilization of the γ phase via microwaves, for which an exact mechanism could not be proposed so far [19].

Due to their commercial importance and wide application, microwave sintering of stainless steels have been studied separately. In these studies, the effect of microwave sintering on the corrosion and erosion resistance besides the microhardness of austenitic and ferritic stainless steels as well as their composites have been investigated in a comparative manner to the conventional sintering route. The densification response of ferritic stainless steels were found to be better than the densification response of austenitic stainless steels via both sintering routes, which was attributed to the enhancement in the diffusion of atoms in more open structure of BCC ferrite [53]. The corrosion and erosion behavior of both stainless steels sintered by microwaves were superior than those of the conventionally sintered ones owing to the fact that microwave sintering results in closed and smoother pore morphologies [54]. In order to study the effect of microwave sintering on stainless steel composites, both ferritic and austenitic stainless steel compacts containing YAG (Atria Aluminum Garnet) dispersion as the reinforcing phase have been microwave and conventionally sintered. Results have indicated that YAG dispersed austenitic and ferritic stainless steel composites couple more effectively with the microwaves and more amenable to microwave sintering [55]. Conventionally sintered YAG composites showed inferior densification response than their microwave sintered counterparts, which displayed improved density at an optimal YAG addition. This difference was thought to mainly arise from local hot spot formation by differentially heating YAG particles under microwave radiation further facilitating diffusion and densification. Under solid state sintering conditions, microwave sintered YAG dispersed austenitic stainless steel composites had improved mechanical properties than their conventionally sintered counterparts, however, under supersolidus sintering conditions microwave sintered composites surprisingly displayed inferior mechanical properties despite their higher densification [55]. Underlying reasons

being still unclear; it has been determined that microwave sintering results in an elongated and irregular pore morphology under supersolidus sintering conditions which causes a decrease in hardness and a brittle characteristic in the failure mode. In contrast to this, both solid state and supersolidus sintering of YAG dispersed ferritic stainless steel composites under microwave radiation resulted in better densification as well as improved hardness. Quantitative metallographic examination revealed not only smoother and rounded pore morphologies but also narrower pore size distributions. Consequently, ferritic stainless steels and their composites processed through microwave sintering route had improved mechanical properties such as sliding wear response, ductility and hardness [53-55].

2.5.2.5. Biomedical Applications of Microwave Sintering

One of the attractive applications of microwave sintering is the production of biocompatible materials. Generally, materials with a porous surface to allow for bonding and load transfer along with a dense core to satisfy strength requirements are desired for biomedical applications, and titanium is a commonly used metal because of its inert surface, high strength and lightweight [56]. Powder metallurgy of titanium alloys are rather challenging due to high melting point and reactivity, as result their sintering is usually carried out under high vacuum conditions and at elevated temperatures [57]. Studies indicated that P/M titanium alloys can be produced with a dense core and porous surface at one step via microwave processing route. This benefit associated with microwave sintering results from the inverse temperature profile and nature of microwave heating, where heat is generated within the sample body and lost to the surroundings from the surface unlike conventional sintering. The thickness of the porous region is mainly controlled by the sintering time with an inverse proportionality, and the pore size is a function of the size of the powders used [56]. It was noted that especially at low temperatures, spark discharge is an encountered phenomenon due to the high vacuum atmospheres to prevent oxidation, disrupting heating uniformity and control of heating rate. However, at temperatures exceeding 800 °C, discharges were eliminated, and controlled heating and sintering of biocompatible titanium alloys was possible [58].

2.5.2.6. Effect of Microwaves on Diffusion Behavior of Selected Metallic Systems

To confirm the anisothermal effects of microwaves and the accelerated sintering kinetics on powder metallurgical compacts neck growth kinetics and concentration profiles of elemental copper and nickel powders and stainless steels have been studied under multimode and single mode microwave radiation. The compacts were placed in the cavity center, where electric field strengths are maximized, since according to the previous knowledge heating effect originating from the interaction of conducting powder metallurgical compacts with the electric field component of the microwaves is more intense and efficient. Results have indicated that the initial heating rates are higher for both metallic systems in single mode cavities as compared to multimode heating, which is expected since the electromagnetic energy is concentrated around the samples [36, 59]. Furthermore, from the neck growth kinetics and the advance of the interparticle contacts, the diffusion coefficients and corresponding activation energies were calculated. The activation energies required for diffusion is almost the same as conventional sintering under multimode radiation, whereas the activation energies for diffusion is anomalously low under single mode sintering being comparable to those in the case of diffusion of copper and nickel atoms in the liquid state [17, 35]. These findings suggested that single mode microwave radiation causes local melting and/or plasma formation in the interparticle regions favoring transport of atoms to the neck region and enhancing densification. In addition to the calculated activation energies, there were some microstructural evidences obtained in the porous copper system supporting this hypothesis, in which porous regions formed especially near the interparticle contact regions could be seen apparently implying sputtering of atoms from the bulk of the particles to the neck region. Under multimode microwave sintering, the activation energies were almost the same as activation energies required for conventional sintering, and the accelerated sintering kinetics and enhanced densification response was thought to be associated with the fast heating, which restricts particle coarsening and pore coalescence, so that more surface area is present at sintering temperatures facilitating densification by providing easy paths for diffusion [18]. Another study investigating the diffusion of nickel atoms into iron lattice (BCC) indicated an asymmetry in the diffusion behavior of nickel despite the symmetrical cubic lattice

of the iron [60]. It was concluded that such an unsymmetric diffusion behavior of nickel is can be related to the nonuniform distribution of electromagnetic waves within the furnace.

CHAPTER 3

EXPERIMENTAL PROCEDURE

3.1.Metal Powders Used In the Study

Microwave and conventional sintering experiments were carried out on compacts composed of prealloyed stainless steel powders and of premixed elemental Nickel (Ni) (Alfa Aesar, Lot #G29T041) and Iron (Fe) (Alfa Aesar, Lot# I29T024) powders at permalloy composition (80 wt% Ni).

The composition and morphologies of the stainless steel powders are seen in the below given SEM micrograph (Figure 3.1) and EDS analysis results (Table 3.1), respectively. From the SEM photo, it is clear that the stainless steel powders have ellipsoid morphology with approximately 55 μm particle size. EDS analysis result indicates that the composition of the prealloyed stainless steel powders matches with that of the austenitic grade 316 stainless steel (Table 3.1).

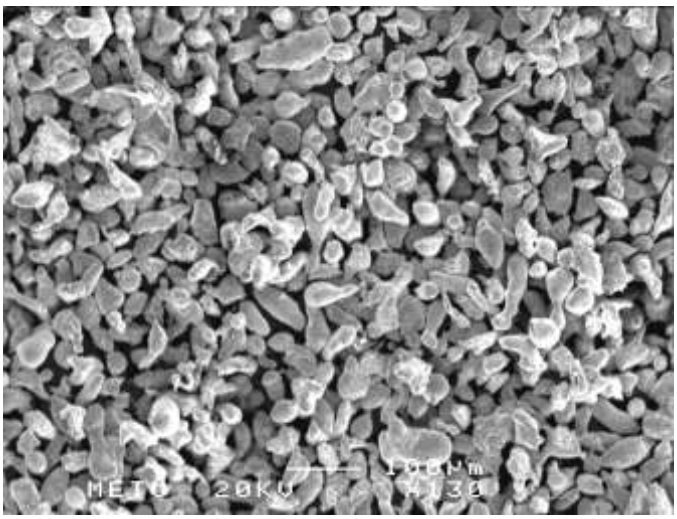

Figure 3.1 .SEM micrograph of the stainless steel powders used in the study.

Table 3.1. Average composition of the stainless steel powder obtained from 5 measurements of EDS results.

Element	*Weight Conc %*	*Atom Conc %*
Si	0.75	1.28
Cr	18.48	16.92
Fe	64.21	54.73
Ni	10.85	8.80
Mo	1.25	0.62

Elemental Nickel and Iron powders of average particle size below 10 μm were used in the permalloy related studies. The average particle size of the powders was deliberately chosen to be below 10μm which is proportional to the room temperature skin depth values of Ni and Fe metals, so that effective coupling with microwave radiation, and hence heating, can occur starting from room temperature. Size and morphology of the Ni and Fe powders can be seen in the below given SEM micrographs (Figure 3.2). Morphology of the Ni powders is irregular rounded, since the production method for Ni powders is water atomization. On the contrary, Fe powders have spherical geometry originating from the inert gas atomization process.

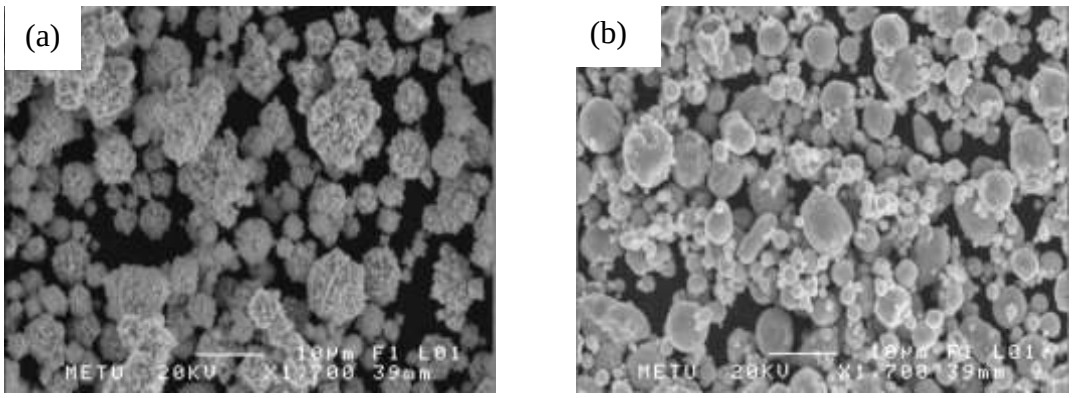

Figure 3.2. SEM micrographs of the elemental Ni (a) and Fe (b) powders used in the study.

3.2. Powder Compaction Stage

For soft magnetic permalloy compacts, elemental Ni and Fe powders were weighed to obtain 4:1 (weight percent) Ni to Fe ratio and hand mixed in porcelain mortar in isopropyl alcohol to obtain a homogenous mixture which were subsequently taken to the compaction stage. Austenitic stainless steel samples were directly taken to the compaction stage after weighing, where no premixing was necessary as the powders were already prealloyed and had the desired composition.

3.2.1. Double-Action Uniaxial Compaction

To study the effect of varying green density on the densification response of the sintered samples, varying double-action uniaxial (Uni) compaction pressures were utilized for the permalloy compacts, which were 50, 100 and 150 MPa. In addition to these, to maximize the green density an alternative compaction procedure composed of double-action uniaxial pressing under 200 MPa followed by cold isostatic pressing under 150 MPa of pressure was also applied. In order to observe the effect of altering compaction method and/or pressure on the green density, weight and dimensions of the green compacts were measured, and green densities of the compacts were determined. Corresponding green densities calculated relative to the theoretical density of bulk permalloy, which is 8.7 g/cm^3 (%TD) with respect to varying compaction pressure and method is given in Table 3.2.

Table 3.2. Applied compaction pressures and methods with corresponding green densities used in the study.

Compaction Pressure	Green Density (%TD)
Uni 50MPa	56%
Uni 100MPa	65%
Uni 150MPa	73%
CIP 150 MPa	65%
Uni 200 MPa + CIP 150 MPa	78%

The sample dimensions obtained via these compaction pressures are given in Figure 3.3.

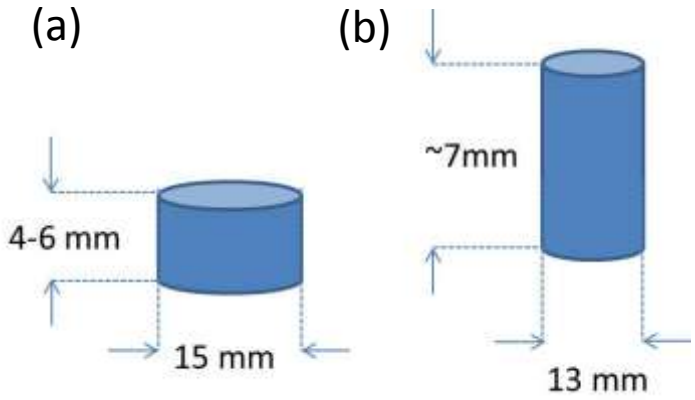

Figure 3.3. Sample dimensions of the samples (a) double action unidirectionally compacted (b) cold isostatically pressed

To study the effect of microwave and conventional sintering on the diffusion behavior of the powder metallurgical compacts in a comparative manner, diffusion couples were prepared from elemental Ni and Fe powders. Initially, 2 grams of Fe powder was pressed uniaxially under 10 MPa of pressure to provide a smooth Fe-Ni interface. Subsequently, Ni powder of the same amount was added into the die, and the Fe-Ni diffusion couple was subjected to 100 MPa of pressure via double-action uniaxial pressing (Figure 3.4). The compaction pressure resulting in the optimized densification response was chosen to compare the effect of microwave and conventional sintering methods on the diffusion behavior of the constituent elements in the studied alloy system. Electron probe microanalysis is done on perpendicular cross sections to the interface to obtain the composition profiles.

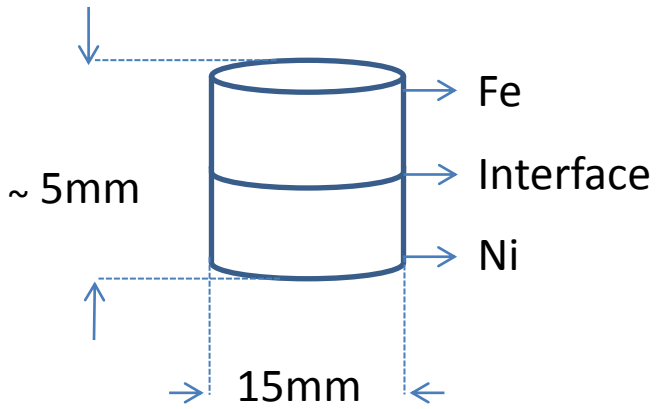

Figure 3.4. Schematic illustration of Fe-Ni diffusion couples.

Stainless steel compacts were consolidated by double-action uniaxial pressing applying 200 MPa of pressure, and the green pellets had relative green densities of approximately 75% that of the theoretical density of the stainless steel alloy.

3.2.2. Cold Isostatic Pressing (CIPing)

Premixed permalloy powders and as-received stainless steel powders were also shaped directly by cold isostatic pressing (CIPing) under 150 MPa of pressure in elastomeric molds. Several elastomeric molds of varying hardness were tried to provide optimum pressure transfer from the compaction fluid to the sample. It was determined that silicone elastomers of hardness 40 Shore A show the optimum performance. Since the elastomeric molds are not as rigid as steel dies used in uniaxial pressing, the aspect ratio of the samples shaped by CIPing differed from that of the pellets compacted via uniaxial pressing, although the inner diameters of the elastomeric mold and steel die were identical. Cold isostatically pressed (CIPed) compacts attained a rod-like geometry, since they underwent lateral contraction more extensively, while uniaxially pressed compacts had a disc-like shape with a lower height to diameter ratio.

Figure 3.5. Representation of the cold isostatic press used in the study.

3.3. Sintering Stage

Microwave and conventional sintering experiments were conducted for both prealloyed austenitic stainless steel and premixed permalloy compacts. The soaking time at the desired sintering temperature was kept constant at 45 minutes, and no protective sintering atmosphere was used during heating cycles. Although both

stainless steels and permalloys can resist to high temperature oxidation considerably, it would have been preferable to use protective atmospheres such as vacuum or Argon in order to prevent any probable oxidation and to achieve “cleaner” grain boundaries and microstructures. However, due to inevitable complications taking place between the candidate sintering atmospheres and the high electric field component of the microwave energy introduced into the microwave sintering cavity; utilization of atmospheric air as sintering atmosphere had been compulsory owing to its high dielectric breakdown strength and ability to withstand high voltages. Sintering experiments for permalloys were carried out at 1200, 1225, 1250, 1275 and 1300 °C via both microwave and conventional sintering routes.

Technical details of the microwave sintering equipment (MKH 4.8, Linn High Therm GmbH, Eschenfelden, Germany) used in this study are given in Figure 3.6. Maximum available microwave power is 4.8 kW supplied by 6 magnetrons each of which is capable of delivering 0.8 kW of power to the heating cavity of net dimensions 135 by 135 by 135 mm. Due to the rapid and volumetric nature of microwave sintering, direct heating of the sample can be achieved and heating rate can be kept constant at 30 °C/min by manually adjusting the microwave power. During microwave sintering experiments, temperature of the specimens are measured using optical pyrometer, since incorporation of thermocouples into the microwave cavity requires additional shielding precautions to prevent microwave leakage as well as arcing on the thermocouple surface.

Figure 3.6. Microwave heating furnace used in the study.

Since direct heating arises from the interaction between microwave energy and powdered compact, heat is lost to the surroundings from the surface of the sample. Therefore, a custom-built special sintering setup, insulation cage, composed Al_2O_3 insulation materials and crucibles was used for the microwave sintering experiments to minimize heat losses from the sample surface and maximize heating uniformity (Figure 3.7). SiC powder was incorporated into the microwave sintering setup as susceptor material to provide preheating and to protect the microwave furnace from standing wave damage.

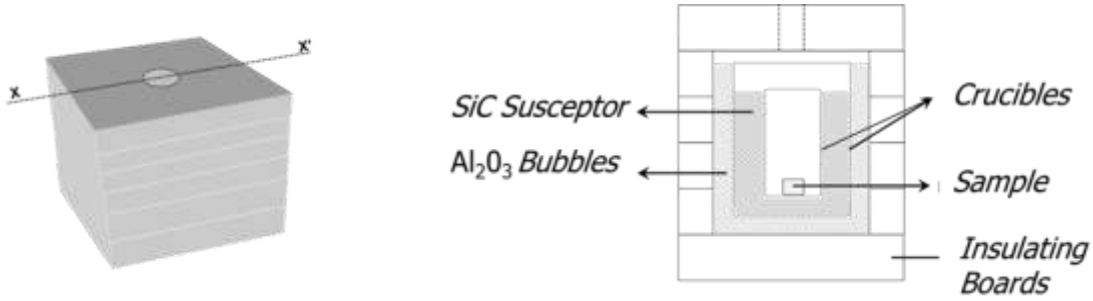

Figure 3.7. Microwave sintering setup

For conventional heating experiments a muffle type furnace was used, where no additional sintering setup was necessary, since heat is delivered to the sample surface from the heating elements via radiation and convection. Heating rates associated with conventional sintering experiments were also set to 30 °C/min on the temperature controller unit of the furnace; however, in reality such high heating rates cannot be achieved in conventional furnaces due to the indirect and ineffective way of heat transfer.

3.4. Characterization of Microwave and Conventionally Sintered Compacts

Both microwave and conventionally sintered compacts were characterized in terms of their densification and microstructural evolution as well as mechanical and soft magnetic properties.

3.4.1. Characterization of Densification Response

To determine the densification response of microwave and conventionally sintered compacts with respect to varying sintering temperatures and compaction pressures, surfaces of the sintered compacts were initially ground by 120 grit SiC abrasive paper to remove all surface oxides and artifacts. Subsequently, the samples were vacuum impregnated in xylene for two hours to make sure that all open pores were filled with xylene. After vacuum impregnation, samples were kept in xylene for 24 hours to fix the presence of xylene in the pores, and then the sintered densities of the compacts were determined via Archimedes' method and calculated using Equation 3.1:

$$\rho_{sint} = \frac{0{,}86 * M_{dry}}{M_{sat} - M_{sus}} \qquad 3.1$$

where ρ_{sint} is the sintered density, 0.86 is the density of xylene, M_{dry} is the dry weight of the ground sample, M_{sat} is the weight of the xylene impregnated sample and M_{sus} is the weight of the sample suspended in xylene. Following the measurement of sintered densities, the densification response was determined in terms of relative densification (%TD) by normalizing the sintered density with the theoretical density of the alloy under consideration.

3.4.2. Characterization of Microstructural Evolution

After measuring the sintered densities of the compacts, the samples were sectioned and their surfaces were prepared by standard metallographic specimen preparation methods for optical and scanning electron microscopy analyses. Since both austenitic stainless steels and permalloys are known for their low hardness values, coarse grinding procedures and prolonged specimen preparation durations, which may cause mechanical damage in depth, were avoided. Samples were ground starting with 15 μm polycrystalline diamond paste and were polished consecutively with 9, 3 and 1 μm polycrystalline diamond suspensions. Due to the low hardness of the samples, smearing and closing of the pores were encountered as a result of extensive plastic

deformation introduced during specimen preparation. To get rid of the deformed layer and to provide full opening of the pores, the samples were immersed in the appropriate etchants of each alloy for 1 minute before the final 1 μm diamond polishing step. Etching-repolishing cycle was repeated twice to ensure accurate revealing of the original microstructure.

Microstructures of the as-polished samples were examined using SEM to investigate pore morphologies. For grain size measurements, optical microscopy images of the etched surfaces were taken. For each sample, grain size measurement was conducted using linear intercept method on at least five representative micrographs, and average of thes"e measurements was reported. Compositions of the etchants used for the austenitic stainless steel and the permalloys are given in Table 3.2. At this point, it is worth noting that etching of the permalloys is complicated owing to the good corrosion resistance of these alloys originating from their high Ni content. Furthermore, etchants used should be fresh and prepared shortly before the etching step, since the grain boundary attack is mainly achieved via the oxidizing activity of the H_2O_2, and this compound can quickly lose its activity due to the high fugacity of 0_2.

Table 3.3. Compositions of the etchants used for austenitic stainless steel and permalloy powder metallurgical compacts.

Marble's Reagent (For Austenitic Stainless Steels)	$CuSO_4.5H_2O$ (saturated) 50 ml Ethyl Alcohol 50 ml distillated water
Permalloy Etchant	25 ml H_2O_2 25 ml distillated water 5 ml HF

3.4.3. Mechanical Characterization

Mechanical properties of microwave and conventionally sintered austenitic stainless steel and permalloy compacts were determined and compared based on Vickers

microhardness measurements. Since microhardness measurements are more precise and sensitive to surface condition, the samples have undergone further final polishing steps down to 0.05 μm colloidal silica to remove any residual surface stress that may originate from the metallographic surface preparation steps, and the surfaces were subsequently etched to reveal the grain boundaries. Microindentation load of 10 gf was applied for 10 seconds by ensuring that the tested area is free of pores, so that the mechanical property of the bulk metal can be determined. At least 5 different measurements were taken from pore free locations in the grain interiors and obtained values were averaged.

3.4.5. Characterization of Magnetic Properties

B-H curves of the samples were obtained via vibrating sample magnetometer (VSM) (EasyVSM 9, ADE Electronics, WI, USA) at external magnetic field values between -20000 and 20000 Oersteds applied with a step size of 2000 Oe/min, where applied external magnetic fields were changing between $\mp 0{,}5\ T$. VSM measurements were conducted on the samples that were compacted via double-action uniaxial pressing under various compaction pressures, and on the samples directly shaped by cold isostatic pressing. Consequently, differential permeability, hysteresis loss and saturation magnetization values of these samples were determined for various processing parameters applied.

3.5. Flowchart of the Experimental Procedure

The outline of the experimental procedure followed in this study for the processing of permalloy compacts is summarized in Figure 3.8. The procedure is identical for the stainless steel compacts except for the initial powder handling steps. Same procedure has been applied in the conventional sintering experiments for both stainless steel and permalloy samples.

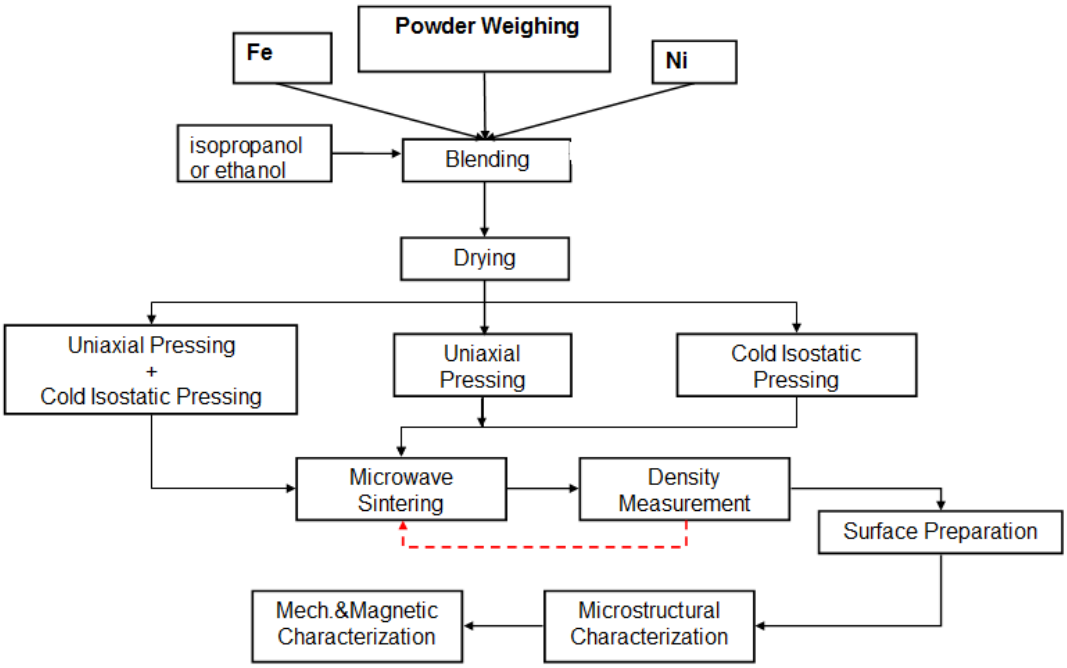

Figure 3.8. Experimental procedure flowchart of this study.

CHAPTER 4

RESULTS AND DISCUSSION

4.1. Microwave Sintering of 316L Stainless Steels

4.1.1. Densification Response with respect to Sintering Temperature

Upon examination of the relative densification (%TD) versus sintering temperature graphs (Figure 4.1) of the 316L austenitic stainless steel compacts, it can be said that the microwave sintered powder metallurgical (P/M) austenitic stainless steels attain higher densification values than their conventionally treated counterparts at sintering temperatures of 1150, 1200, 1225 °C. Here relative densification is determined as the ratio of the measured sintered density of a compact to the theoretical density of 316L austenitic stainless steel, which is 7.99 g/cm^3. As it can be noted from Figure 4.1, densification versus sintering temperature graphs of both samples follow roughly the same slope implying a similar temperature dependence of sintering behavior for both microwave and conventionally sintered compacts. Although the temperature dependence, and consequently, the densification mechanism during sintering stage appears to be similar for both sintering routes, differences in the final densification values are thought to be arising from the different heating rates employed via two sintering processes. During microwave sintering high heating rates exceeding 30 °C/min can be reached, where direct and volumetric heating of the compact is possible resulting in shorter heating durations to the sintering temperatures on the order of tens of minutes. In contrast, in the case of conventional heating heat is delivered from the heating elements to the whole furnace cavity, and the overall heating time to the sintering temperature is on the order of hours. Owing to the faster heating rates and processing cycles associated with microwave sintering, particle

coarsening and pore coalescence can be suppressed, which in turn provides refined microstructures with more available interparticle contacts and grain boundaries. Increased surface and contact area enhances diffusion, and hence final density of the compacts produced via microwave sintering route (Table 4.1)

Table 4.1. Sintering temperature versus final density values of microwave sintered (M) and conventionally sintered (C) samples.

Sintering Temperature (^{0}C)	Density (g/cm^3)	
1150	6.58 (M)	6.39 (C)
1200	6.73 (M)	6.50 (C)
1225	6.83 (M)	6.60 (C)

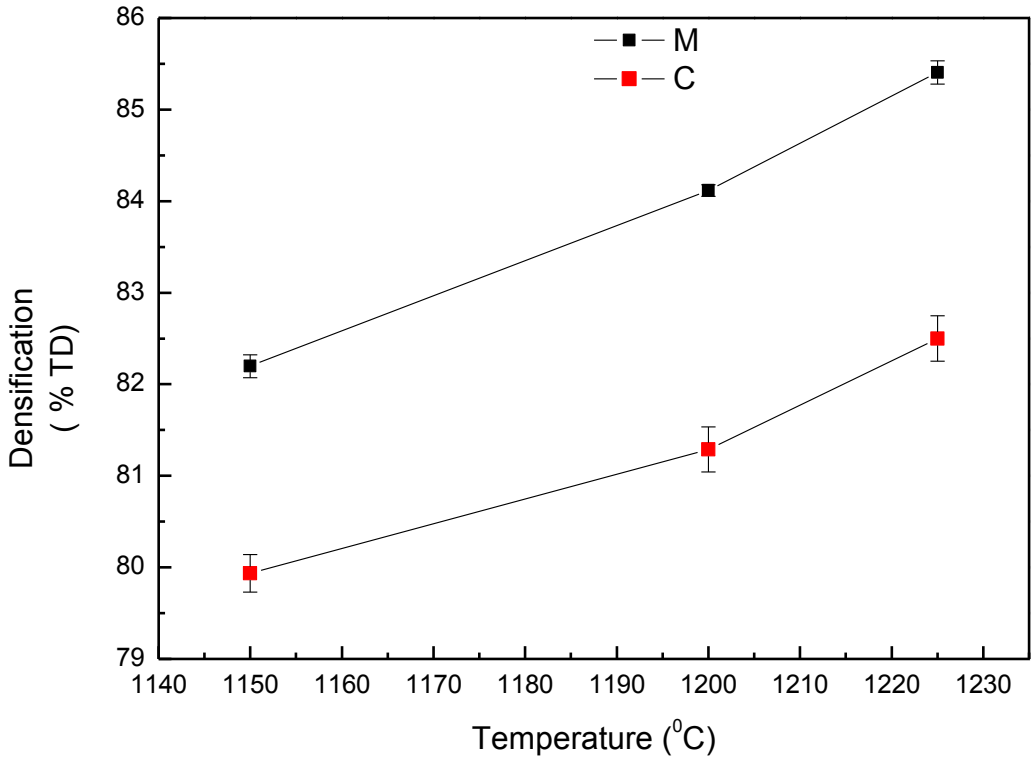

Figure 4.1. Densification versus sintering temperature values of the double-action pressed and microwave (M) and conventionally (C) sintered samples.

The sintering behavior of cold isostatically pressed (CIPed) samples with changing sintering temperature differs from that of the uniaxially compacted samples (Figure

4.2.). Optimum sintering condition seems to be achieved at temperature 1150 ^{0}C for both microwave and conventionally sintered samples. Sintered densities of the samples decrease at increasing sintering temperatures (Table 4.2.), which might be caused by pronounced oxidation at higher temperatures hindering inter-particle diffusion. This situation is thought to be related to the lower green densities of the CIPed samples compared to those of the uniaxially compacted ones. In addition to this, increased amount of porosity in the green compacts has adverse effects on sintered density with increasing temperature owing to the pronounced pore coalescence and pore growth at elevated temperatures. Furthermore, the fact that the densification values achieved in CIPed samples are lower compared to uniaxially pressed samples at the same sintering temperatures is also a consequence of the lower green density of the CIPed green compacts.

Table 4.2. Sintered density of the cold isostatically compressed samples after microwave (M) and conventional (C) sintering at different temperatures.

Sintering Temperature(^{0}C)	Density (g/cm^{3})	
1150	6.06 (M)	5.68 (C)
1200	5.97 (M)	5.60 (C)
1225	6.02 (M)	5.62 (C)

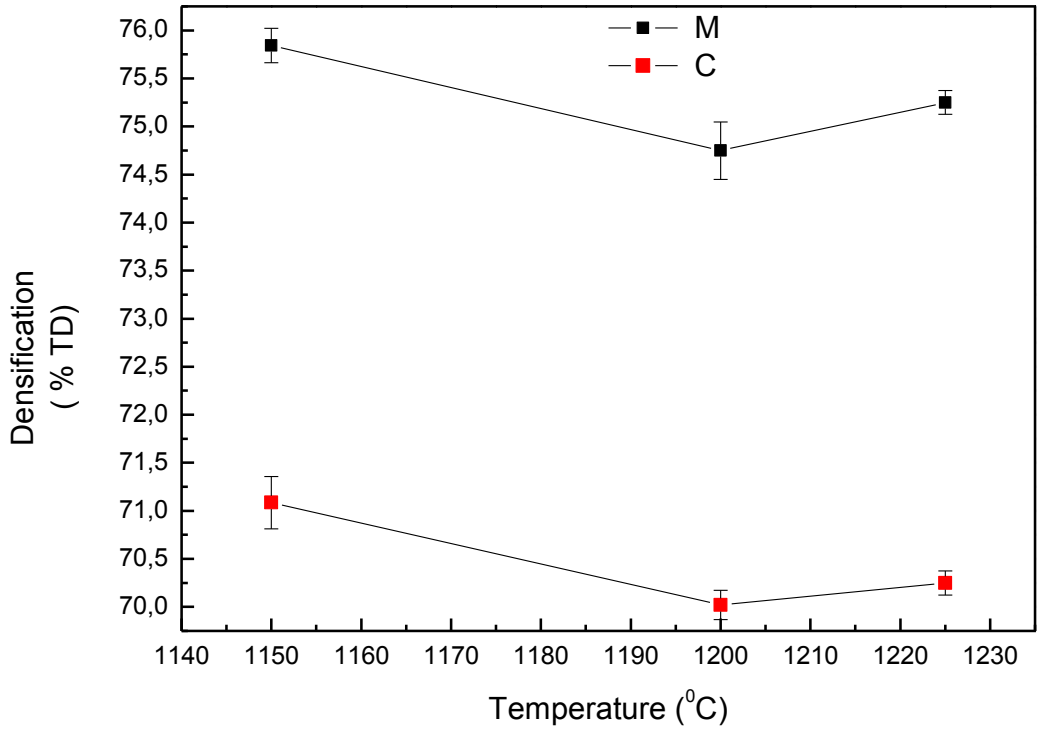

Figure 4.2. Densification versus sintering temperature of the cold isostatically pressed samples after microwave (M) and conventional (C) sintering.

4.1.2. Microstructural Evolution in Stainless Steel Compacts by Sintering

Microstructural examination under SEM revealed that microwave sintered samples have lower amount of porosities along with pore rounding compared to their conventional counterparts at all sintering temperatures and compaction pressures (Figures 4.3 a-f and 4.4 a-d).

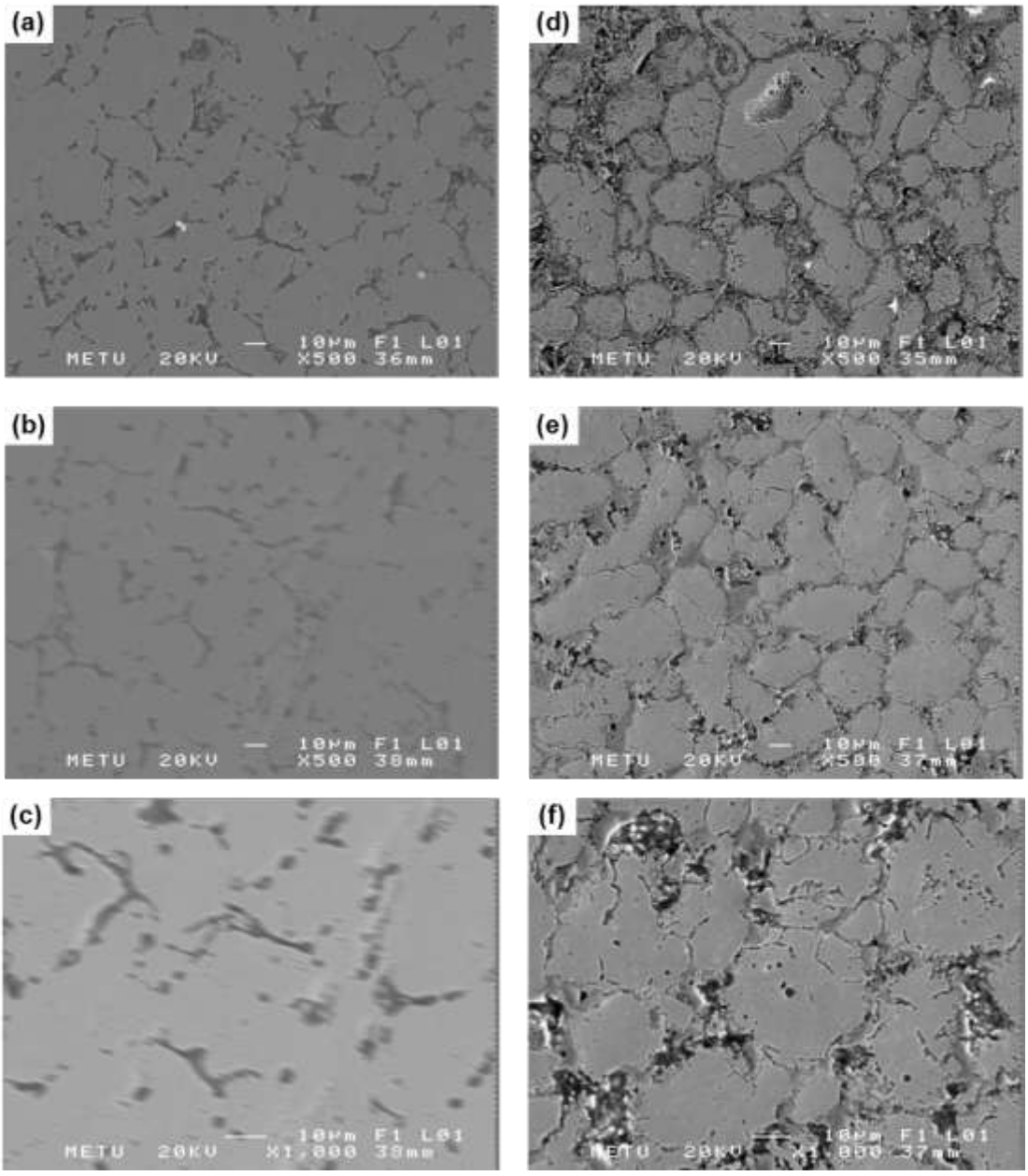

Figure 4.3.SEM micrographs of samples compacted via double-action pressing under 200 MPa of pressure; microwave sintered at 1150 (a), 1200 (b) and 1225 ^{0}C (c); Figure conventionally sintered at 1150 (d), 1200 (e) and 1225 ^{0}C (f).

Annealing twins, which are sign of good quality sintering were present in the samples with optimized densities in the case of microwave sintering, which were absent in the samples produced via conventional route at any sintering condition. In addition to improved densification and pore morphologies, presence of annealing twins implies that superior sintering of the samples with microwave energy can be achieved even at lower temperatures (Figure 4.5).

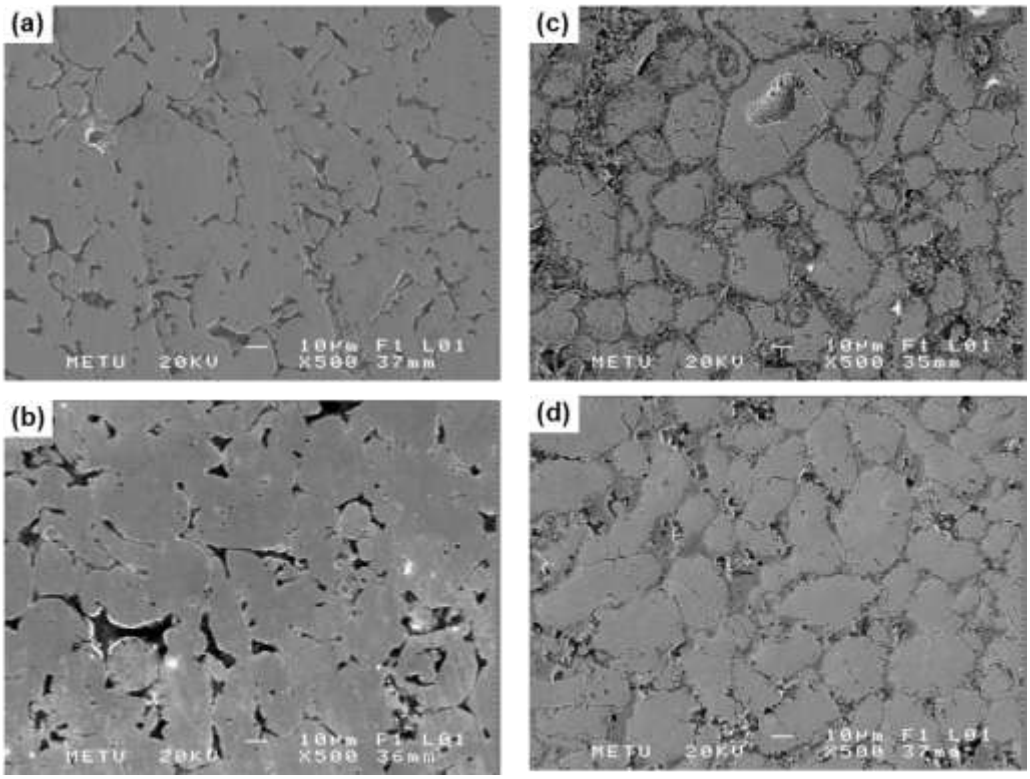

Figure 4.4. SEM micrographs of samples compacted via cold isostatic pressing under 150 MPa of pressure and microwave sintered at 1150 (a), 1200 ^{0}C (b) Figure and conventionally sintered at 1150 (c), 1200 ^{0}C (d)

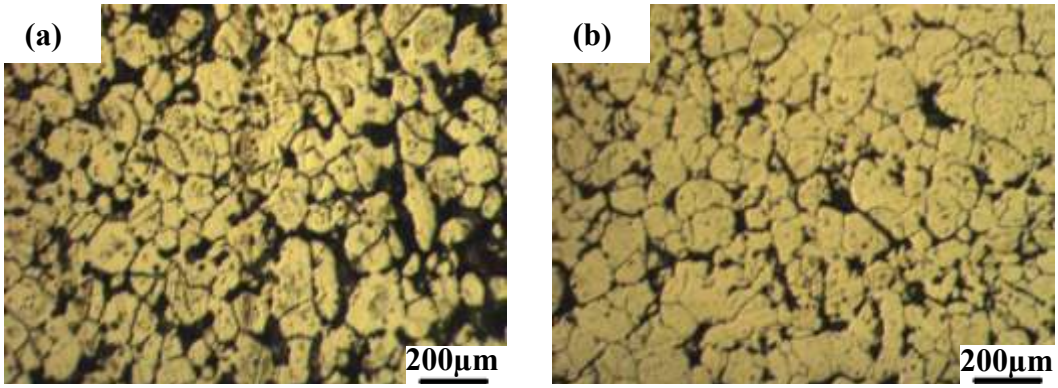

Figure 4.5. Representativeoptical micrographs of the samples compacted via cold isostatic pressing under 1500 bars of pressure and microwave (a) and conventionally (b) sintered at 1225^0C.

For grain size measurement, optical microscopy images have been employed to get a good statistical distribution and representative values for each sintered sample. For both sintering techniques, the increase in the sintering temperature resulted in microstructural coarsening and grain growth. Both increased amount of particle contacts and enhanced diffusion rates at elevated temperatures are thought to contribute to this outcome in the case of double-action pressed compacts. One other point worth considering is that microwave sintered samples attain smaller grain sizes as compared to the conventionally sintered ones and exhibit decreased amount of porosity (Table 4.3.)

Table 4.3. Average grain sizes of the austenitic stainless steel samples compacted via cold isostatic pressing (CIP) and uniaxial double action (UNI) and microwave (MW) and conventionally (C) sintered at 1150, 1200, 1225^{0}C

Sintering Temperature (^{0}C)	1150	1200	1225
Compaction Route	Average Grain Size (μ)		
CIP	20± 3(MW)	35 ±4 (MW)	40 ± 5(MW)
	30 ± 5(C)	45 ± 3(C)	50 ±4 (C)
UNI	20 ± 4(MW)	25 ±4 (MW)	30 ± 5(MW)
	27 ± 5(C)	35 ± 5(C)	42 ± 5(C)

4.1.3. Mechanical Characterization

Microhardness measurements were utilized to characterize the mechanical properties of microwave and conventionally sintered stainless steel P/M compacts. Microhardness vs. sintering temperature data of the samples compacted via double-action pressing under 200 MPa of pressure (Figure 4.6) show that microwave sintered samples attain higher microhardness values than the conventionally sintered samples under identical conditions. This result is expected, since sintered density and residual porosity are key parameters determining final properties of the powder metallurgical parts. Higher final densities of the microwave sintered samples result in improved mechanical properties compared to the conventionally sintered samples.

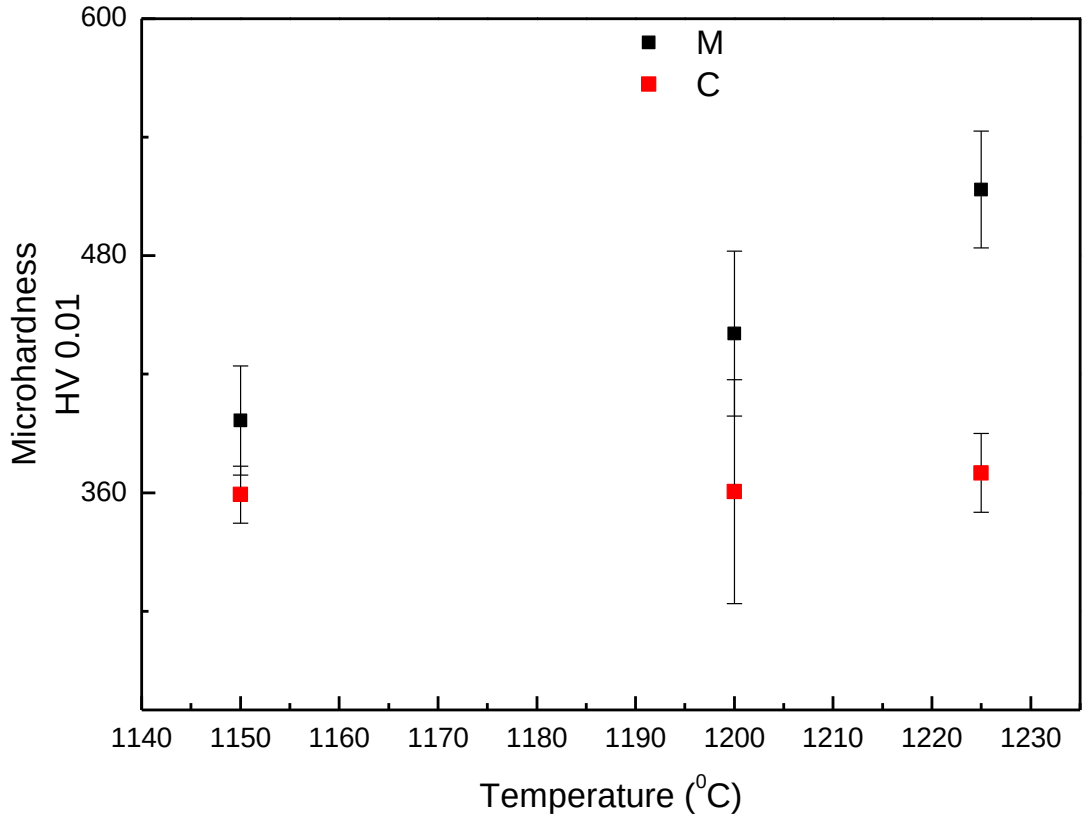

Figure 4.6. Microhardness versus sintering temperature graph of the samples uniaxially compacted via double-action pressing under 200 MPa of pressure and sintered at 1150, 1200, 1225 ^{0}C by both techniques.

Similarly, microhardness versus sintering temperature data of the cold isostatically pressed samples followed a similar behavior to their densification response (Figure 4.7). From Figure 4.7 it is clear that microhardness values are optimized at 1150^{0}C as in the case of the sintered density values. Due to lower green densities achieved by cold isostatic pressing resulting in microstructural coarsening and pore coalescence phenomena associated with the decrease in the final densities, corresponding microhardness values are lower at higher sintering temperatures.

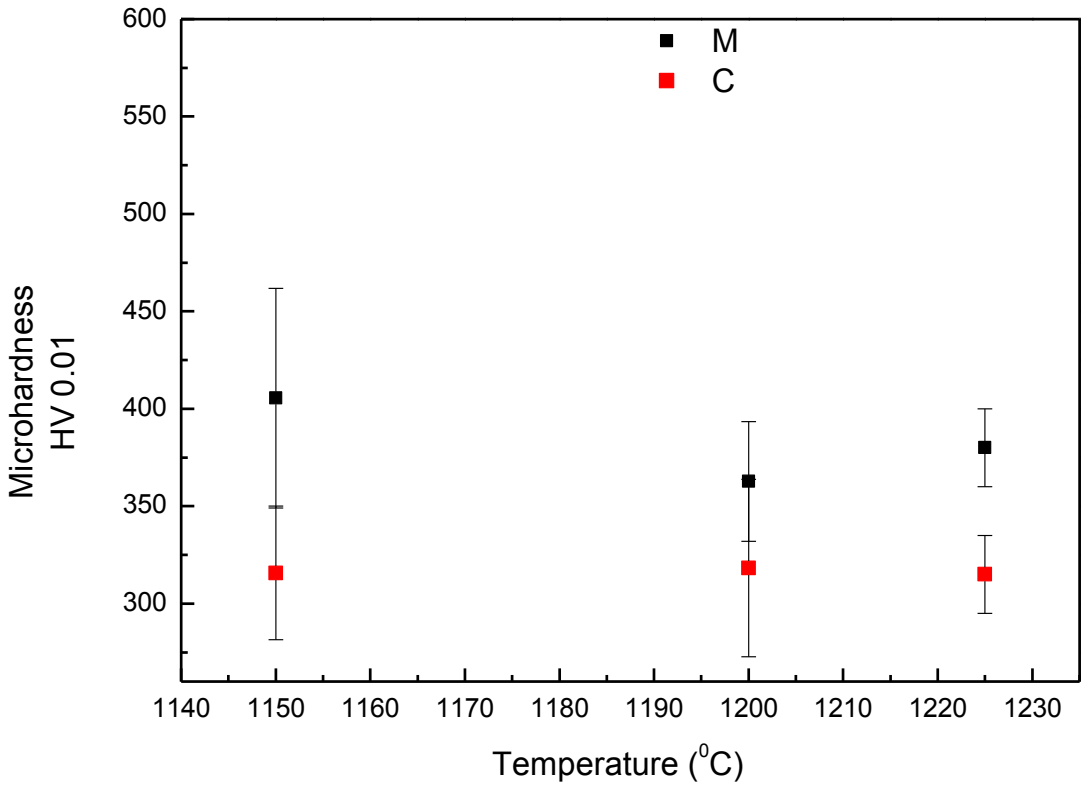

Figure 4.7. Microhardness versus sintering temperature data of compacts cold isostatically pressed under 150 MPa of pressure after microwave (M) and conventional (C) sintering at 1150, 1200 and 1225 °C.

4.2. Microwave and Conventional Sintering of Premixed Permalloys

In this section, densification response, microstructural evolution along with mechanical and magnetic properties of the Ni-Fe alloy of 4:1 (wt%) composition compacted by various techniques under various pressures and then sintered at different temperatures by both microwave and conventional sintering methods will be discussed. The effect of several sintering parameters on the engineering properties of the powder metallurgical permalloy compacts will be discussed in a comparative manner to enlighten the differences and similarities between microwave and conventional sintering routes in a detailed manner.

4.2.1. Densification Response of the Microwave and Conventional Sintered Permalloys compacted via 2-D Uniaxial Pressing

From Table 4.4; it can be seen that the densification response of microwave sintered samples with varying sintering parameters differs from that of the conventionally

sintered samples. To begin with, in most of the samples it is observed that microwave sintering is advantageous in the sense it results in higher sintered densities compared to conventional sintering for the same soaking times and compaction pressures. Furthermore, microwave sintering provides higher heating rates and shorter processing cycles. From the densification behavior of the microwave sintered samples, it seems that faster heating rates and processing cycles not only results in improved process efficiency along with time and energy savings but also enhanced densification. Faster rates of microwave heating result in shorter time intervals that the samples dwell at elevated temperatures till they reach to the sintering temperature leading to microstructural refinement. This microstructural refinement, leaves larger surface area providing easier paths for the atoms to diffuse through. Consequently, with the aid of the enhanced diffusion, densification response of the microwave sintered samples precedes that of their conventional counterparts.

Table 4.4. Densification response of the microwave (M) and conventionally (C) sintered samples for varying uniaxial compaction pressures at 3 different sintering temperatures**.**

Sintering Temperature		Densification (%TD)							
		1200 ^{0}C		1225 ^{0}C		1250 ^{0}C		1275 ^{0}C	
Compaction Pressure (MPa)	Green Density (%TD)	M	C	M	C	M	C	M	C
50	56	83.0	80.0	85.5	81.0	88.0	83.5	89.3	84.3
100	65	85.6	83.3	87.0	85.0	88.8	86.5	90.1	87.7
150	73	84.5	84.8	85.8	86.0	88.3	87.5	89.5	88.9

In the case of the conventionally sintered samples, sintered density increases continuously with both increasing sintering temperature and green density, which is expected and in good agreement with the conventional sintering theories. In contrast, final density of the microwave sintered samples increases with increasing compaction pressure, and hence green density, up to a certain level after which it starts to decline. The optimization behavior related to the compaction pressures and green densities associated with the microwave sintering route is thought to be arising

from the unique mechanism of the heat generation within the powdered compacts. During microwave sintering electromagnetic waves penetrate to the sample body, and as the microwaves propagate through the sample, the waves are attenuated where electromagnetic energy is absorbed and converted to heat. Since sintering and consequent densification relies on the heat generated within the body, the penetration and interaction of microwaves within the sample is essential. The decrease in the sintered densities with increasing compaction pressure implies that the efficiency of penetration and absorption of the microwave radiation in the compact decreases beyond a certain green density. This is understandable in the sense that the conductivity of the green compacts increases with increasing compaction pressure due to enhanced inter-particle contacts and necks, therefore, the penetration depth of the microwaves decreases and incident electromagnetic radiation is reflected from the external surface of the compact due to this shielding effect. Consequently, a balance between efficient interaction and green density exists, which results in an optimized sintered density by microwave heating. From Figure 4.3, it is seen that the optimum compaction pressure is 100 MPa for the present permalloy composition. At the compaction pressure of 150 MPa, conventionally sintered samples attain slightly higher densities than the microwave sintered ones particularly at lower sintering temperatures, at which grain growth and microstructural coarsening does not have a pronounced negative effect on densification.

In addition to this, temperature dependence of the sintered densities of microwave sintered samples differs from that of the conventionally sintered samples (Figure 4.8). The sintered densities of microwave sintered samples rise more steeply with increasing sintering temperature. The difference in the slopes of densification vs. sintering temperature graphs obtained by microwave and conventional sintering processes may arise from a change in the activation energies required for diffusion in two processes implying that different mechanisms of diffusion are active in the two processes. Alternatively, increased interfacial area for easy diffusion of atoms associated with rapid and volumetric nature of microwave sintering can lead to accelerated densification behavior with respect to sintering temperature. The discussion whether the diffusion mechanisms are altered with the sintering method

applied is done in the succeeding sections related to composition profile of the diffusion couples produced from elemental Ni and Fe powders.

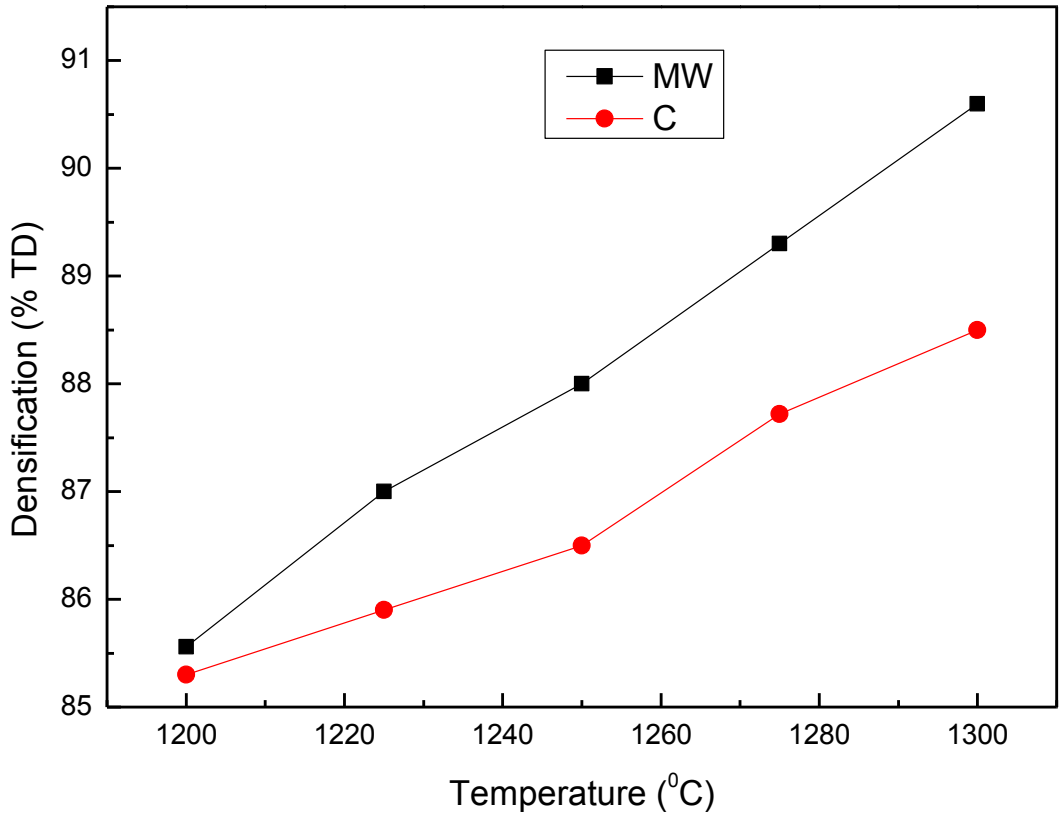

Figure 4.8. Densification versus sintering temperature graphs of microwave (M) and conventionally (C) sintered samples.

4.2.2. Microstructural Evolution of Double-Action Uniaxially Compacted Samples

From the optical microscope microstructural examinations of the sintered permalloy compacts given in Figures 4.9, 4.10 and 4.11 for varying uniaxial compaction pressures and sintering temperatures, it can be seen that porosity is the least for 100 MPa pressure for all sintering temperatures. The tone difference in the color observed in the optical micrographs has been mainly caused by the varying effect of the etching process. Especially in the case of lower compaction pressures, the advantage of microwave sintering is pronounced with significant elimination of porosity as compared to conventional sintering. The difference between microwave and conventionally sintered samples compacted at 50 MPa may originate from a

weaker dependence of densification response on green density in the case of microwave heating due to the accelerated sintering kinetics by microstructural refinement. Moreover, the difference may also result from the shorter exposure times of the samples to oxidation during faster sintering cycle in microwave sintering route. Owing to the high amount of porosity in the green state at lower compaction pressures, the oxidation of grain boundaries is especially enhanced for conventional sintering where oxide layers present at boundaries restricting particle necking and densification at 50 MPa (Figure 4.9 a-f, Figure 4-10 a-f, Figure 4-11 a-f, 4-12 a-b).

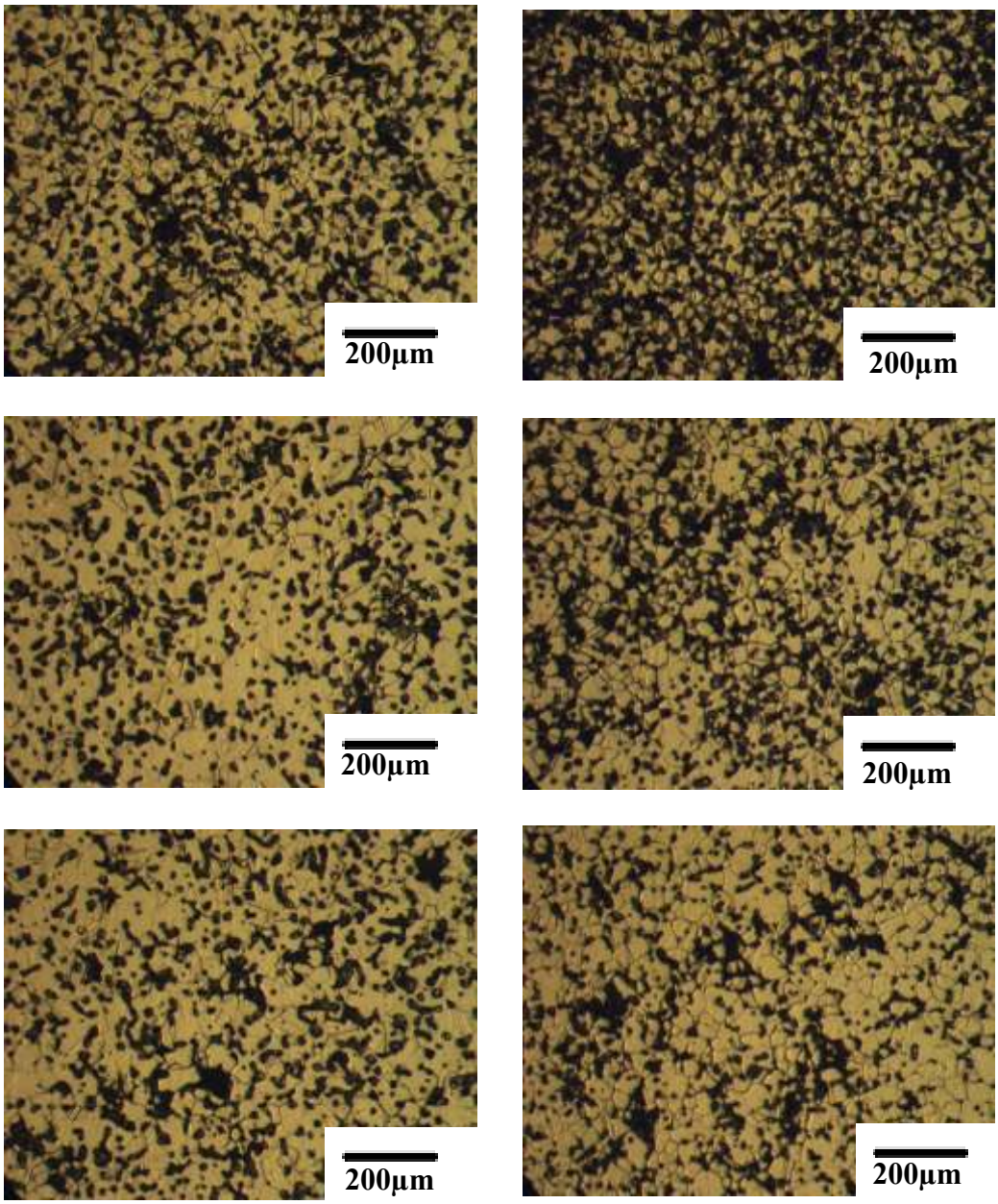

Figure 4.9. Optical micrographs of the samples compacted via double-action uniaxial pressing under 50 (a), 100 (c) and 150 (e) MPa of pressure and microwave sintered at 1200 °C along with optical micrographs of the samples compacted via double-action uniaxial pressing under 50 (b), 100 (d) and 150 (f) MPa of pressure and conventionally sintered at 1200 °C.

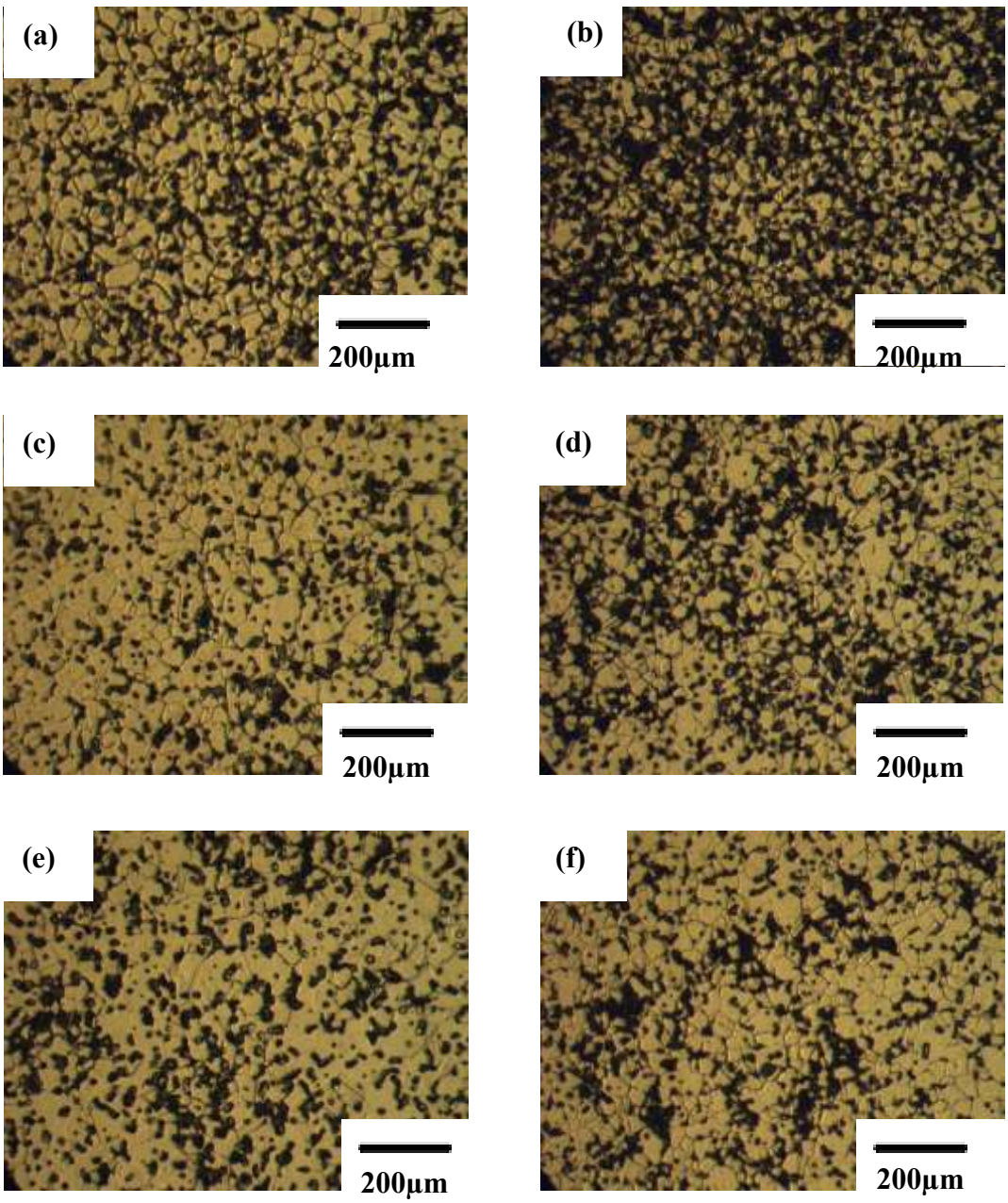

Figure 4.10. Optical micrographs of the samples compacted via double-action uniaxial pressing under 50 (a), 100 (c) and 150 (e) MPa of pressure and microwave sintered at 1225 °C along with optical micrographs of the samples compacted via double-action uniaxial pressing under 50 (b), 100 (d) and 150 (f) MPa of pressure and conventionally sintered at 1225 °C.

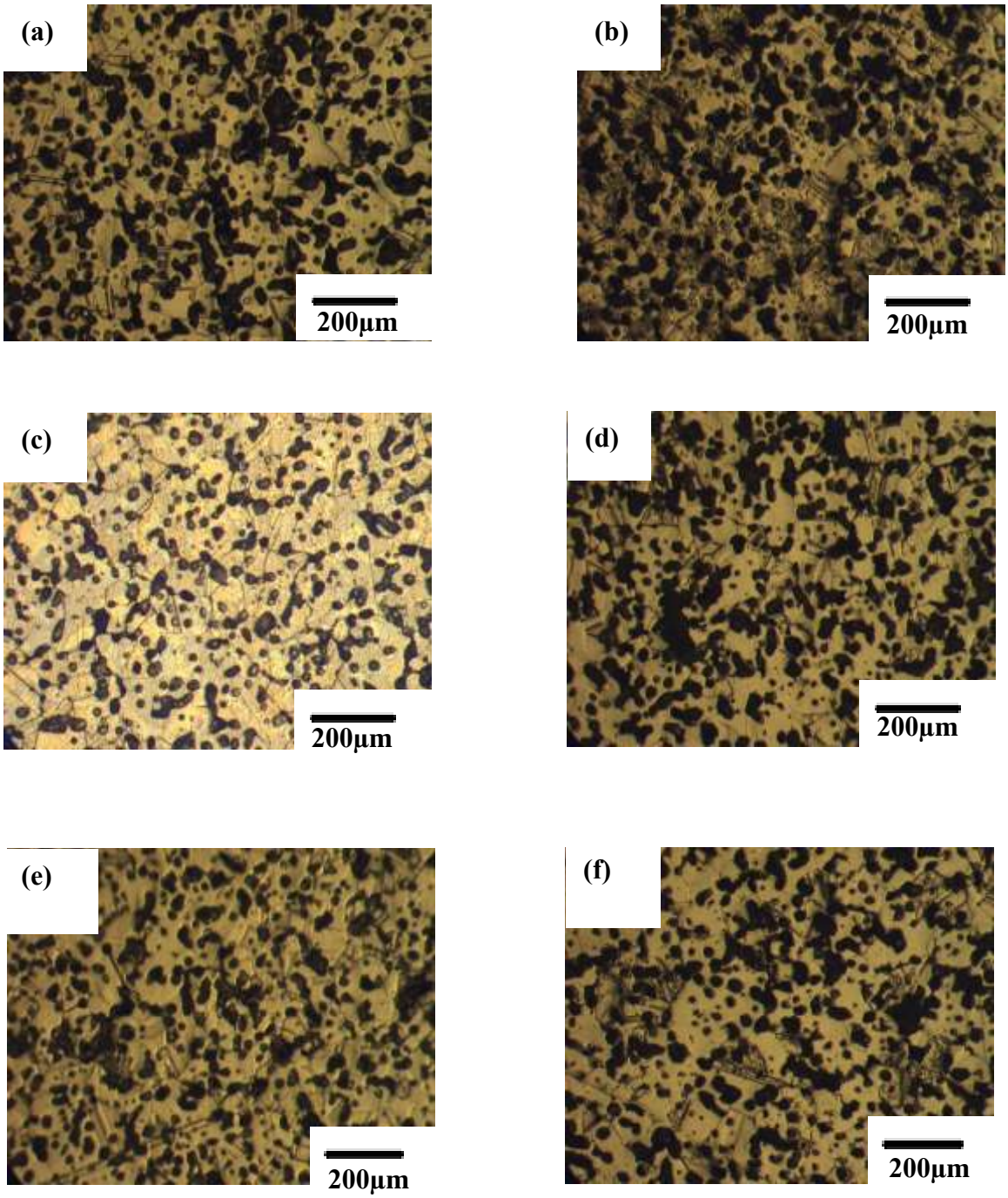

Figure 4.11. Optical micrographs of the samples compacted via double-action uniaxial pressing under 50 (a), 100 (c) and 150 (e) MPa of pressure and microwave sintered at 1250 °C along with optical micrographs of the samples compacted via double-action uniaxial pressing under 50 (b), 100 (d) and 150 (f) MPa of pressure and conventionally sintered at 1250 °C.

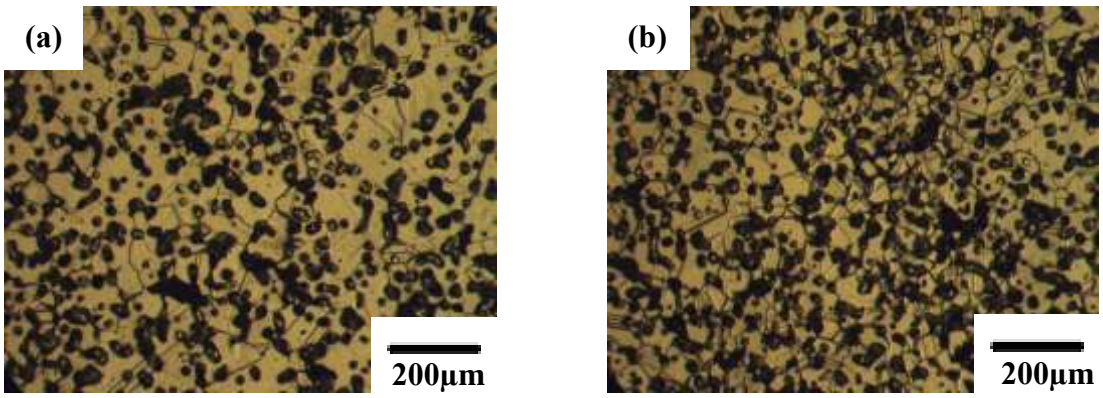

Figure 4.12. Optical micrographs of the samples compacted via double-action uniaxial pressing under 100 MPa of pressure and then microwave (a) and conventionally (b) sintered at 1300 °C.

Microstructural evolution of samples uniaxially compacted under 150 MPa indicates that pore elimination via conventional sintering starts to be as effective as the microwave sintering route that can clearly be seen in Figure 4.12. This demonstrates improved sintering efficiency achieved by microwave heating with lower green densities due to effective interaction of the microwaves with the highly porous powdered compact. This effectiveness starts to diminish for higher green densities, which provide increased sintering efficiency for conventional heating especially at higher temperatures that is based on the presence of high amount of contact area between the particles available for faster atomic diffusion in the relatively denser green compact.

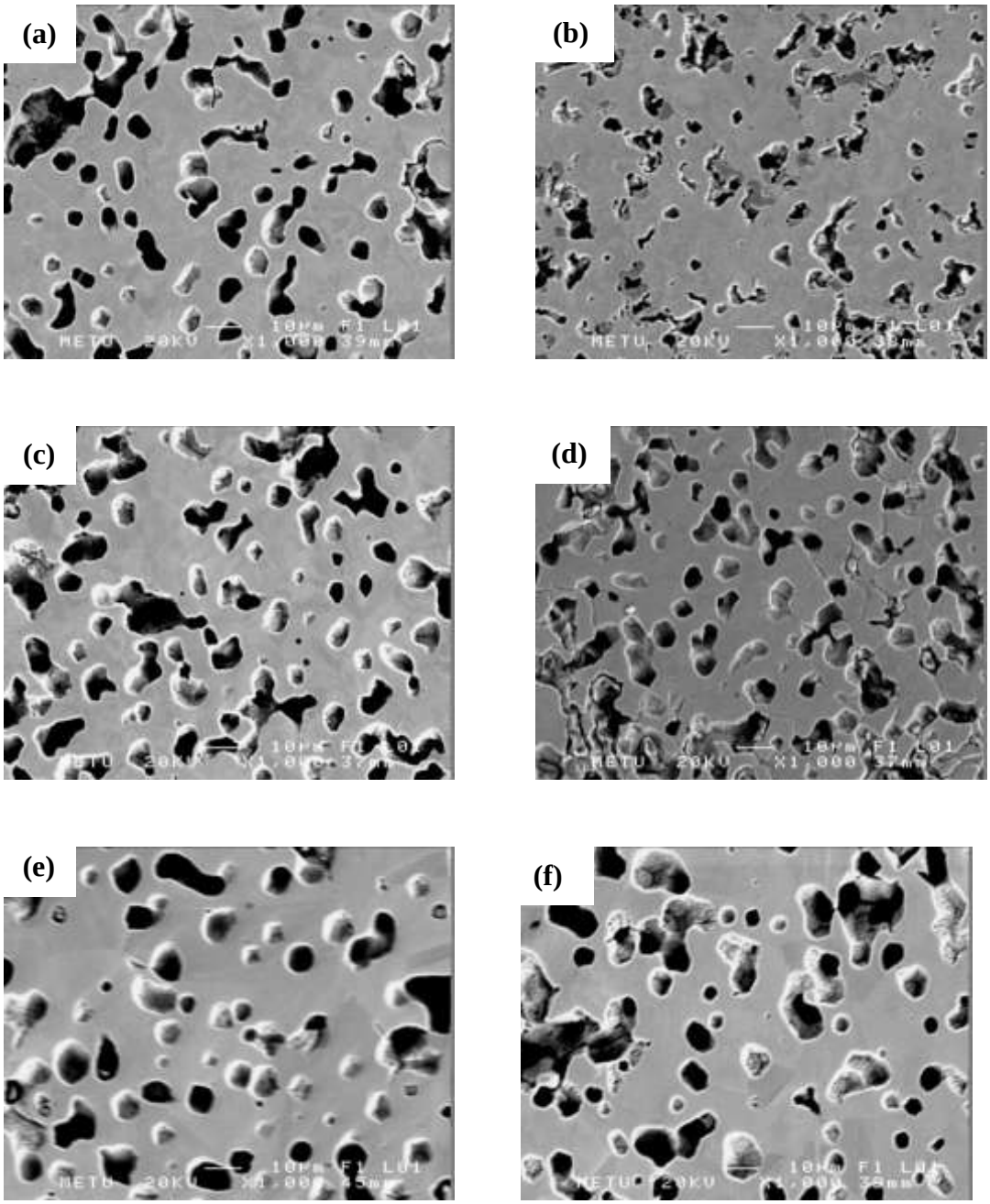

Figure 4.13. SEM micrographs of the samples compacted via double-action uniaxial pressing under 150 MPa pressure and microwave sintered at 1200 (a), 1225 (c) and 1275 (e) °C along with the SEM micrographs of the samples compacted via double-action uniaxial pressing under the same pressure and conventionally sintered at 1200 (b), 1225 (d) and 1275 (f) °C.

Average grain size values of the sintered compacts for varying green densities (compaction pressure) and sintering temperature are given in Table 4.5. From the presented data, it can be seen that the microstructural coarsening phenomenon

associated with the conventional sintering route is much pronounced as compared to microwave sintering route, in particular at higher sintering temperatures where rapid grain growth and pore coalescence occur. On the contrary, owing to the faster heating rates and decreased processing cycles obtained, microwave sintered samples are exposed to high temperatures for a shorter period of time, hindering grain growth, which is especially observed in the compacts with low green densities achieved by lower compaction pressures. The refined grain size and increased grain boundary area results in a higher number of pores surrounded by boundaries aiding atomic movement towards the pores, and consequently shrinkage and elimination of pores especially at relatively lower sintering temperatures can be achieved effectively.

In addition to its effect on the amount of porosity in the sintered compacts, microwave heating has a profound effect on the pore morphology as well. Examination of pore morphologies via SEM micrographs (Figure 4.13) revealed that elimination and rounding of pores via conventional sintering is retarded at sintering temperatures as high as 1275 °C whereas rounder and smoother pores can be obtained with microwave sintering starting from 1200 °C . However, the cylindrical shape of the pores imply that intermediate stage sintering is not complete and moved onto final stage.

Table 4.5. Average grain size values of microwave (M) and conventionally (C) sintered samples for varying sintering temperature and green density.

Temperature	1200 °C		1225 °C		1275 °C	
	Average Grain Size (μm)					
Green Density (%TD)	M	C	M	C	M	C
%56	55±4	49±5	63±3	57±3	79±4	89±9
%65	60±5	61±2	69±4	71±6	85±8	96±7
%71	62±3	63±3	69±2	66±6	85±8	96±7

4.2.3. Mechanical Characterization of Uniaxially Compacted Permalloys

Effect of microwave sintering compared to conventional sintering on the mechanical properties of unidirectionally compacted permalloy samples has been studied by microhardness measurements. For conventionally sintered samples, generally microhardness values increase with increasing green density (Figure 4.14). This is related to the direct increase in the sintered density with increasing green density in the case of conventional heating. In the case of microwave sintered samples; however, the microhardness values tend to get optimized around 65% green density (Figure 4.15). Similar to conventionally sintered samples, the maximum microhardness values of microwave sintered samples correspond to the maximum sintered densities, yet as it has already been discussed in Section 4.2.1., the sintered densities are maximized at 65% green density in microwave heating. Therefore, the microhardness values follow a similar trend with respect to the sintered and green densities.

Another important point to consider about the microhardness change is the relative decrease in the microhardness values at the sintering temperature of 1275 °C. Despite the increasing sintered density, microhardness values fail to improve for both microwave and conventionally sintered samples. However, the rate of decrease in microhardness values is much pronounced in the conventionally sintered samples as compared to microwave sintered ones. The reason can be correlated to the excessive microstructural coarsening originating from slow heating rates and prolonged processing cycles associated with conventional heating. Referring to Table 4.5, it can be seen that there is extensive grain growth taken place at 1275 °C especially for the conventionally sintered samples, which is responsible for the deterioration of microhardness properties. Upon a further increase in the sintering temperature, namely at 1300 °C**,** the microhardness values got slightly improved with respect to the values obtained at 1275 °C accompanied by an increase in the sintered density with comparable grain sizes. The combined effect of an increase in sintered density and average grain sizes on microhardness of the microwave and conventionally sintered samples are represented in figure in the normalized microhardness versus

grain size graph (Figure 4.14). Here, normalized microhardness term stands for the microhardness values of the samples divided by their percent theoretical density values to cancel the effect of residual porosity on the hardness data. In this graph, it is seen that for low sintering temperatures, microwave and conventionally sintered samples attain similar normalized microhardness values with respect to grain size, due to the restricted grain growth. However, with increasing sintering temperatures, the normalized microhardness values of the conventionally sintered samples become inferior to the normalized microhardness values of the microwave sintered samples due to the excessive grain growth taking place in the conventional sintering case.

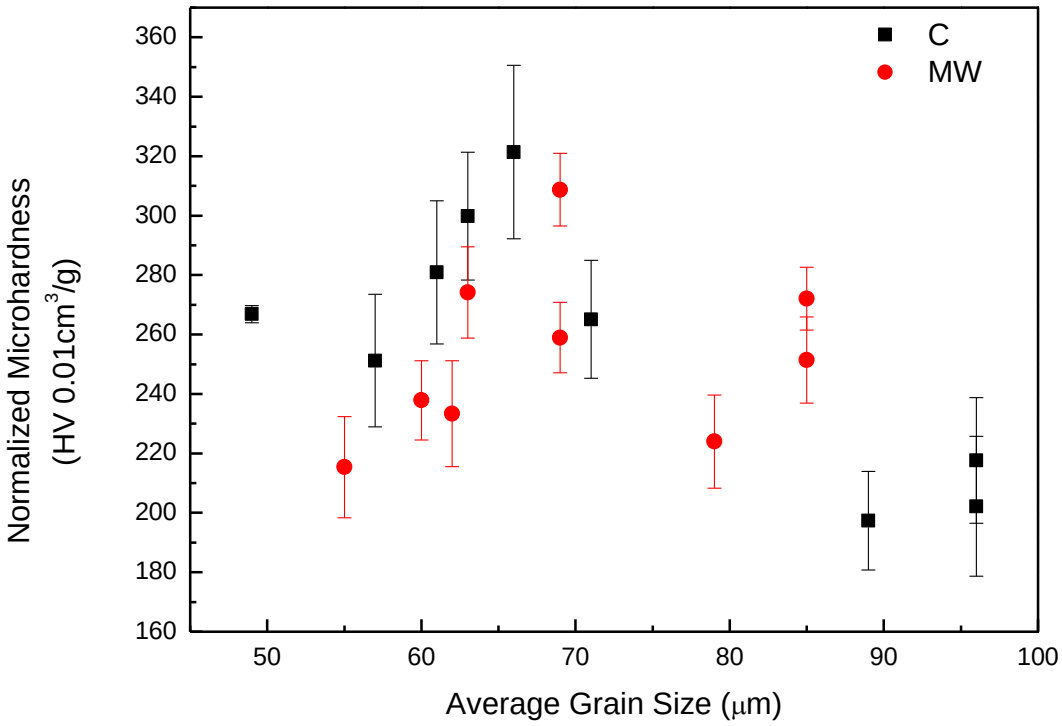

Figure 4.14. Normalized microhardness versus average grain size values of the microwave (MW) and conventionally (C) sintered samples.

To sum up, in the case of the microhardness values for samples produced either by microwave or conventional sintering, the general trend is to attain the maximum microhardness value at the maximum sintered density at constant or similar sintering temperatures, and hence, comparable final grain sizes. With altering sintering temperatures, an optimization in microhardness occurs at intermediate temperatures,

where achieved sintered density and grain size balance each other to give the optimum values. Furthermore, conventionally sintered samples appear to be affected more from the increase in sintering temperatures due to longer exposure times associated with prolonged sintering cycles, therefore, grain growth is more dominant in conventionally sintered samples than the microwave sintered ones, so the decrease in microhardness is more severe as compared to microwave sintering case (Figures 4.15 and 4.16).

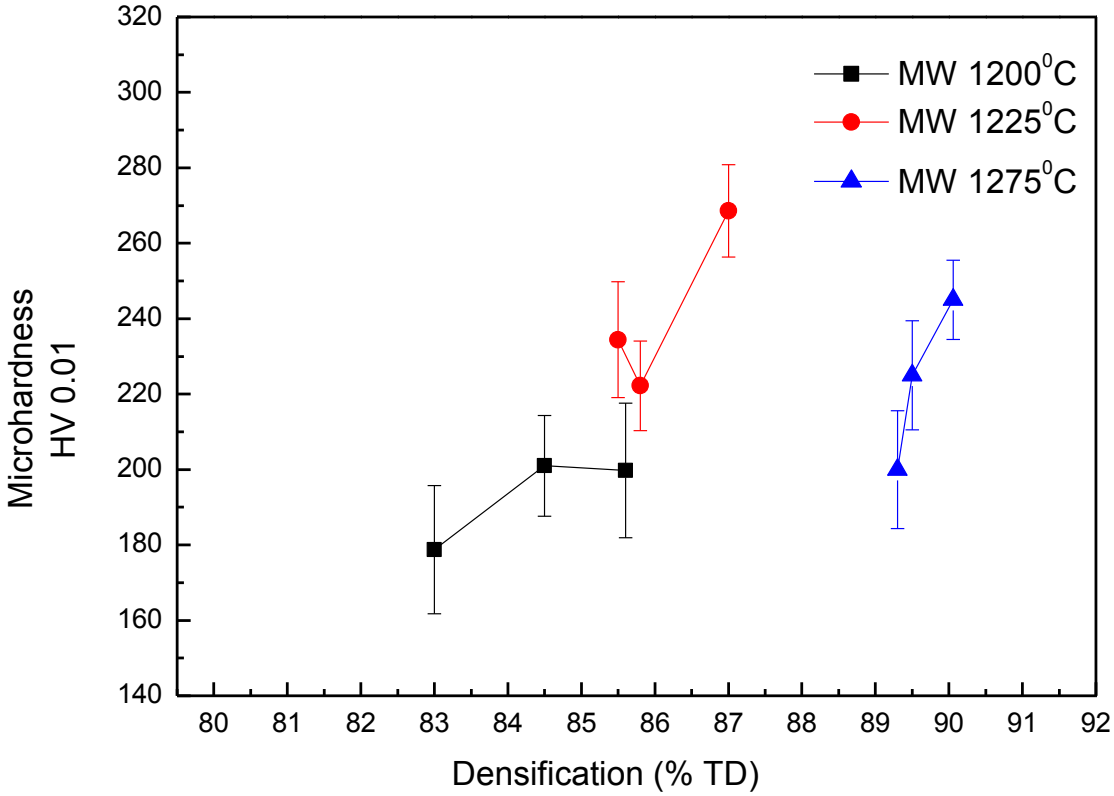

Figure 4.15. Microhardness variation of microwave sintered (MW) samples at 1200, 1225, 1275 °C with respect to densification.

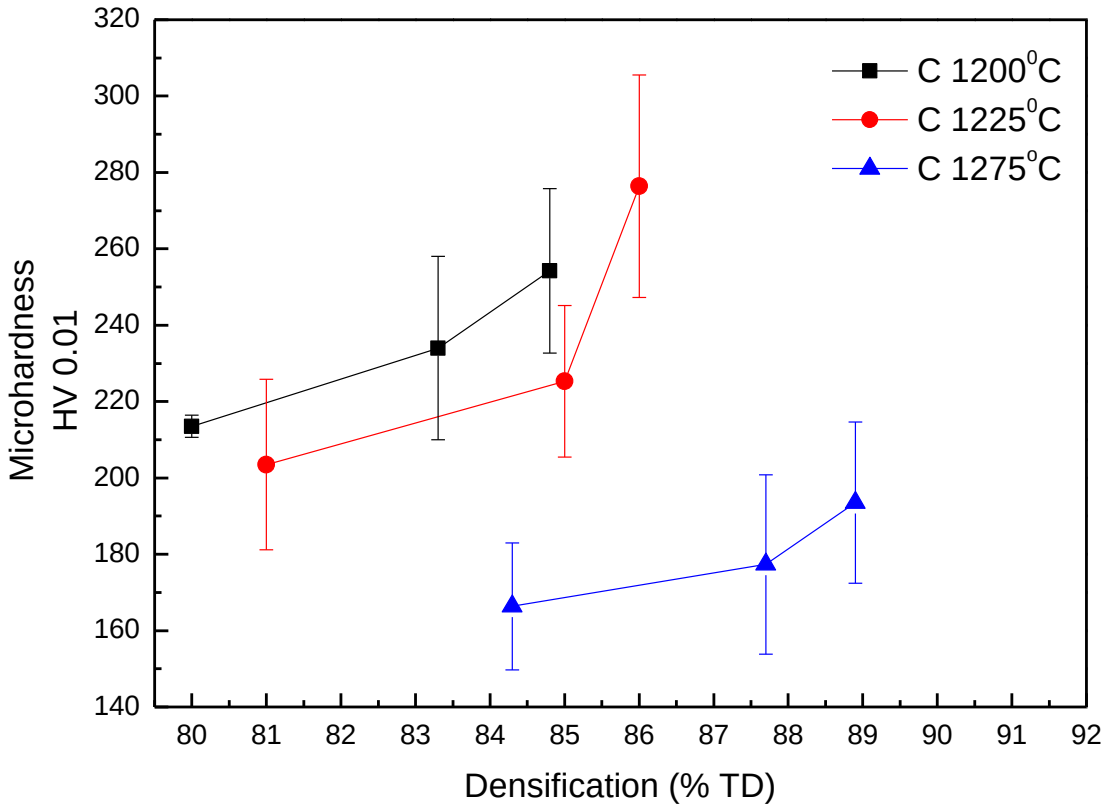

Figure 4.16. Microhardness variation of conventionally sintered (C) samples at 1200, 1225, 1275^{0}C with respect to densification.

4.2.4. Magnetic Characterization of Uniaxially Compacted Permalloys

Differential permeability curves and hysteresis loops of the powdered permalloys were investigated to observe the effect of microwave sintering on their soft magnetic properties in comparison to those achieved by conventional sintering. For powder metallurgical soft magnetic materials porosity and grain size are the key microstructural parameters which determine the soft magnetic response. For high initial and maximum permeability coarse grained microstructure is desired, since grain boundaries are major obstacles to the alignment of magnetic domains in conjunction with the applied external field. In the same sense, round pore morphology with minimized amount also optimizes the response of soft magnetic material to the external field. Moreover, magnetic induction is also controlled mainly by the residual porosity, as any air gap present in the sample is a source of demagnetization deteriorating the magnetic induction within the sample. Other than

high permeability and magnetic induction; narrow hysteresis loops are also desired for soft magnetic materials, where minimization of the area bounded by the hysteresis curve represents decreasing amount of energy losses during the hysteresis cycle.

In Figure 4.17 - 4.20, differential permeability and hysteresis loops of microwave and conventionally sintered powdered permalloy samples are given,. As it can be seen in Figure 4.17, maximum permeability of the microwave sintered samples has been achieved as the sintering temperature increased from 1250 to 1275 °C. This result is not surprising in the sense that with increasing sintering temperatures, both grain size and densification increases leading to a reduction in the amount of the obstacles resisting the motion of domain walls, which results in higher initial and maximum permeability. Upon a further increase in the sintering temperature to 1300 °C, permeability drops and the hysteresis curve widens (Figure 4.19). Despite the increase in densification and grain size, domain wall motion is restricted due to the extensive oxidation of grain boundaries at elevated sintering temperatures, which lowers the permeability and increases hysteresis losses. However, in the case of the alloy microwave sintered at 1300 °C, the permeability is almost constant around the maximum value indicating the presence of a uniform and homogenous microstructure imposed by the higher temperature.

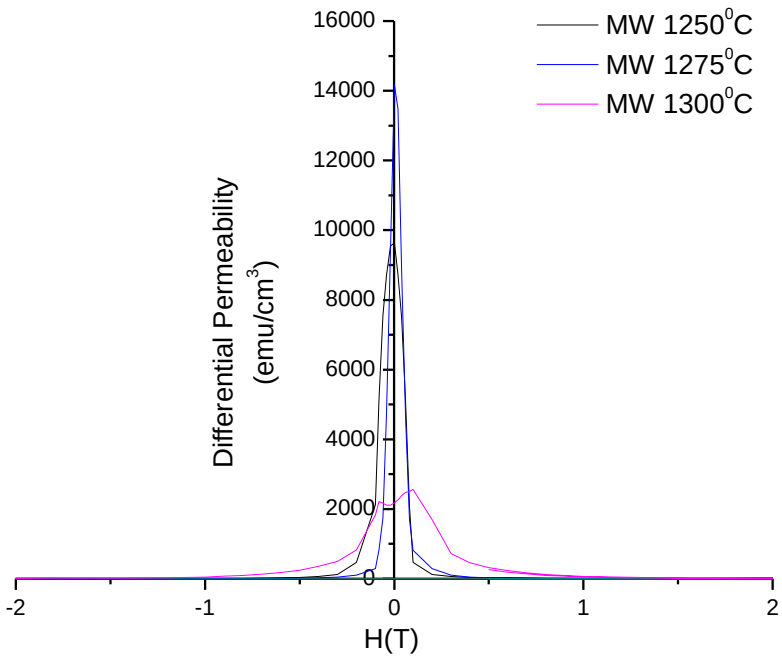

Figure 4.17. Differential permeability versus applied field graphs of the permalloy samples uniaxially compacted under 100 MPa and microwave sintered at 1250, 1275 and 1300 °C .

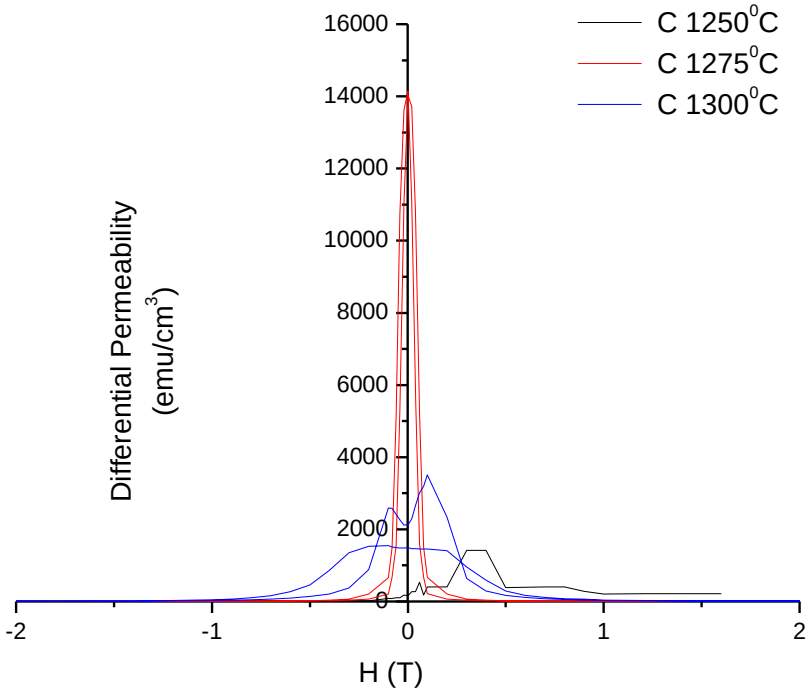

Figure 4.18. Differential permeability of the permalloy samples uniaxially compacted under 100 MPa and conventionally sintered at 1250, 1275 and 1300 °C.

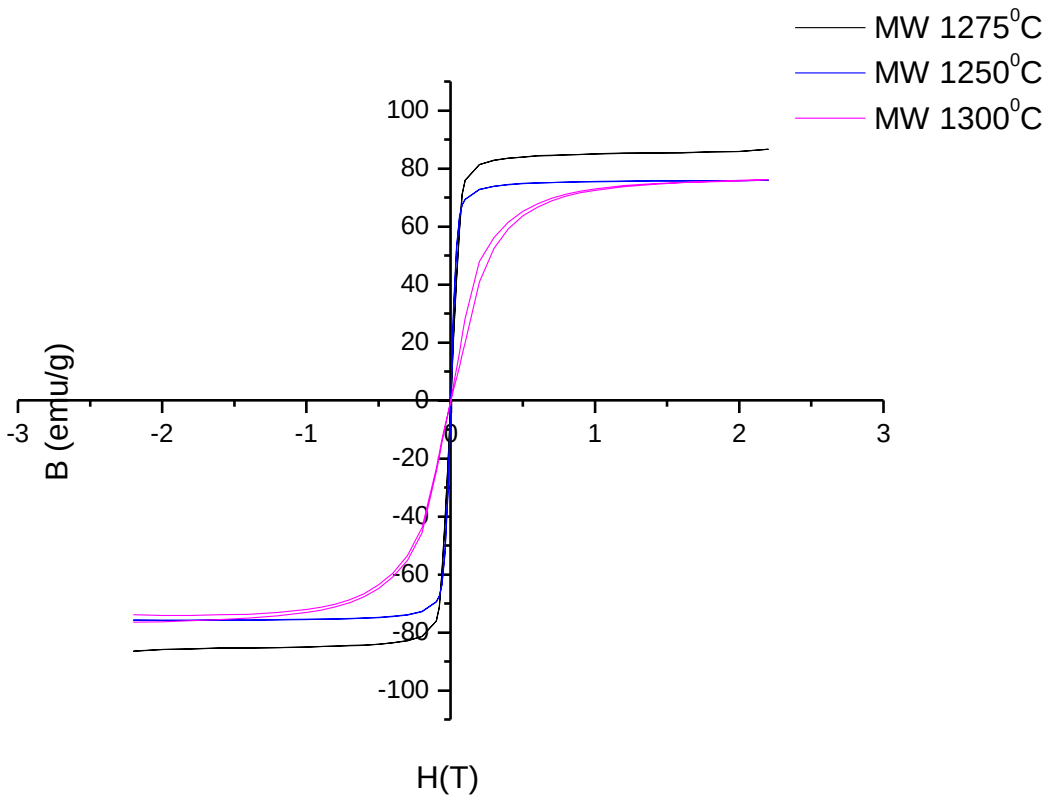

Figure 4.19. Hysteresis loops of the samples uniaxially compacted under 100 MPa and microwave sintered at 1250, 1275 and 1300^{0}C.

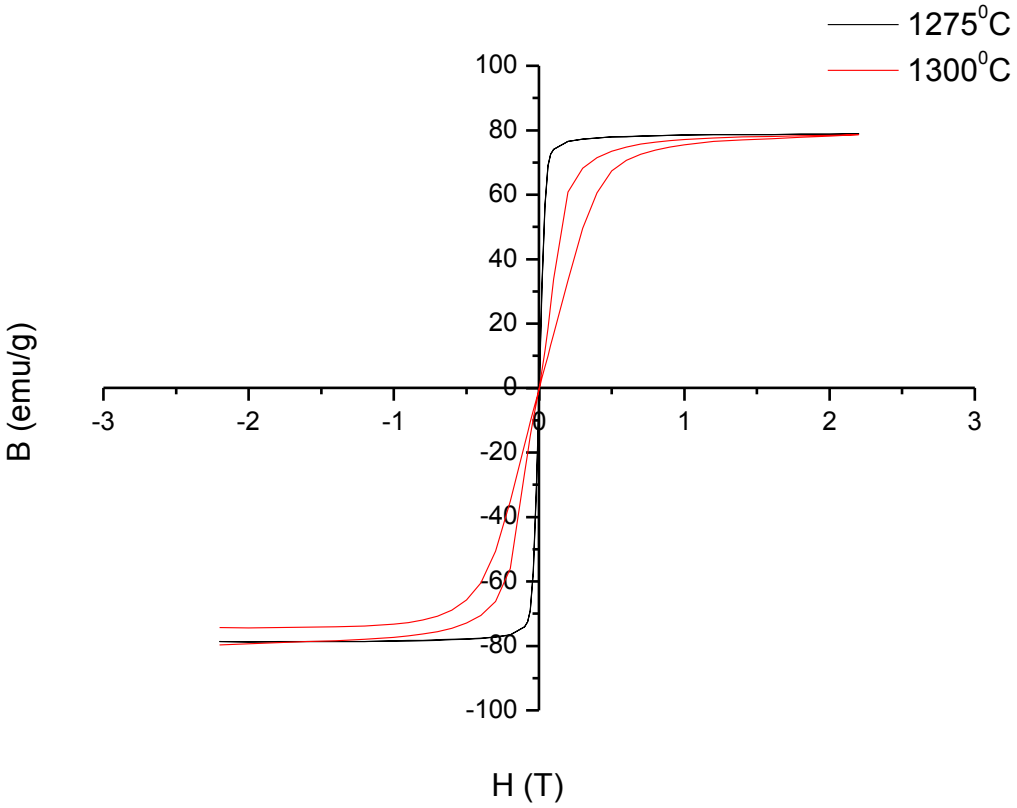

Figure 4.20. Hysteresis graphs of the samples uniaxially compacted under 100 MPa and conventionally sintered at 1250, 1275 and 1300^{0}C**.**

The permeability of conventionally sintered samples show a similar dependence on sintering temperature like their microwave sintered counterparts (Figure 4.18). In this case, the permeability is also maximized around 1275 °C due to the compromise obtained between densification, grain coarsening and grain boundary oxidation. From the hysteresis curves of the conventionally sintered samples (Figure 4.19), it can be seen that at 1300 °C, the hysteresis curves widens and losses increase with a decrease in permeability (Figure 4.18) suggesting detrimental contribution of enhanced oxidation kinetics to the deterioration of the soft magnetic properties at elevated sintering temperatures.

To study the effect of sintered density on the soft magnetic properties at constant temperature obtained via changing compaction pressures, differential permeability and hysteresis loops of the samples with varying green densities, yet sintered at 1225

°C were obtained. From the permeability data (Figure 4.21 and 4.22), it can be seen that for both microwave and conventionally sintered samples, the permeability values do not alter significantly with changing sintered densities at constant temperatures. Although a slight change occurs with changing compaction pressures, sintered samples with approximately same grain sizes (~ 70-80µm) were obtained, since grain growth is enhanced effectively with increasing sintering temperature rather than compaction pressure. Furthermore, microwave sintered samples exhibit slightly higher permeability values compared to their conventionally sintered counterparts. This difference may have arisen from the contributions of improved sintered densities and inhibited grain boundary oxidation obtained via the shorter processing cycle of microwave sintering process.

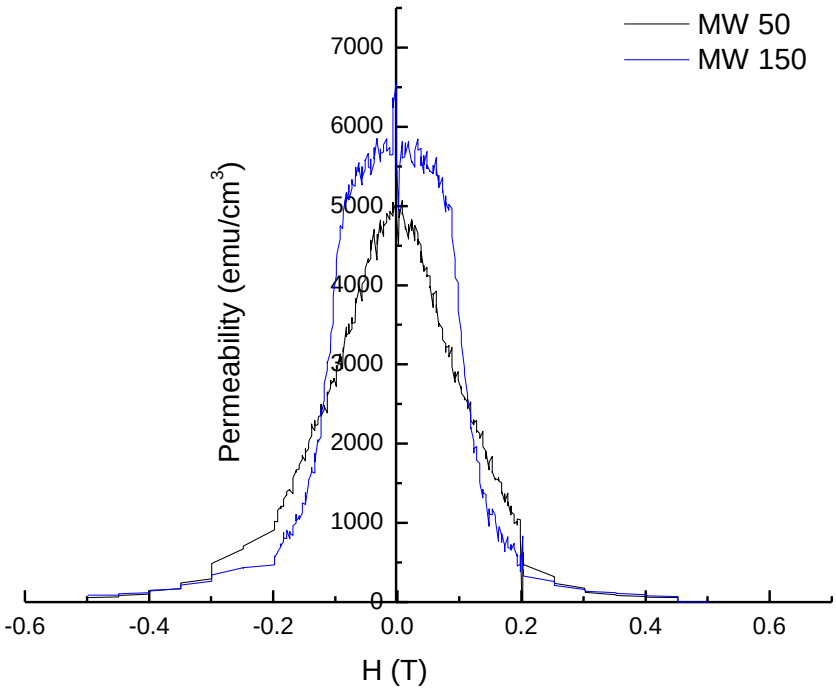

Figure 4.21. Differential permeability versus applied field graphs of the samples uniaxially compacted under 50 (MW 50) and 150 MPa (MW 150) then microwave sintered at 1225 °C with final densification of 85.5% and 85.8%, respectively.

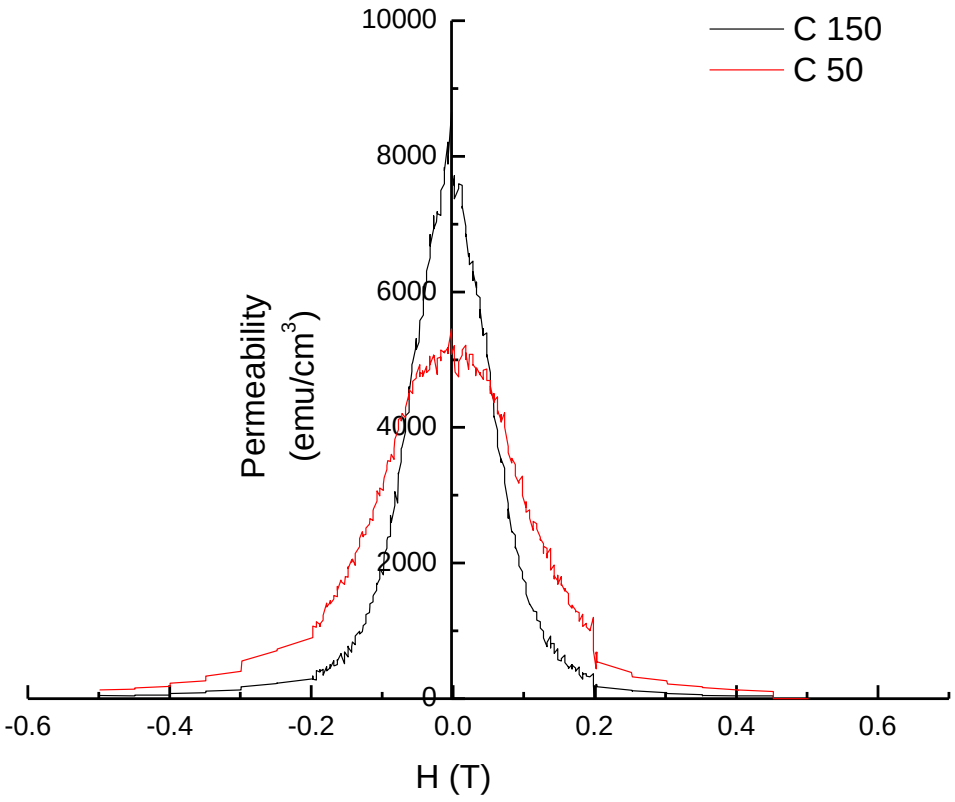

Figure 4.22. Differential permeability versus applied field graphs of the samples uniaxially compacted under 50 (C 50) and 150 MPa (C 150) then conventionally sintered at 1225 °C with final densification of 81 and 86%, respectively**.**

Hysteresis loops of microwave and conventionally sintered permalloy samples sintered at constant temperature with varying green densities presented in Figure 4.23 and 4.24, respectively, also revealed the effect of final densification on the soft magnetic properties in microstructures with comparable grain sizes. For microwave sintered samples, samples compacted under 150MPa reaches higher magnetic saturation values than the 50MPa compacted samples, since the sintered densities of the two samples are similar, the difference may arise from the grain boundary oxidation. Owing to the low green density of the sample compacted under 50MPa, severe oxidation of grain boundaries which is detrimental to soft magnetic properties occurred. For conventionally sintered samples, samples compacted under 150MPa pressure reaches higher magnetic saturation as expected due to its higher sintered

density and decreased susceptibility to grain boundary oxidation because of its high green density.

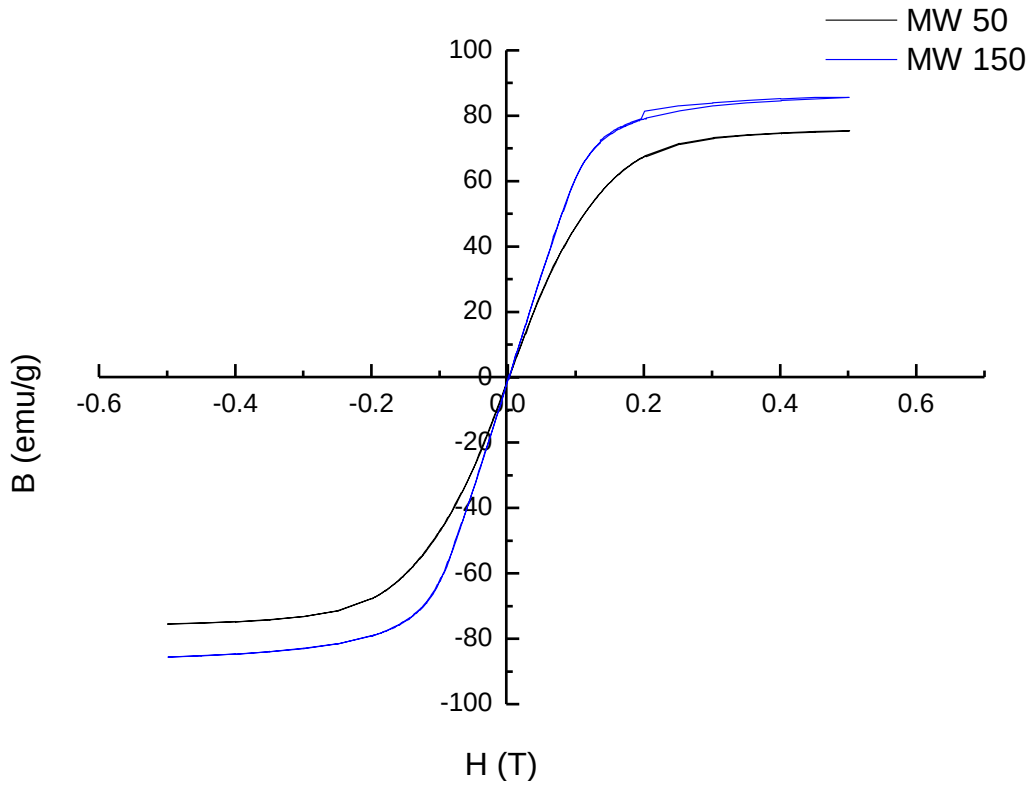

Figure 4.23. Hysteresis loops of the samples uniaxially compacted under 50 (MW 50) and 150 MPa (MW 150) then microwave sintered at 1225 °C**.**

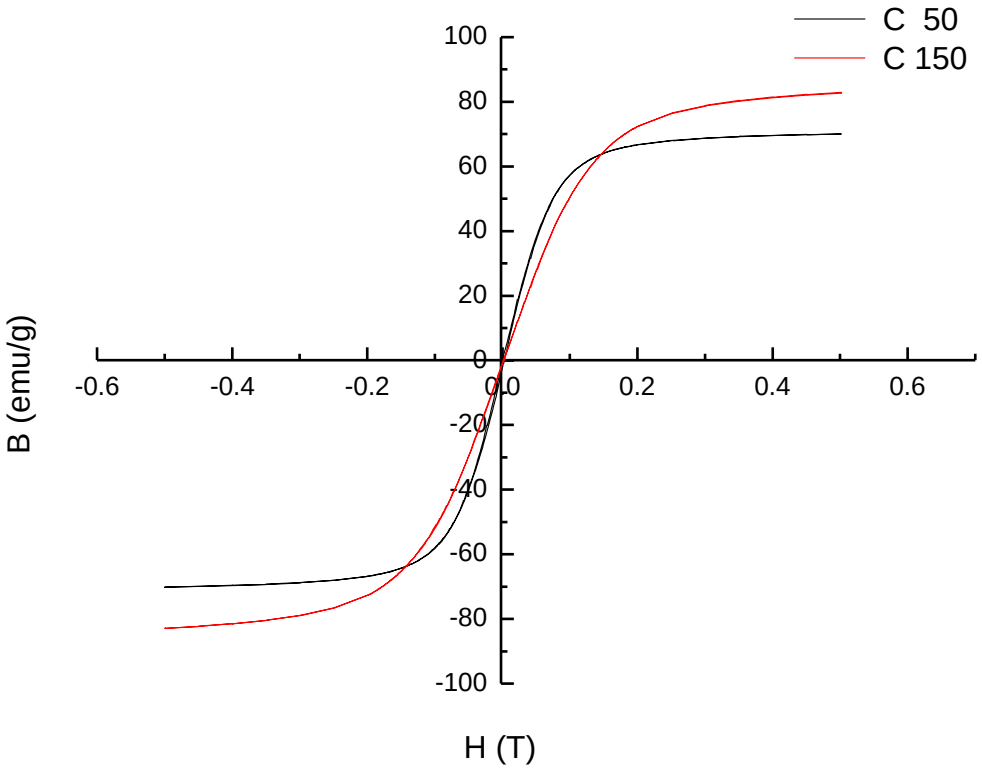

Figure 4.24. Hysteresis loops of the samples uniaxially compacted under 50 (C 50) and 150 MPa (C 150) then conventionally sintered at 1225 °C.

4.3. Powdered Permalloys Directly Formed by Cold Isostatic Pressing (CIPing)

4.3.1 Densification Response of Permalloy Compacts Directly Formed by CIPing

To study the effect of compaction method on the densification, permalloy samples directly formed by cold isostatic pressing from the initial powders under 150 MPa of pressure were microwave and conventionally sintered at 1200, 1250 and 1300°C and characterized in terms of microstructural, mechanical and soft magnetic properties.

In Figure 4.25, the change of sintered density with respect to sintering temperature is depicted. For both microwave and conventionally sintered samples, maximum sintered density was obtained at around 1250 °C. Contrary to the conventional sense, further increase in the sintering temperature resulted in a drop in the final density of samples for both sintering methods, which can be related to microstructural coarsening and pore coalescence hindering atomic transport from the interfacial regions with more open structure despite the significant acceleration in the diffusion

kinetics at elevated sintering temperatures. The inert oxide layer formation in the form of a network on grain boundaries will slow down the diffusion of atoms between the particles, thereby suppressing densification.

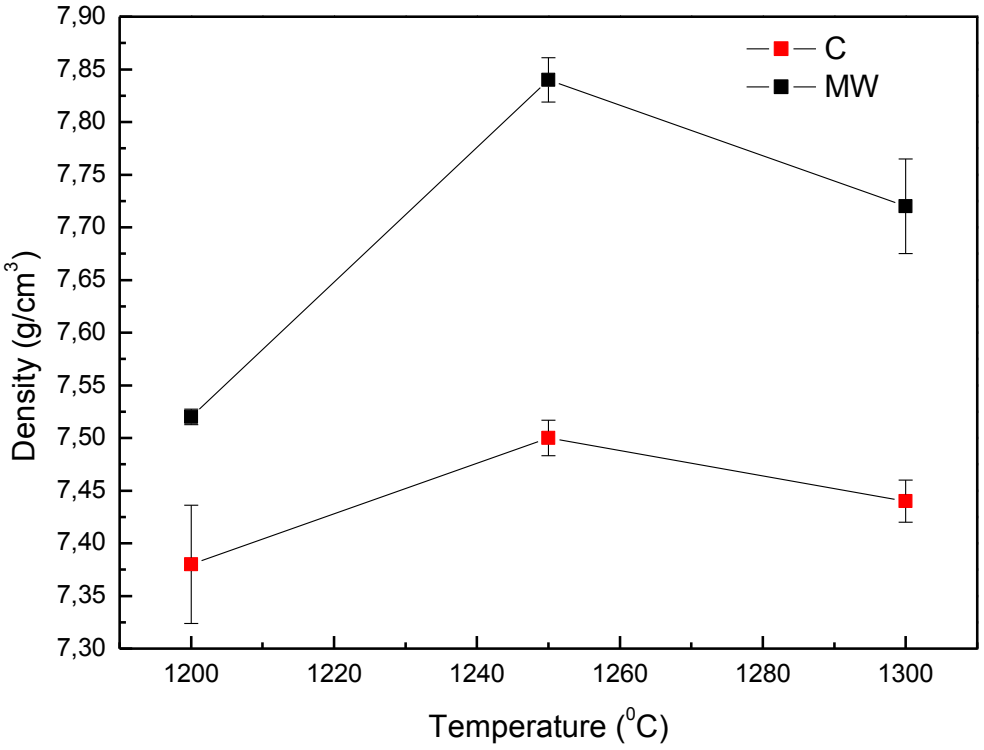

Figure 4.25. Sintered density versus sintering temperature graph for conventionally (C) and microwave sintered samples sintered at 1200, 1250, 1300 °C formed by CIPing.

In Table 4.6, relative densification values of the microwave and conventionally sintered samples calculated from the data of Figure 4.25 are presented. It can be seen that microwave sintered samples reveal higher densification than their conventionally sintered counterparts owing to the volumetric and rapid nature of heating associated with microwave sintering. Furthermore, since the overall processing cycles are shorter in microwave sintering, the adverse contribution of grain boundary coarsening is less pronounced in the case of microwave heating.

Table 4.6. Densification behavior of the microwave (M) and conventionally (C) sintered samples with respect to sintering temperature formed by CIPing**.**

Sintering Temperature (^{0}C)	Densification (%TD)	
1200	86.4 (M)	83,2 (C)
1250	90.6 (M)	86,4 (C)
1300	88.7 (M)	85,3 (C)

4.3.2. Microstructural Evolution of the Compacts Formed by CIPing

In the below given optical micrographs (Figure 4.26), it can be seen that single phase austenitic Ni-Fe alloy could be obtained via both sintering procedures. The presence of annealing twins is a sign of an acceptable sintering. Table 4.6 indicates the grain size values for conventionally and microwave sintered samples. Grain size measurement results indicates that there is significant microstructural coarsening at 1300 °C in the case of both sintering methods, where this effect is more pronounced for the conventional sintering resulting from prolonged processing cycles. The microstructural coarsening as well as extensive grain boundary oxidation is the underlying reasons behind the inferior densification response of the conventionally sintered samples than the microwave sintered samples, which has been shown in Figure 4.25 and Table 4.7.

Table 4.7. Average grain size versus sintering temperature values for conventional (C) and microwave (M) sintered samples cold isostatically compacted under 150 MPa of pressure and sintered at 1200, 1250 and 1300 °C.

Sintering Temperature (°C)	Average Grain Size (μm)	
	M	C
1200	85±8	94±6
1250	89±7	110±9
1300	101±10	116±8

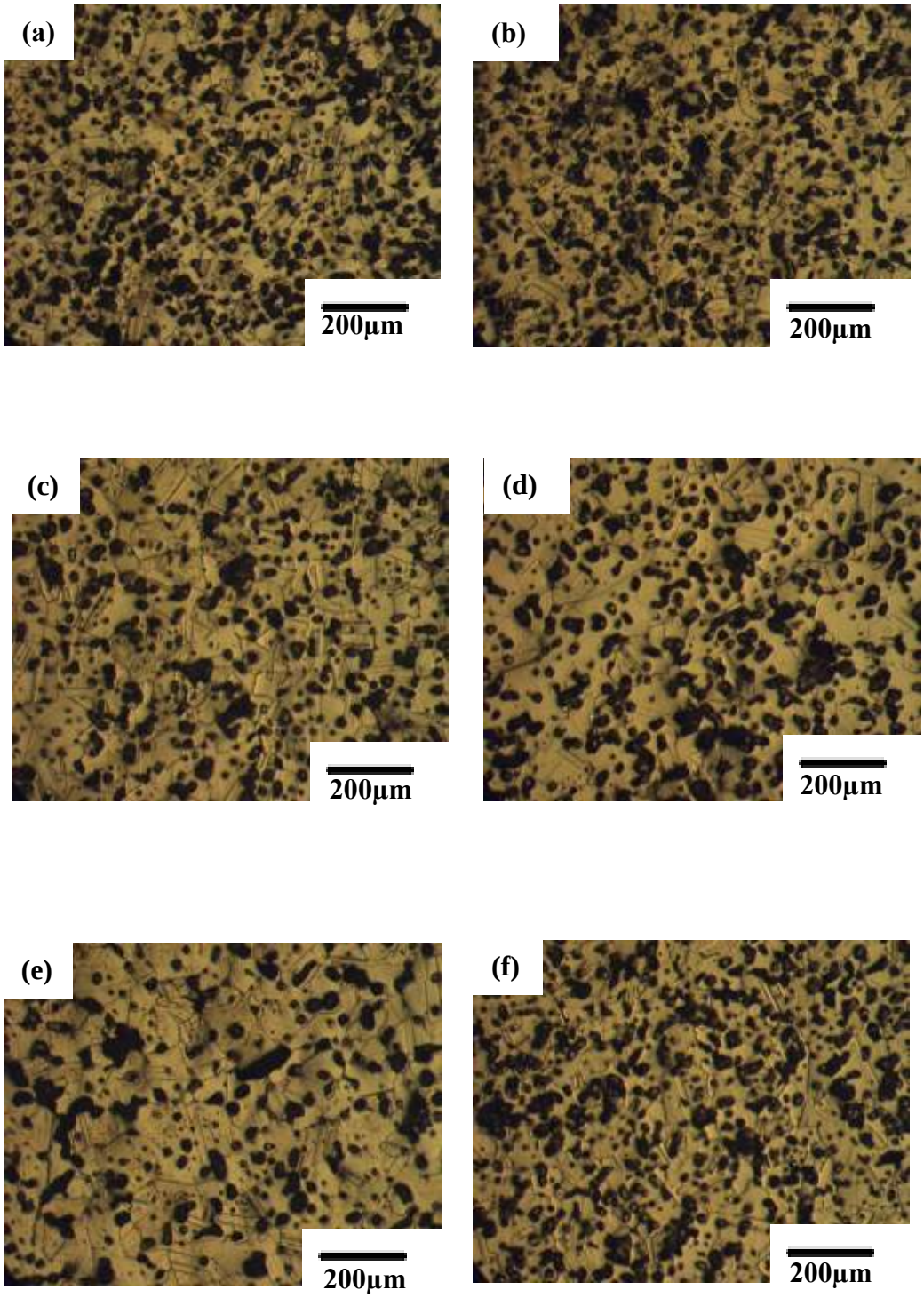

Figure 4.26. a-c-e. Optical micrographs of the samples microwave sintered at 1200 (a) and 1250 (c) and 1300 °C (e). **Figure 4.26. b-d-f.** Optical micrographs of the samples conventionally sintered at 1200 (b), 1250 (d) and 1300 °C (f).

Investigation of pore morphologies via SEM indicated that there is significant pore rounding at 1250 °C corresponding to the optimum densification temperature (Figure

4.27). Moreover, there is significant residual deformation damage from the metallographic specimen preparation steps, particularly for the microwave sintered specimen processed at 1200 °C and for almost all of the conventionally sintered samples, despite the heavy etching and re-polishing procedures applied. The consequent inferior mechanical properties and soft magnetic behavior of the samples is mainly the result of this residual deformation. Another worth noting feature in the SEM micrographs of the samples is the difference in pore morphologies. The pores in the conventionally sintered samples acquire more skewed morphology especially at the lower sintering temperatures, while the pores are more rounded in microwave sintered samples.

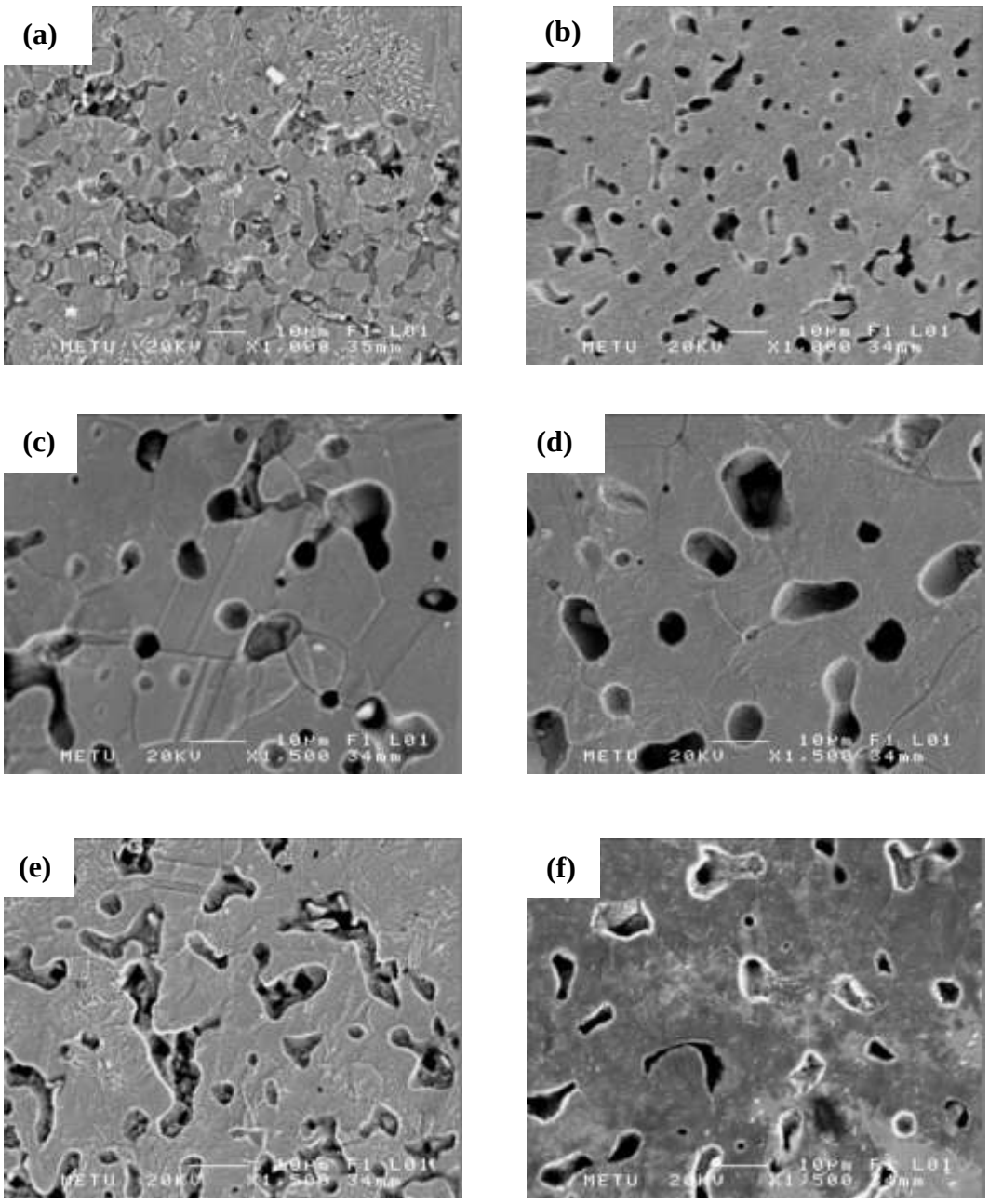

Figure 4.27. SEM micrographs of the samples microwave sintered at 1200 (a) and 1250 (c) and 1300 °C (e). **Figure 4.27. b-d-f.** SEM micrographs of the samples conventionally sintered at 1200 (b), 1250 (d) and 1300 °C (f).

From the hardness vs. sintering temperature graphs (Figure 4.28), it is evident that microwave sintered samples reach higher microhardness values compared to

conventionally sintered samples at the applied sintering temperatures, and an increase in microhardness values is observed with increasing final densities as expected. The higher microhardness values of the microwave sintered samples can be attributed to both improved final densities and refined microstructures as compared to the conventional sintering case. The microhardness values of the conventionally sintered samples are slightly changing with altering sintering temperatures, most probably because of the balance achieved between the two contradicting factors, which are accelerated grain growth and improvement in density with increasing temperature.

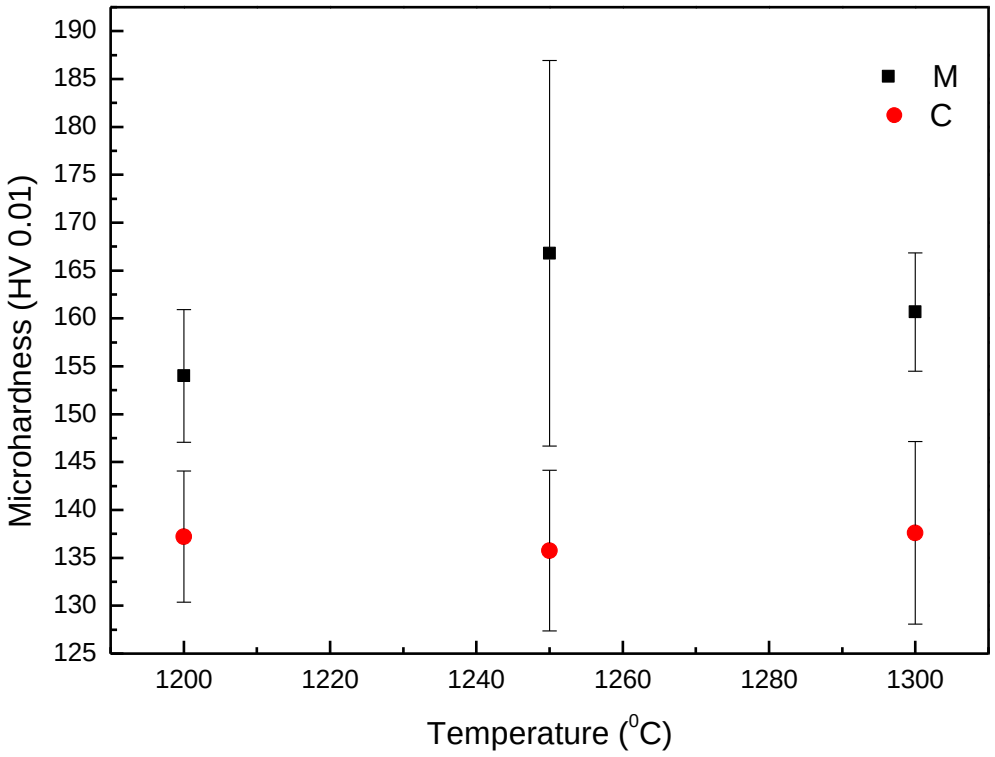

Figure 4.28. Microhardness values of the samples formed directly by CIPing under 150 MPa of pressure then microwave (MW) and conventionally (C) sintered at 1200, 1250 and 1300 °C.

4.3.4. Magnetic Characterization of the Compacts Formed by CIPing

In Figures 4.29 and 4.30, it is observed that optimum soft magnetic properties was achieved in the permalloy samples sintered at 1200 °C for both microwave and conventional sintering routes, which is evident from the highest saturation

magnetization values seen at this temperature. For conventional sintering case, the permeability of the samples follows the maximum grain size values. Adverse Contribution of oxide layer is suppressed by the excessive grain growth at elevated temperatures; since the processing time does not change significantly with increasing temperatures, so exposure to oxidation do not vary to a great extent.

For the microwave sintering case, maximum permeability corresponds to the samples sintered at the lowest temperature, although the sintered density and grain size combination is minimal at these temperature. This finding implies the strong effect of grain boundary oxidation on most magnetic response of the microwave sintered samples. Furthermore, samples sintered at 1300^0C display improved permeability than the samples sintered at 1250^0C, owing to the microstructural coarsening at this temperature.

Conventionally sintered samples at higher temperatures display improved permeability than their microwave sintered counterparts, due to the exaggerated grains associated with longer processing cycles. However, microwave sintered samples at 1200^0C have superior magnetic permeability than their conventionally sintered counterpart, owing to the better densification and restricted grain boundary oxidation.

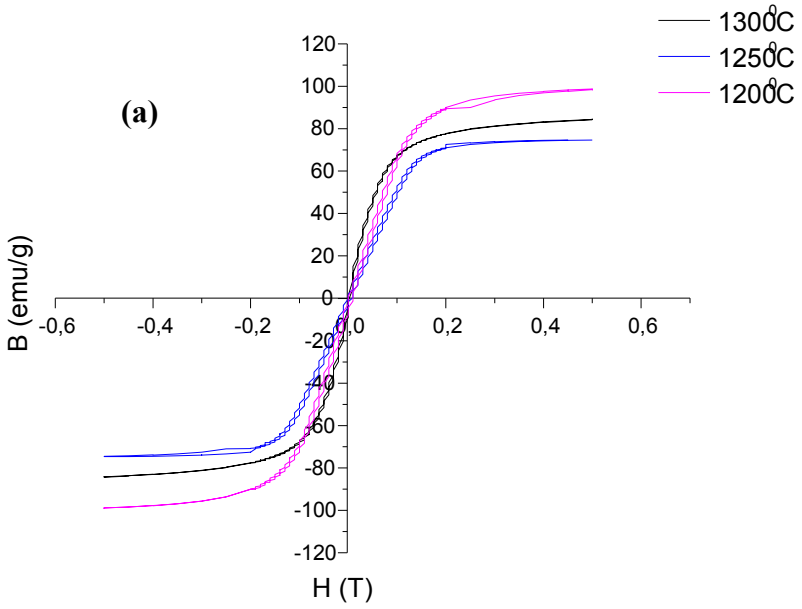

Figure 4.29. Hysteresis loops of the samples microwave (a) and conventionally (b) sintered samples which were formed directly by CIPing.

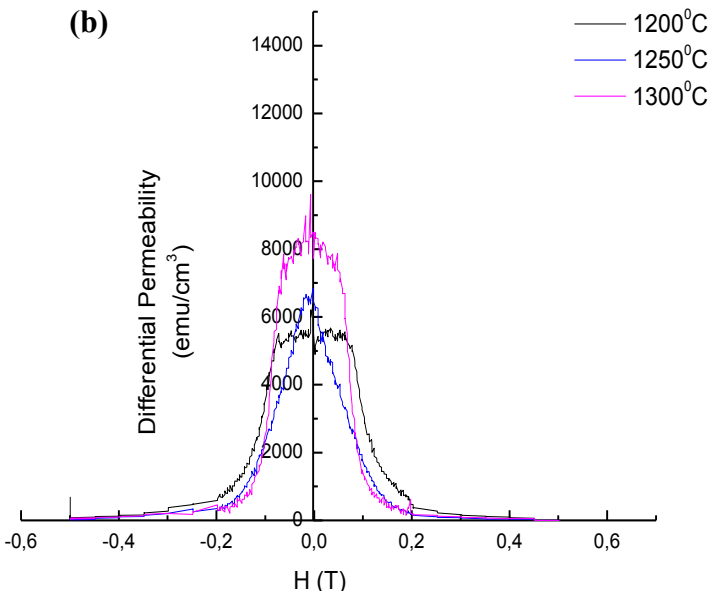

Figure 4.29. Hysteresis loops of the samples microwave (a) and conventionally (b) sintered samples which were formed directly by CIPing (continued).

A similar behavior has been encountered in the microwave sintered samples. In this case, once more samples sintered at the lower temperature showed improved soft magnetic properties in terms of permeability and magnetic induction, which is thought to be originating from the enhanced grain boundary oxidation at higher temperatures.

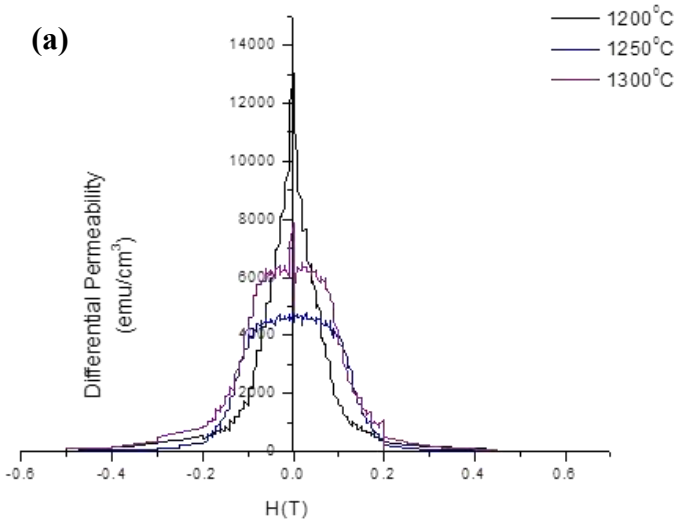

Figure 4.30. Differential permeability versus applied field graphs of the microwave (a) and conventionally (b) sintered samples which were formed directly by CIPing.

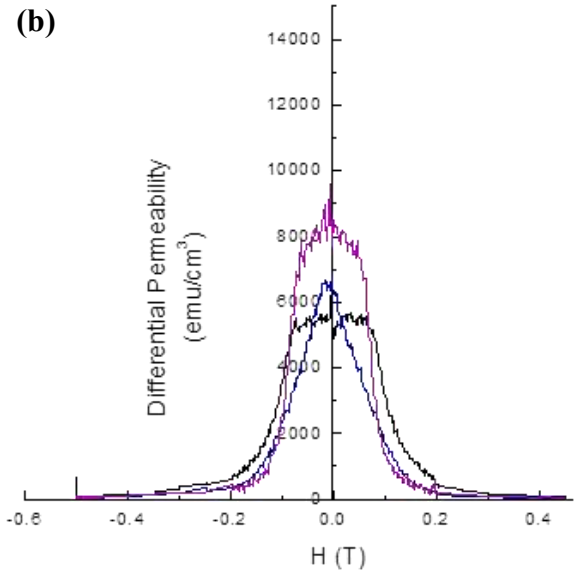

Figure 4.30. Differential permeability versus applied field graphs of the microwave (a) and conventionally (b) sintered samples which were formed directly by CIPing (continued).

4.4. Powdered Permalloys Formed by Uniaxial Pressing Followed Cold Isostatic Pressing (CIPing)

4.4.1. Densification Response of the Permalloy Compacts Formed by Uniaxial Pressing Followed by CIPing

Sintered density versus sintering temperature of the samples formed by uniaxial pressing followed by cold isostatic pressing which were then microwave or conventionally sintered is shown in Figure 4.31. For conventionally sintered samples, sintered density gets optimized at 1250 °C, and sintered density falls upon further increase in temperature, which is thought to be originating from microstructural coarsening and grain boundary oxidation. On the contrary, sintered density of the microwave sintered samples increases with increasing temperature, differing from

the previous case of CIPed samples. The difference mar originate from the fact that double action uniaxially pressed followed by CIPing samples acquire higher green density than samples compacted only via CIPing, so oxygen exposure is less, therefore inert oxide layer formation hindering densification is less pronounced.

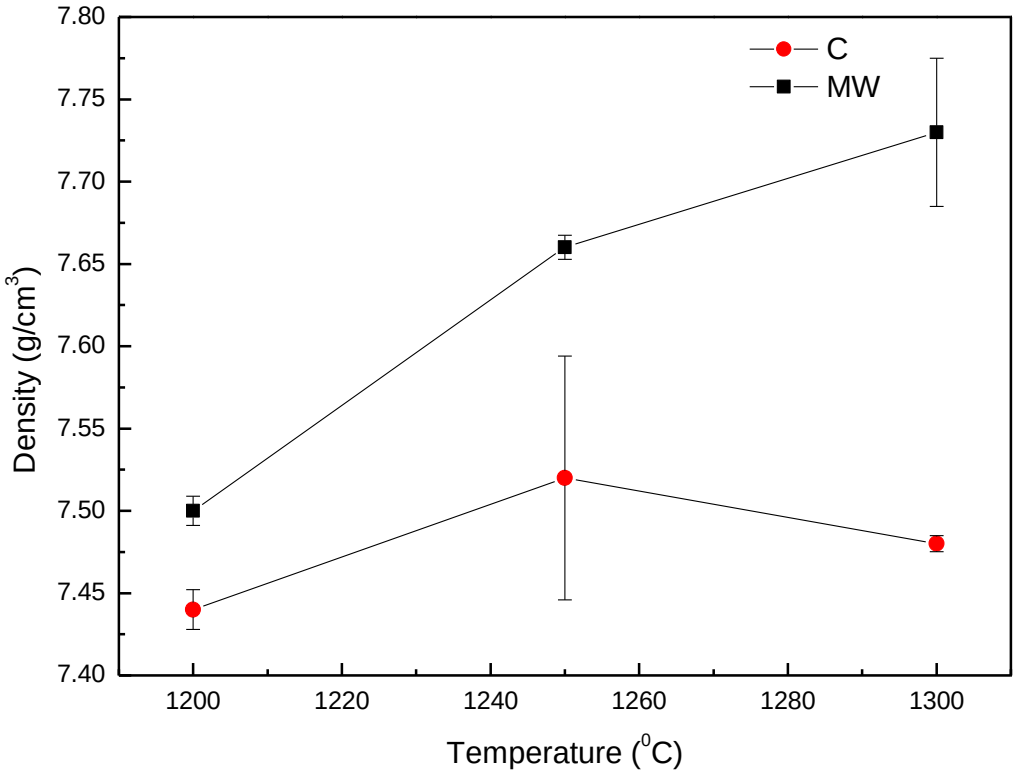

Figure 4.31. Sintered density vs. temperature graphs of the samples microwave (MW) and conventionally (C) sintered at 1200, 1250 and 1300 °C.

4.4.2. Microstructural Evolution of the Permalloy Compacts Formed by Uniaxial Pressing Followed by CIPing

Microstructural examination of the sintered samples (Figure 4.32)revealed that there is excessive grain growth taking place in the conventionally sintered samples (Table 4.8.), and microstructural changes such as grain growth and reduction in residual porosity balance each other at the sintering temperature of 1250 °C, which is in good agreement with the densification findings. In the microwave sintering case, amount of porosity decreases with increasing sintering temperature, and in the micrograph of the sample sintered at 1300 °C (Figure 4.32 (e)) significant pore rounding is observed.

Table 4.8. Average grain sizes for samples microwave (M) and conventionally (C) sintered at 1200, 1250 and 1300 °C**.**

Sintering Temperature (°C)	Average Grain Size (μm)	
	M	C
1200	96	109
1250	106	135
1300	110	150

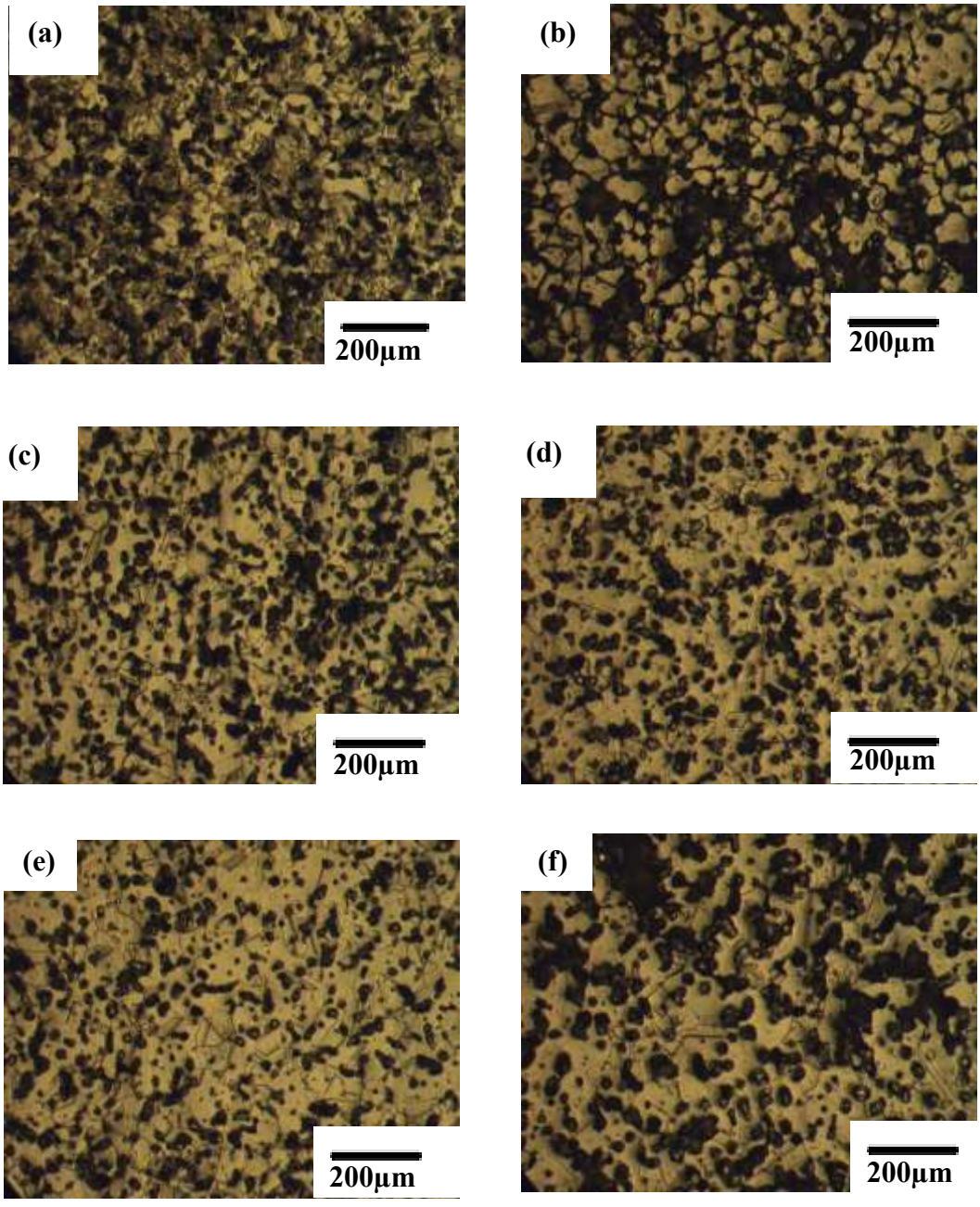

Figure 4.32. Optical micrographs of the samples microwave sintered at 1200 (a) and 1250 (c) and 1300 °C (e). **Figure 4.32.b-d-f.** Optical micrographs of the samples conventionally sintered at 1200 (b), 1250 (d) and 1300 °C (f)

Change in the amount of porosity and in pore morphology of the samples examined using SEM revealed that residual porosity decreases with increasing temperatures for the microwave sintered samples (Figure 4.33). For conventional sintering, it can be seen that pore coalescence took place in the samples sintered at 1300 **°C**. Moreover, pore rounding seems to have occurred in microwave sintered samples, while pore morphology is more skewed in the conventionally sintered ones. Furthermore, there is significant smearing in the pores of the conventionally sintered samples detectable at higher magnifications, which is caused by the plastic deformation incorporated into the sample during metallographic specimen preparation step owing to the relatively low hardness values of conventionally sintered alloys.

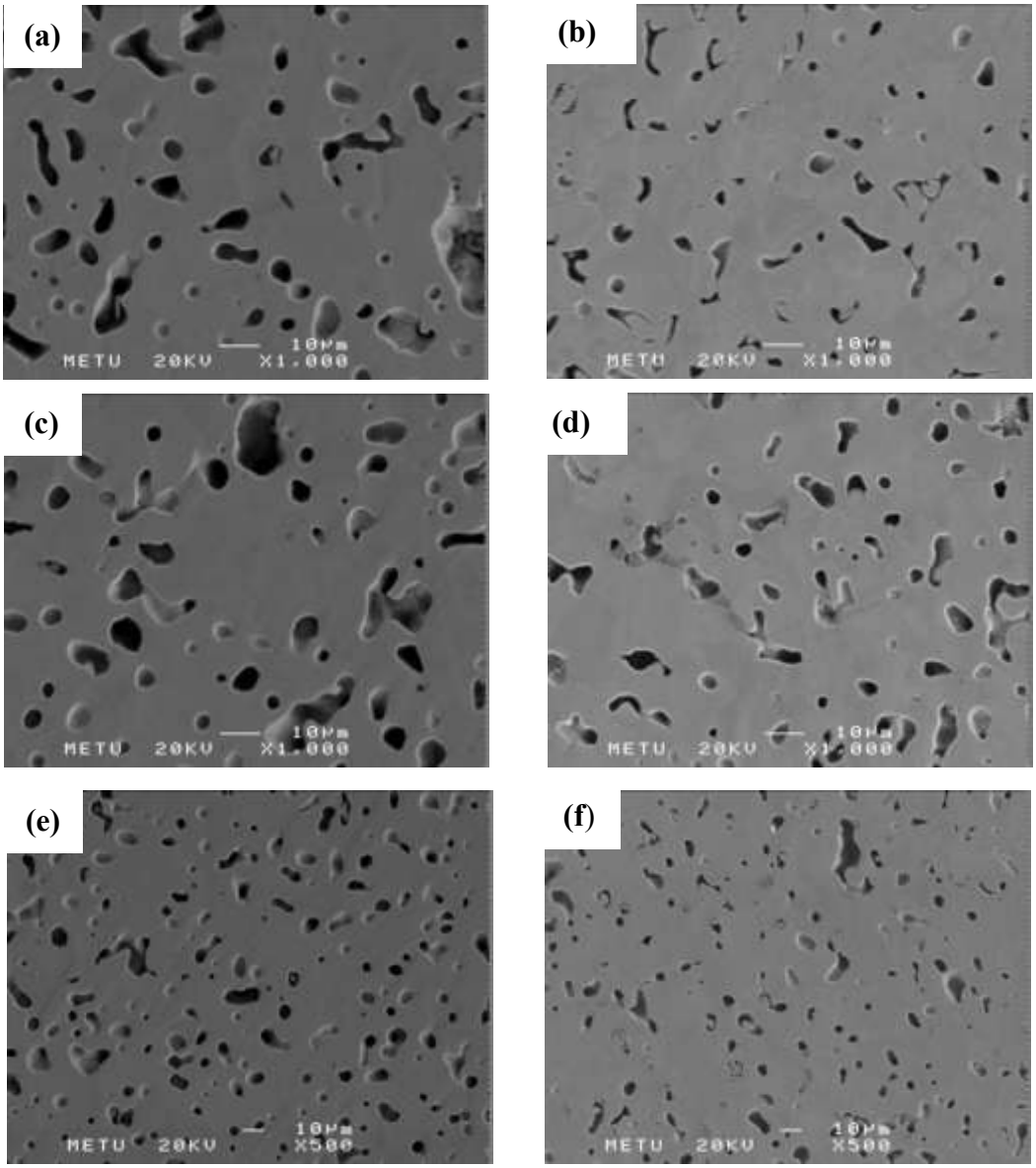

Figure 4.33. SEM micrographs of the samples microwave sintered at 1200 (a), 1250 (c) and 1300 °C (e). **Figure 4.33. b-d-f.** SEM micrographs of the samples conventionally sintered at 1200 (b) and 1250 (d) and 1300 °C (f).

4.4.3. Mechanical Characterization of the Permalloy Compacts Formed by Uniaxial Pressing Followed by CIPing

Microhardness values of the samples reach to an optimum value where the sintered alloy assumes the maximum sintered density, which is expected as the sintered density is the key property of powder metallurgical samples determining the engineering characteristics. In conventional sintering case, microhardness of the samples sintered at 1300 °C shows the minimum value due to the enhanced grain

growth and pore coalescence taking place at relatively higher temperatures (Figure 4.34).

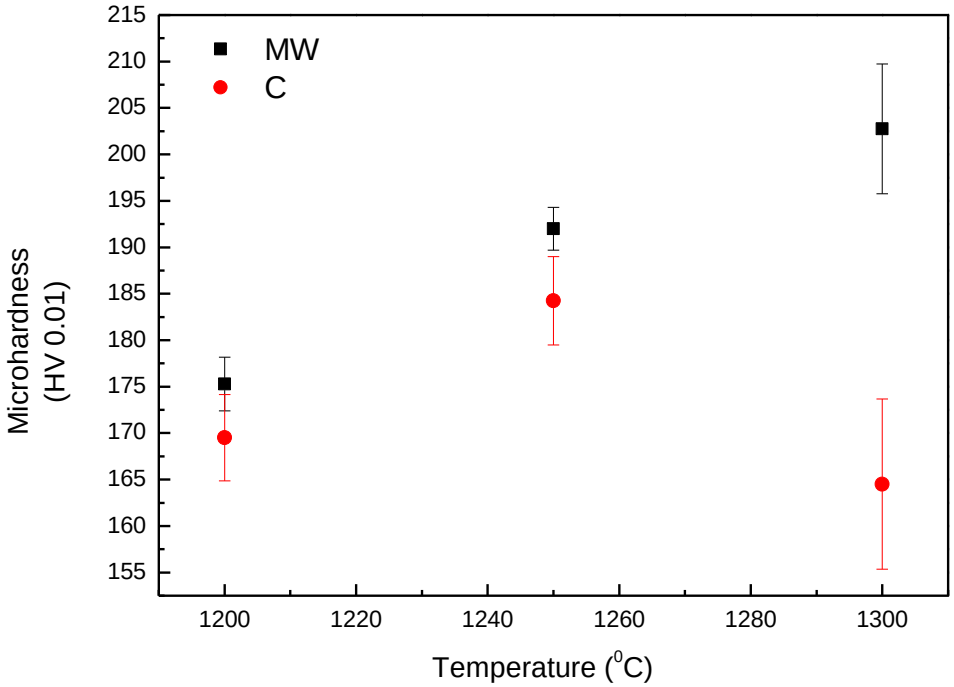

Figure 4.34. Microhardness values of the samples microwave (MW) and conventionally sintered at 1200, 1250, 1300 °C.

4.4.4. Magnetic characterization of the Permalloy Compacts Formed by Uniaxial Pressing Followed by CIPing

From the permeability and hysteresis curves of the sintered permalloys given in Figure 4.35 and 4.36, respectively, maximum permeability values have been achieved at the sintering temperature of 1200 °C for both conventional and microwave heating cases, although the sintered density and the grain sizes are minimal at these temperature. When excessive grain growth yielding grain sizes exceeding 100μm even at the lowest sintering temperatures, these findings indicate that grain boundary oxidation is dominant and because of this reason, at the maximum sintering temperature, maximum permeability could not be obtained despite the increased average grain sizes. The permeability of the microwave sintered samples acquire close values at different sintering temperatures, since oxidation is not as tremendous as in the case of the conventionally sintered samples due to the shorter processing cycles. However, extensive grain boundary oxidation in the

conventionally sintering case seems to be compensated by excessive grain growth to some extent, this way conventionally sintered samples exhibit superior soft magnetic properties than their microwave sintered counterparts.

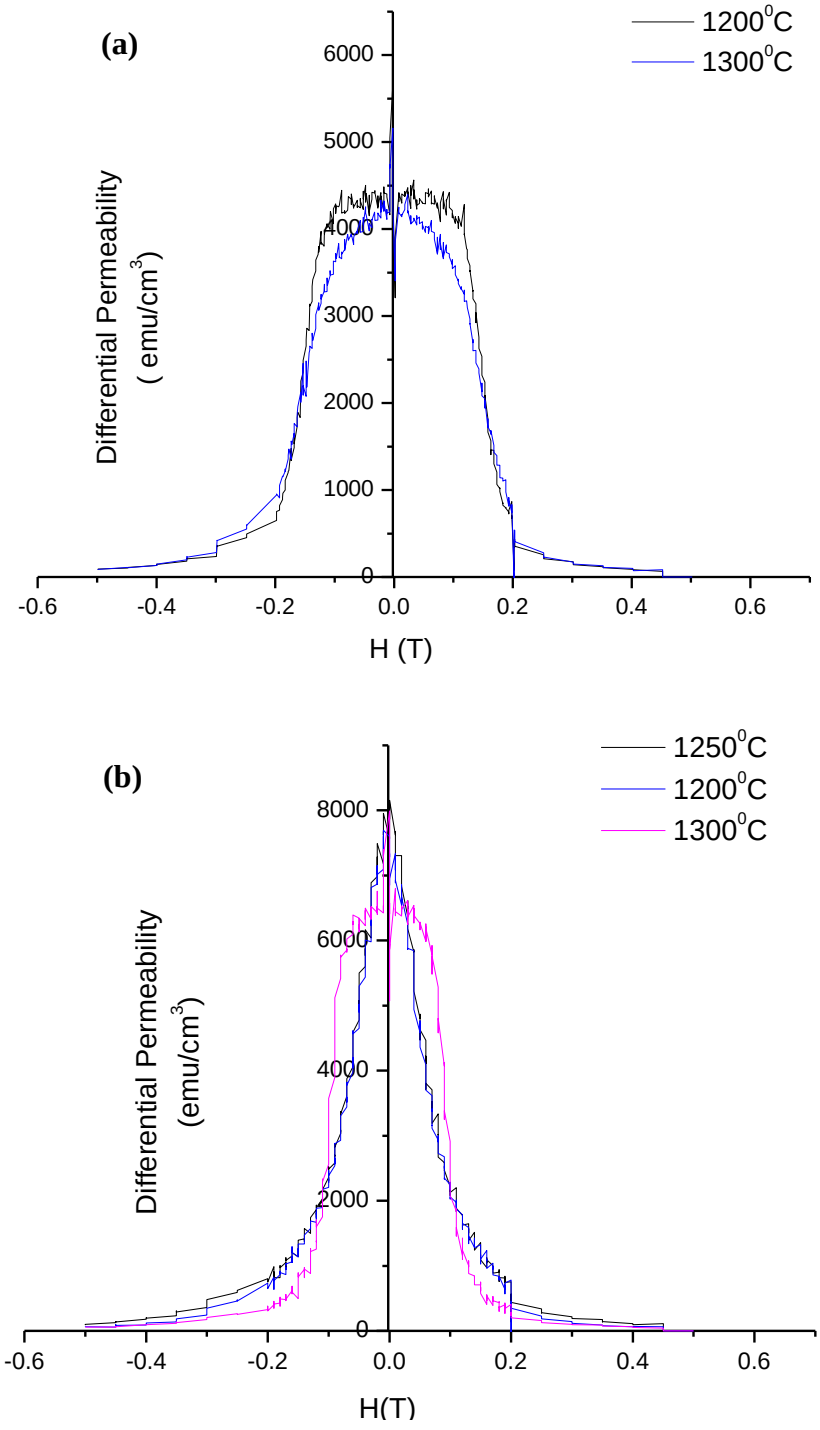

Figure 4.35. Differential permeability versus applied field curves of the samples formed by uniaxial pressing followed by CIPing and then microwave sintered (a) and conventionally sintered (b) at various temperatures.

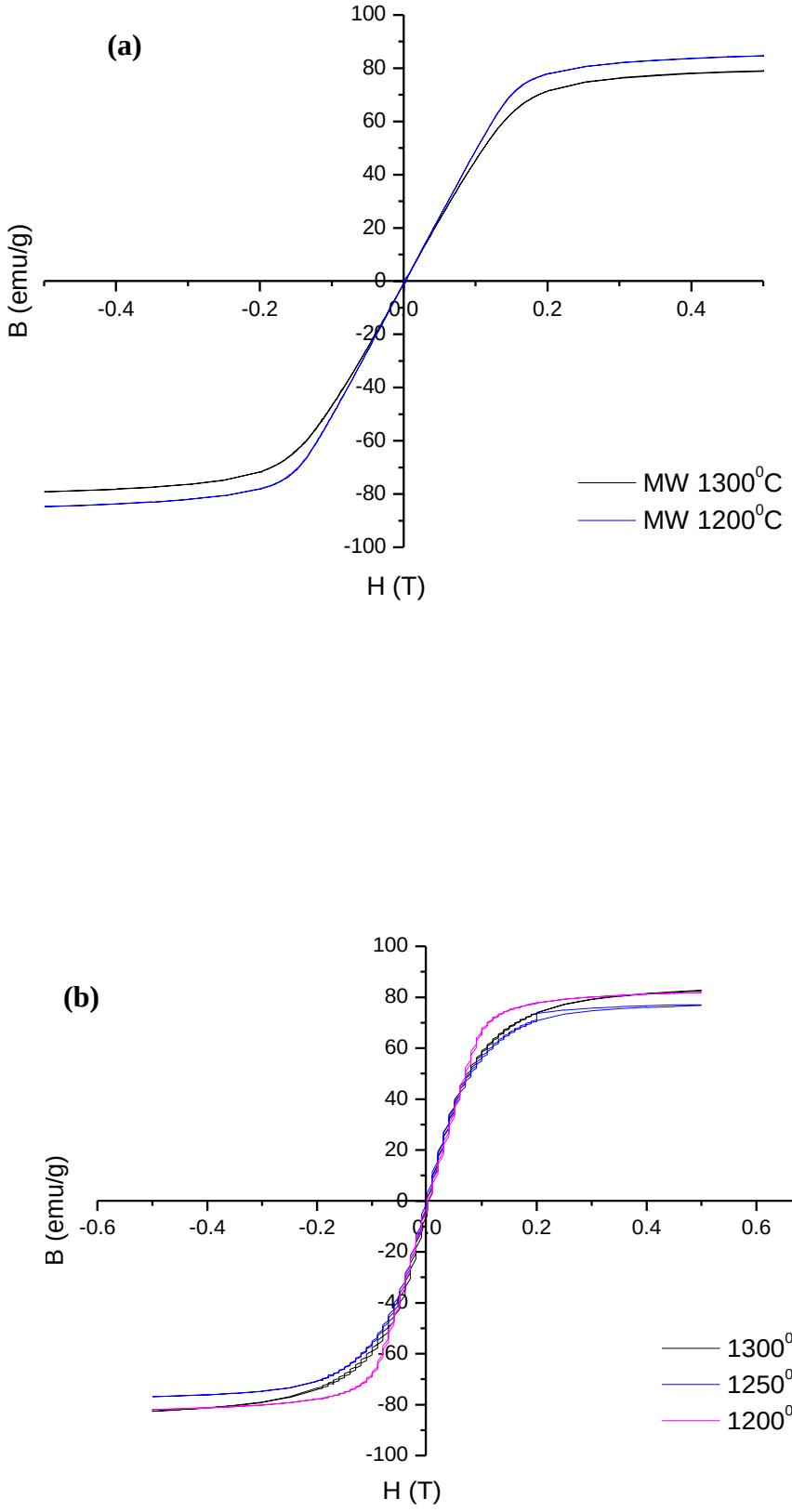

Figure 4.36. Hysteresis loops of the samples formed by uniaxial pressing followed by CIPing and then microwave sintered (a) and conventionally sintered (b) at various temperatures.

4.6. Overall Evaluation of Microstructural Features and Magnetic Properties of the Powdered Permalloys Compacted by Different Methods

To assess the effect of compaction routes on microstructural evolution and magnetic properties of the powdered permalloys, samples that were formed directly by cold isostatically pressing under 150 MPa and samples compacted via uniaxial pressing under 100 MPa were compared in terms of residual porosity, sintered average grain size along with permeability and hysteresis curves.

Table 4.9. Percent porosity and grain size values of the samples formed by cold isostatic pressing (CIP) or by double-action uniaxial compaction (Uni 100) and then microwave (M) or conventionally (C) sintered at various sintering temperatures.

Sintering Temperature	Porosity (%)		Grain Size (μm)	
(°C)	(M)	(C)	(M)	(C)
1200 (CIP)	13.5	16.8	85	91
1250 (CIP)	9.4	13.6	90	102
1300 (CIP)	12.3	14.7	100	116
1200 (Uni 100)	14.4	16.7	61	60
1250 (Uni 100)	11.7	13.5	63	72
1300 (Uni 100)	9	14.6	61	96
1200 (CIP + Uni)	14	14.5	96	109
1250 (CIP + Uni)	12	14	106	135
1300 (CIP + Uni)	11	14.3	110	150

Referring to Table 4.9, it can be seen that only the compaction method has been changed, since samples CIPed under 150 MPa and uniaxially compacted under 100 MPa of pressure have the same green density of 65%. From Table 4.5, it is seen that conventionally sintered samples attain approximately the same sintered density independent from the compaction procedure. However, there is significant grain coarsening in the CIPed samples, although the sintering temperature has been kept

constant. This situation may arise from the more severe plastic deformation and neck formation introduced to the samples during cold isostatic pressing. In contrast, microwave sintered samples differ in sintered density considerably with changing compaction technique, although the starting green densities are the same. The samples compacted via cold isostatic pressing attain higher sintered densities than the samples compacted via uniaxial pressing at the same sintering temperature. These differences may originate from the variation in the geometries of the as-pressed samples. As explained earlier in the "Experimental Procedure" chapter, cold isostatically pressed samples acquire a more rod-like geometry while the uniaxially pressed samples have a more disc-like shape. Correspondingly, aspect and surface to volume ratios of the green samples are different. CIPed samples in the form of a rod geometry have a lower surface to volume ratio, whereas the surface to volume ratio of disc-like uniaxially pressed samples is larger. Since heat is generated within the sample and lost to the surroundings from the external surface of the samples during microwave heating, rod-like geometries could be heated more effectively, and densification was improved. As in the case of conventional sintering, CIPed samples reach coarser grain sizes at the same sintering temperature by microwave heating. Consequently, from Figure 4.37 (a) and 4.38 (a), it is clear that the permeability of samples increase to a great extent for both microwave and conventional sintering cases if cold isostatic pressing is applied at the stage of compaction. As mentioned earlier, permeability of microwave sintered samples surpasses that of the conventionally sintered ones because of the adverse contribution of extensive grain boundary oxidation phenomena in the conventional sintering case. When magnetic properties of the samples compacted via double-action uniaxial pressing followed by CIPing to maximize green density is concerned, the best soft magnetic properties can be observed for these samples in the conventional sintering case, which can be linked to the fact that the maximum sintered density and largest grain size corresponds to the maximum green density for the conventionally sintered samples referring to Table 4.9. However, the situation is different for the microwave sintered samples. Since the largest grain size – minimal porosity combination occurs in the cold isostatically compacted samples, permeability of the compacts shaped by uniaxial pressing followed by cold isostatic compaction are inferior compared to those of the

cold isostatically pressed samples. Moreover, despite higher sintered density, soft magnetic properties of uniaxially compacted samples are inferior to those of the uniaxially compacted and CIPed samples, which is most probably due to the smaller average grain size achieved in the case of the former.

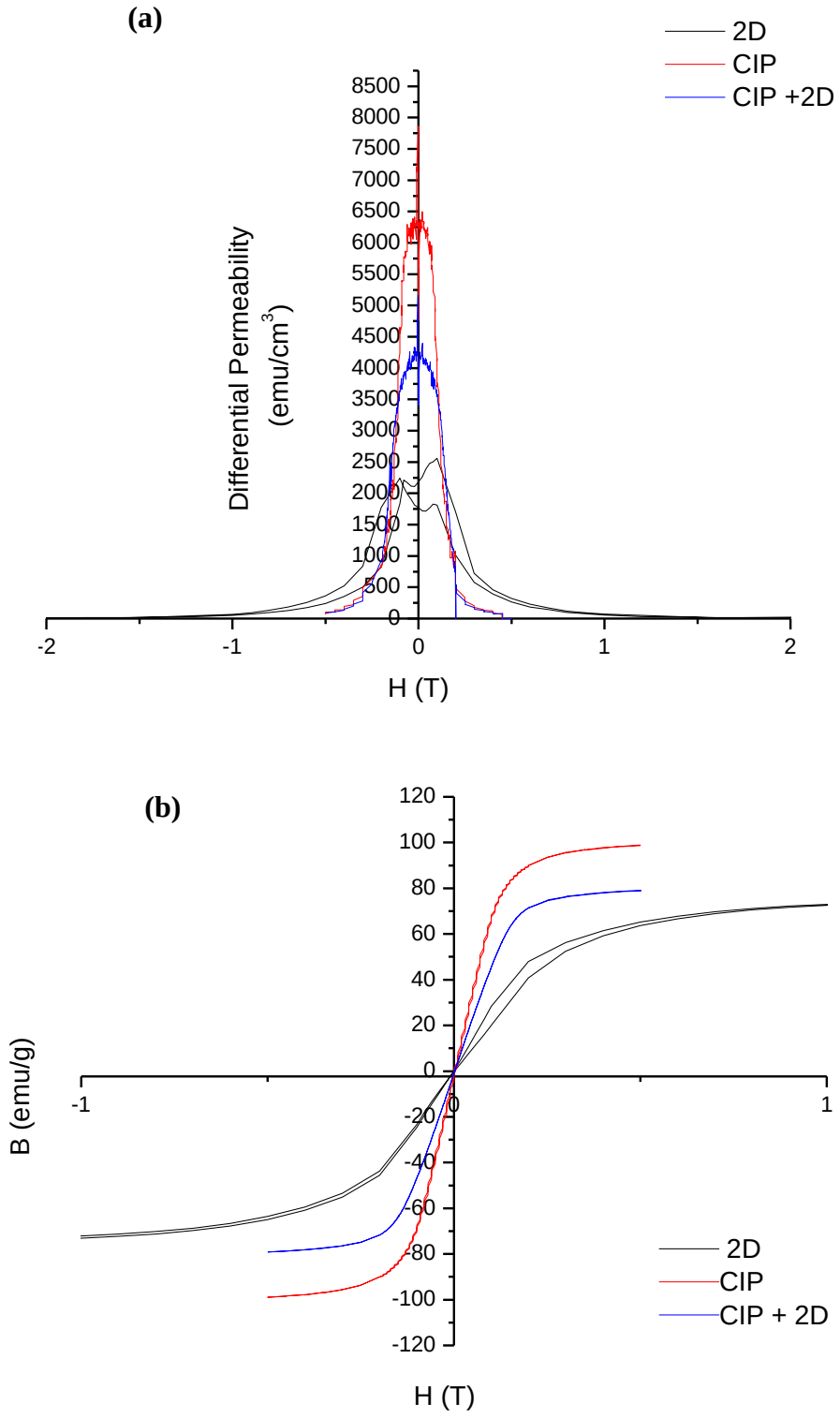

Figure 4.37. Hysteresis loop (a) and differential permeability versus applied field (b) of the samples compacted via various methods at varying compaction pressures and microwave sintered at 1300 °C.

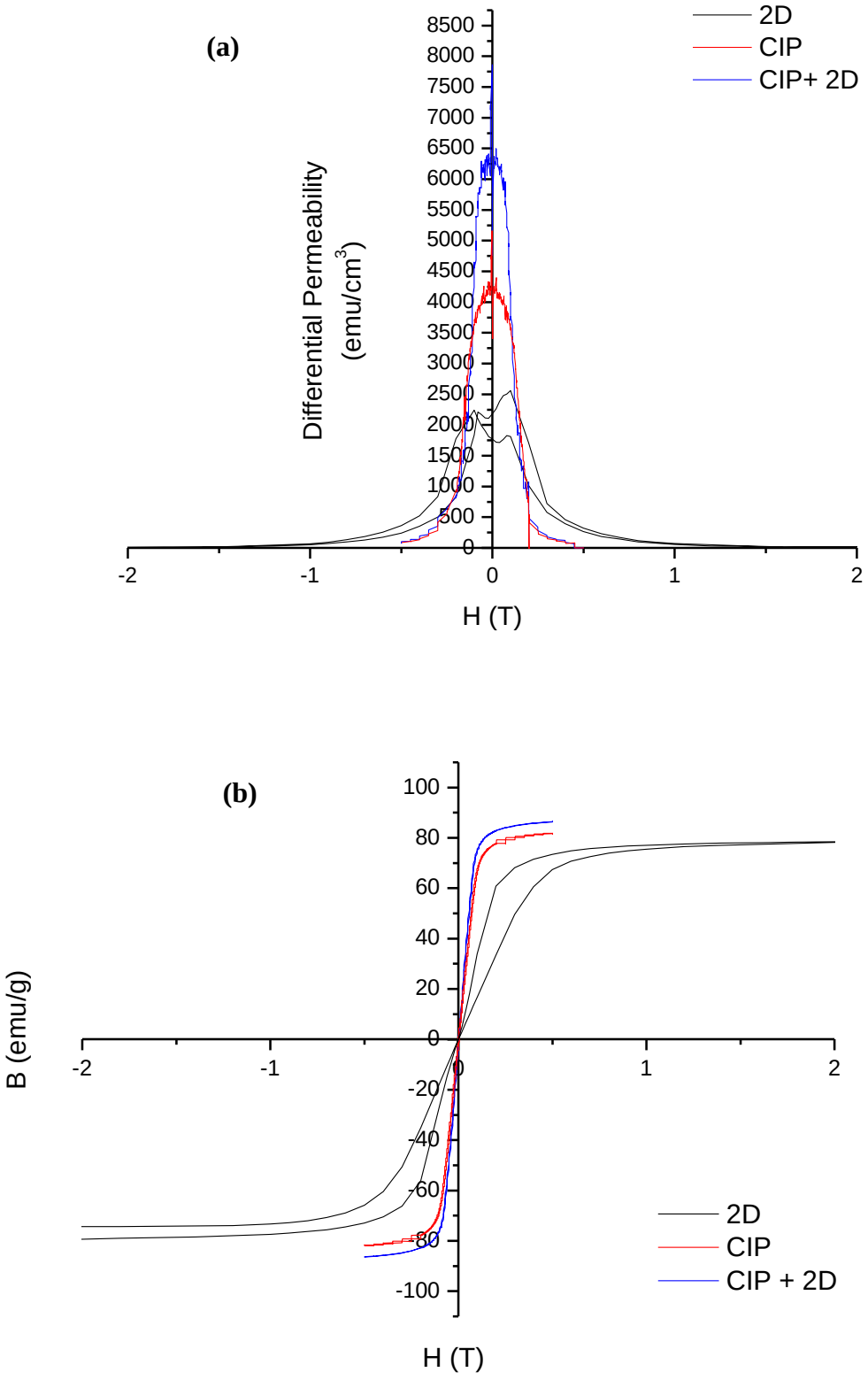

Figure 4.38. Hysteresis loop (a) and differential permeability versus applied field (b) of the samples compacted via various methods at varying compaction pressures and conventionally sintered at 1300 °C.

When the normalized microhardness values of the samples compacted via CIPing and CIPing followed by uniaxial pressing is investigated, the dominant effect of pronounced grain growth in the conventional sintering case is seen (Figure 4.39). Owing to the enhanced grain growth in conventional sintering case; normalized microhardness values of the microwave sintered samples are superior to their conventionally sintered counterparts.

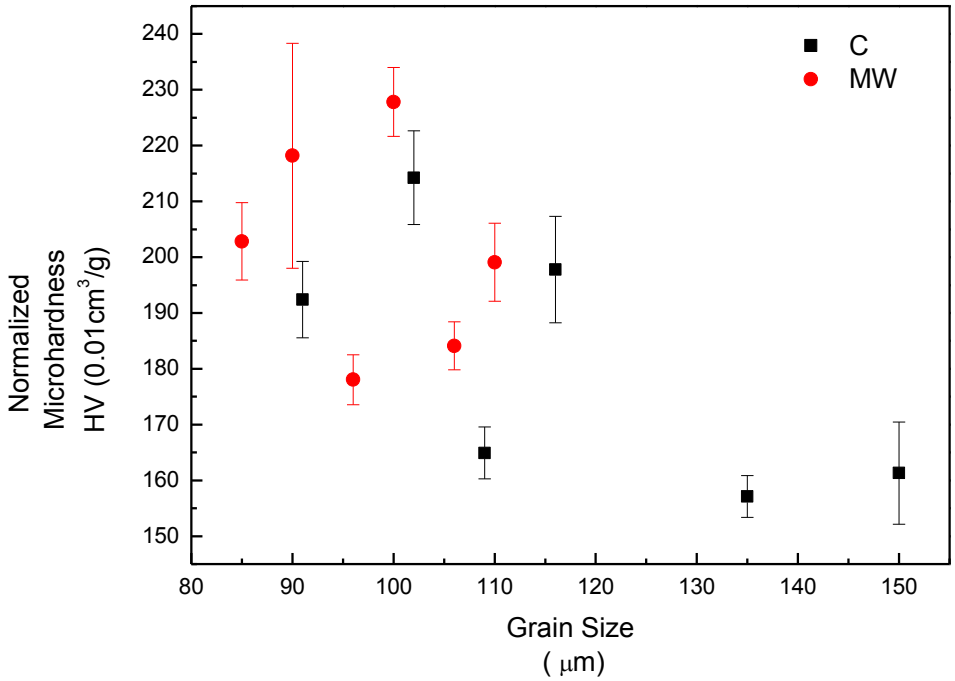

Figure 4.39. Normalized microhardness versus average grain size values of microwave (MW) and conventionally (C) sintered samples.

4.6. Interpretation of Diffusion Couples

From the examination of the concentration profiles of the diffusion couples produced via conventional and microwave sintering of pure Fe and Ni powders, it can be seen that diffusion of iron into nickel is faster than diffusion of nickel into iron for both sintering routes (Figure 4.40-4.47). Assuming that majority of the significant atomic motion has taken place during isothermal holding at the sintering temperatures, these difference can be linked to the larger diffusivity of iron compared to nickel owing to its smaller atomic size. For either sintering route, an increase in the isothermal holding temperature enhanced the diffusion and the distance that both species can travel, as expected.

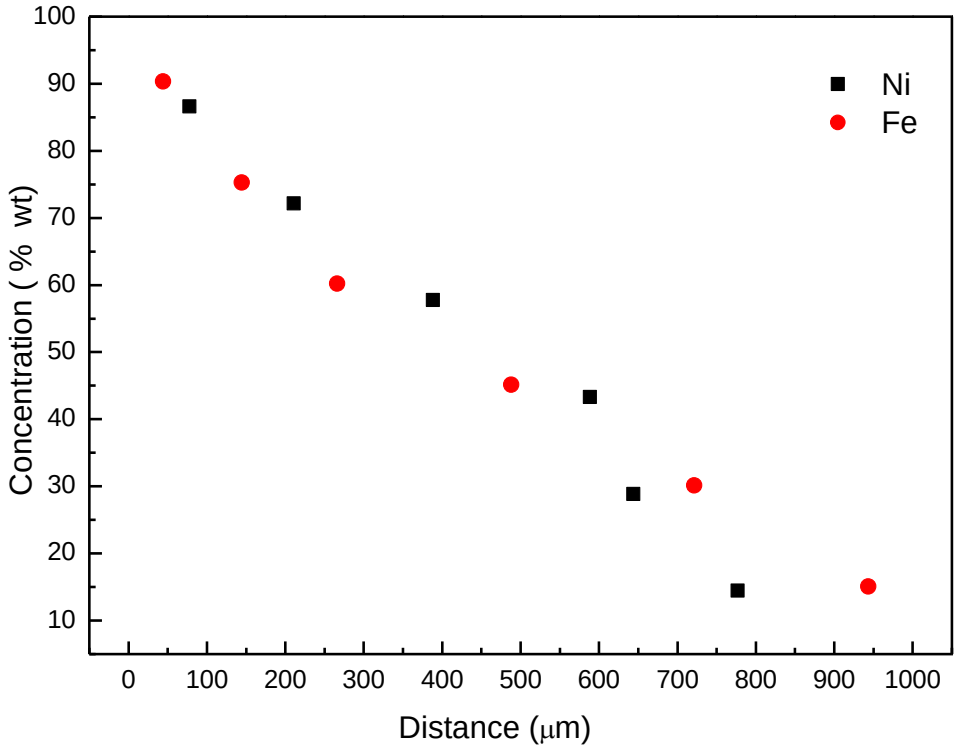

Figure 4.40. Concentration profiles of the Fe-Ni diffusion couples compacted via double-action uniaxial pressing and then conventionally sintered at 1050 °C.

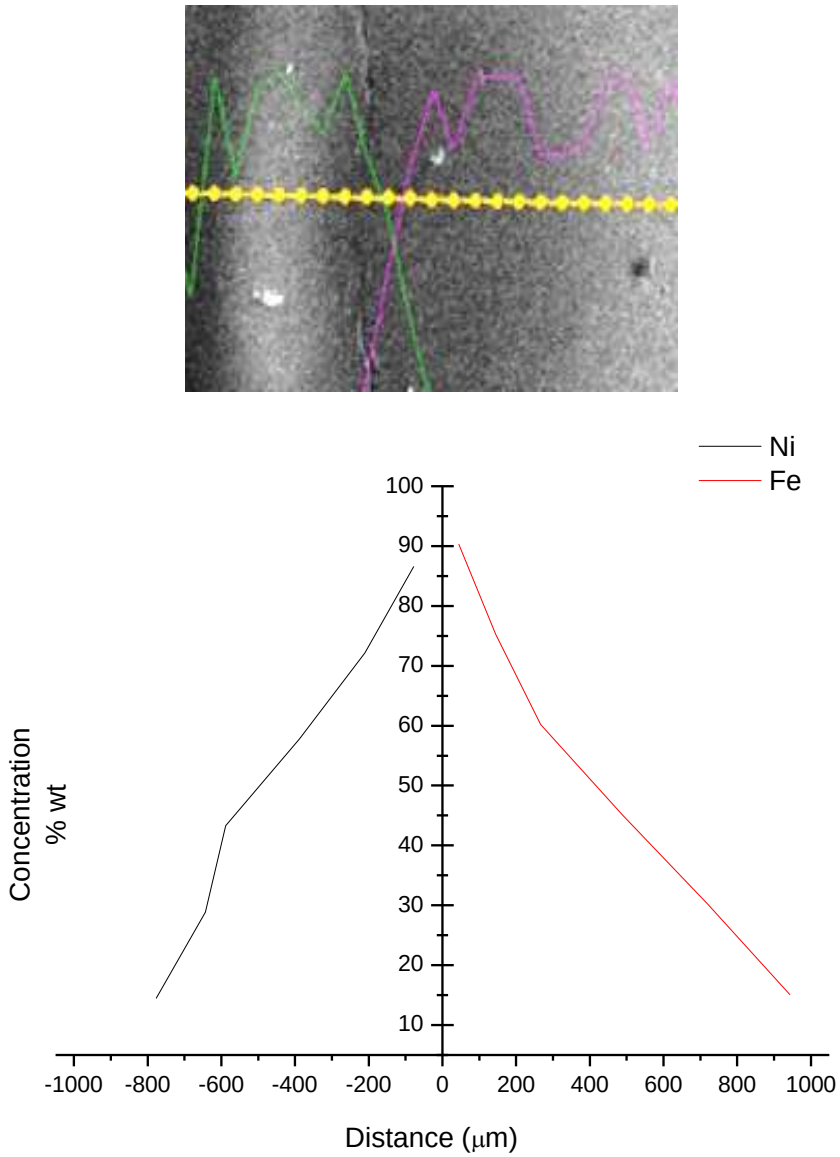

Figure 4.41. Concentration profiles of the Fe-Ni diffusion couples compacted via double-action uniaxial pressing and then conventionally sintered at 1050 °C with respect to interface.

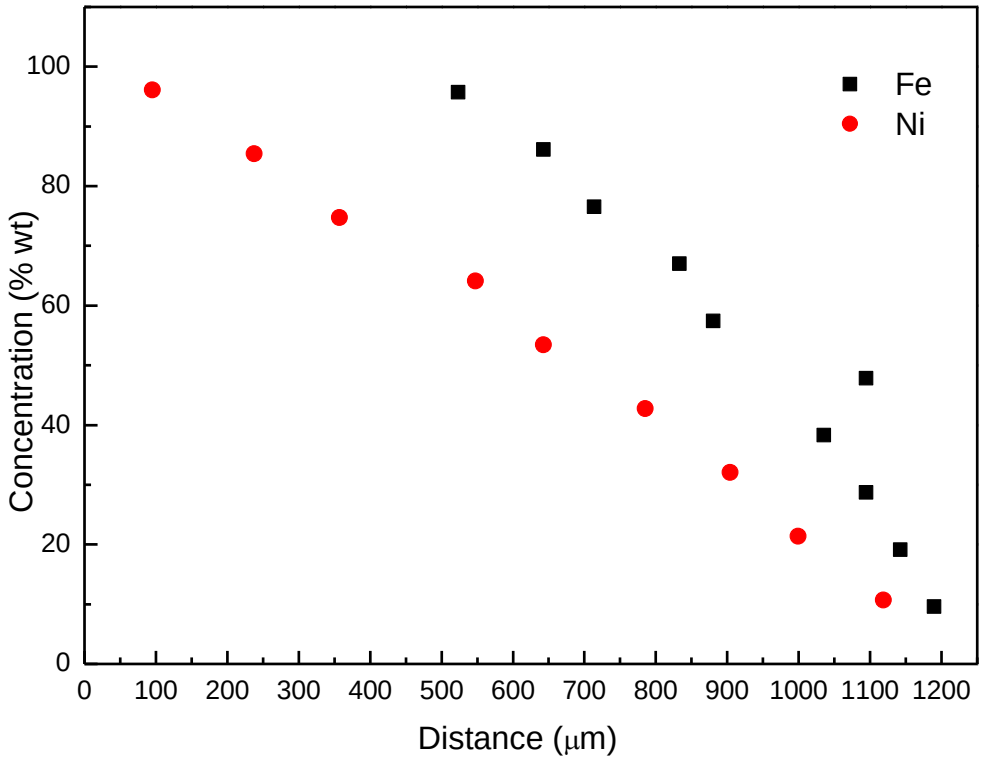

Figure 4.42. Concentration profiles of the Fe-Ni diffusion couples compacted via double-action uniaxial pressing and conventionally sintered at 1100 °C.

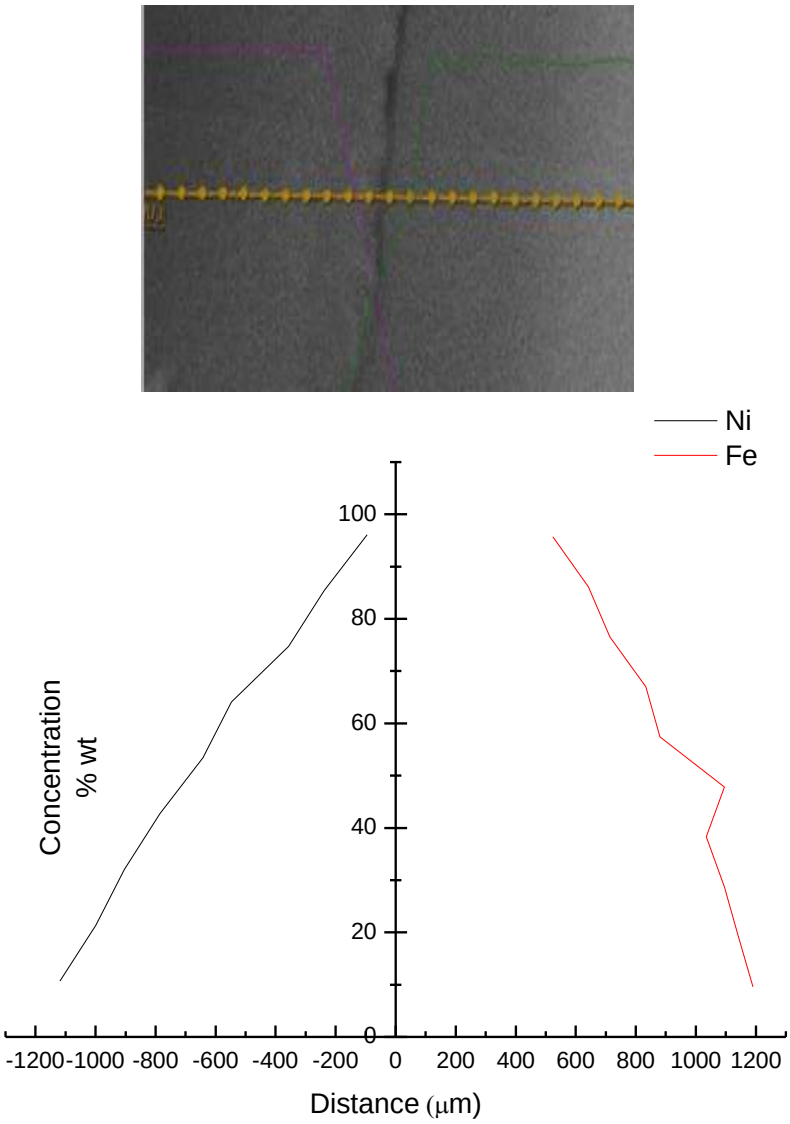

Figure 4.43. Concentration profiles of the Fe-Ni diffusion couples compacted via double-action uniaxial pressing and conventionally sintered at 1100 °C with respect to the interface.

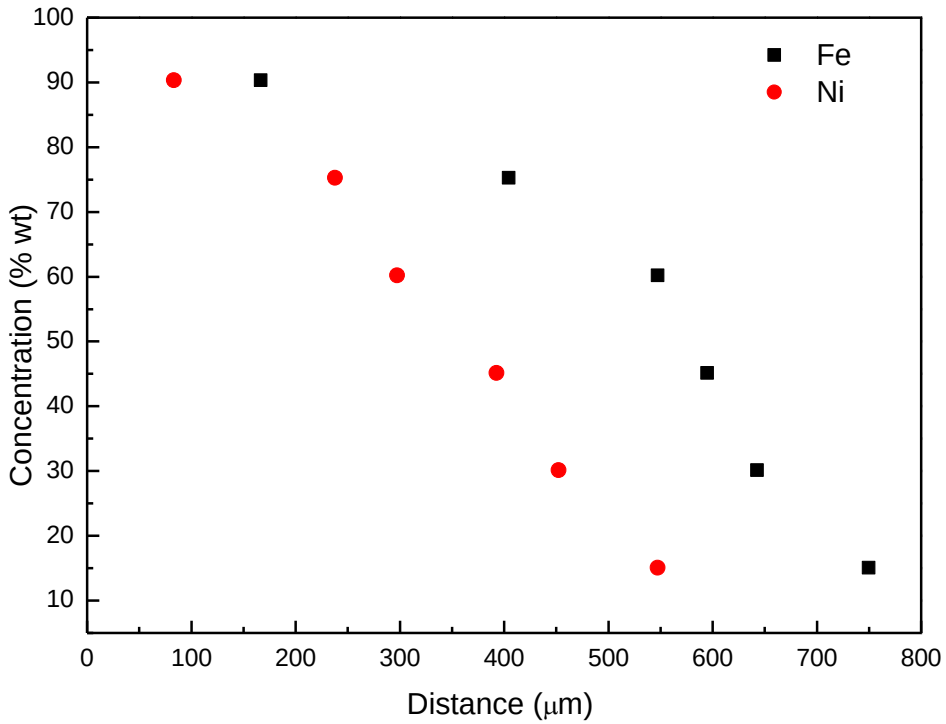

Figure 4.44. Concentration profiles of the Fe-Ni diffusion couples compacted via double-action uniaxial pressing and microwave sintered at 1050 °C.

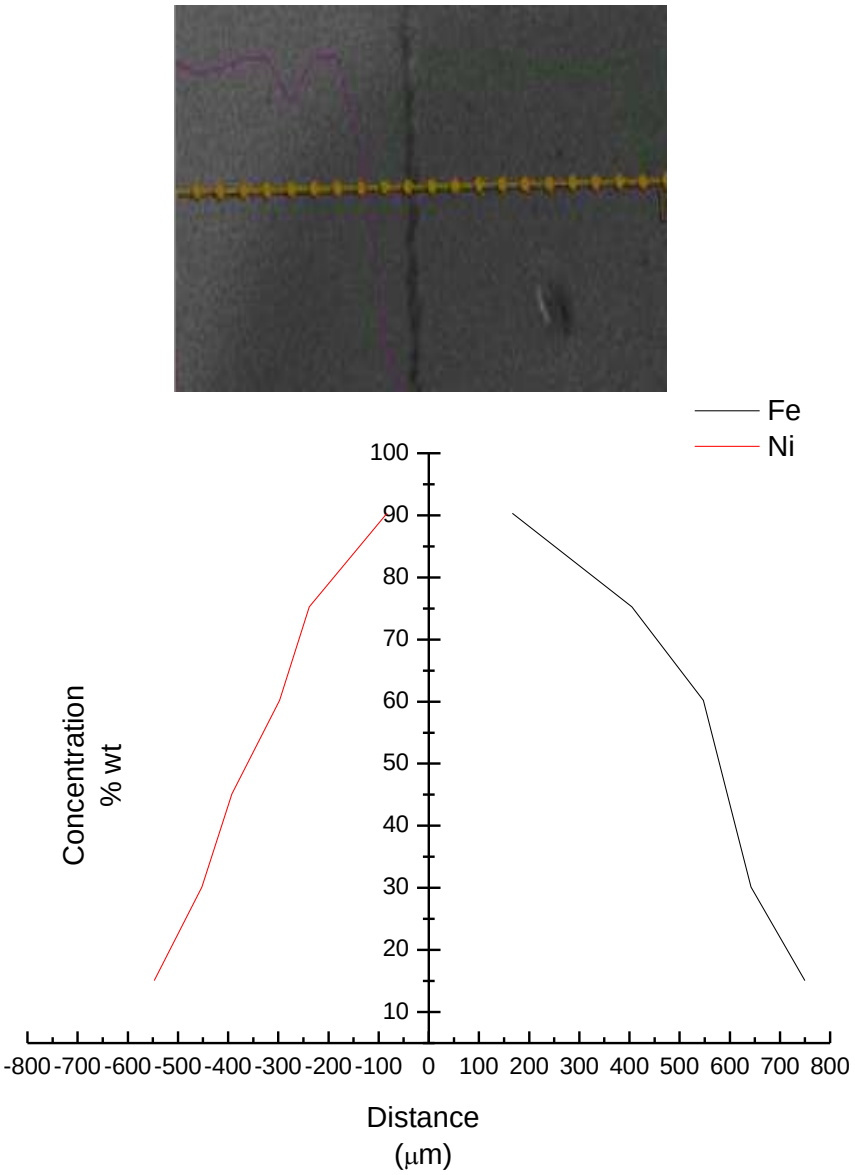

Figure 4.45. Concentration profiles of the Fe-Ni diffusion couples compacted via double-action uniaxial pressing and microwave sintered at 1050 °C with respect to interface.

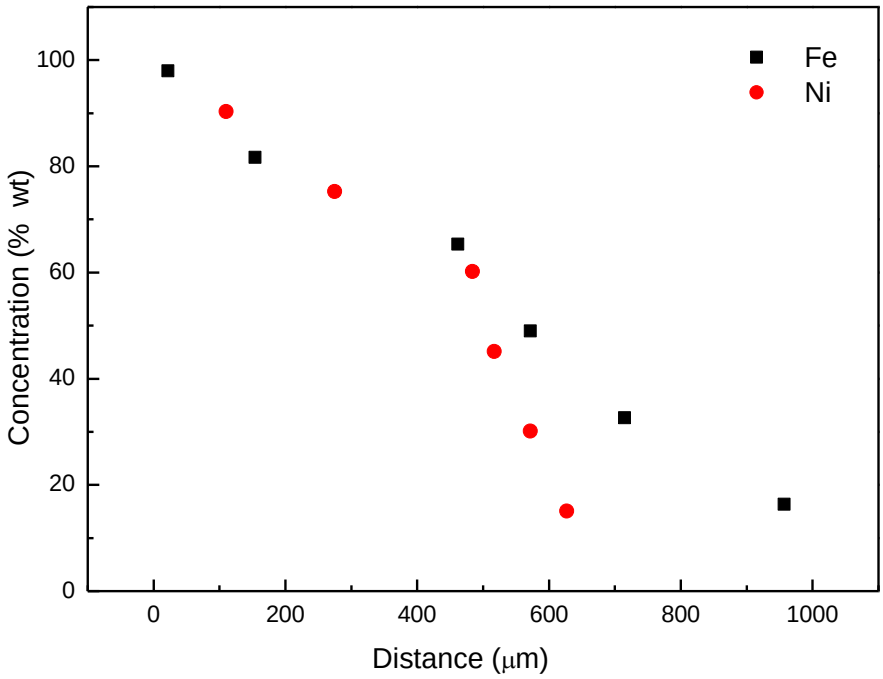

Figure 4.46. Concentration profiles of the Fe-Ni diffusion couples compacted via double-action uniaxial pressing and microwave sintered at 1100 °C.

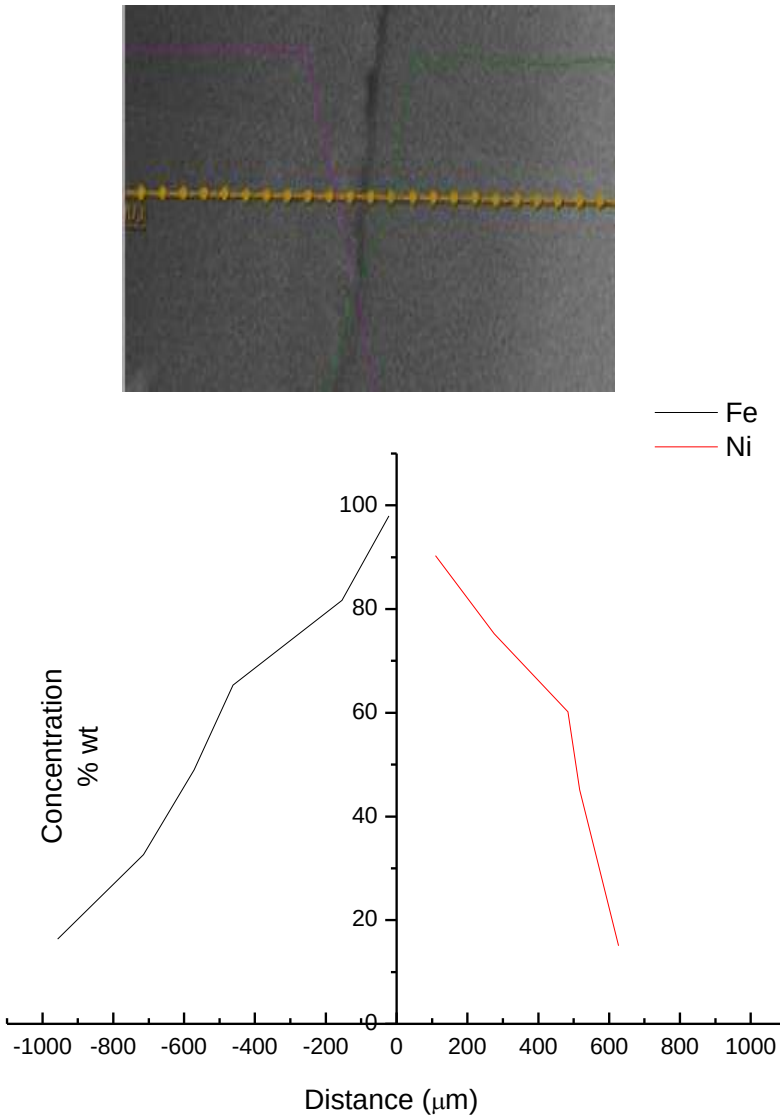

Figure 4.47. Concentration profiles of the Fe-Ni diffusion couples compacted via double-action uniaxial pressing and microwave sintered at 1100 °C with respect to interface.

Comparative investigation of concentration profiles with respect to the sintering routes revealed that both cases show quiet resemblance to each other, and no considerable difference in the diffusivities of the Fe and Ni atoms was observed under the two heating methods (Figure 4.48). The similarity of the concentration profiles obtained via conventional and microwave processing methods suggests that there is no change introduced in the diffusion mechanism of Fe and Ni atoms during microwave sintering process at these temperatures. In the literature, studies concerning diffusion behavior and activation energies conducted under multimode and single mode microwave heating indicated that such mechanism changes accompanied by accelerated bulk diffusion kinetics can be observed if heating takes place at the maximum magnetic field position of the single mode cavities; whereas in multimode cavities the main advantage that comes with the microwave heating is the rapid and volumetric heating without much effect on the diffusivities of the atoms in the systems [17, 18, 35].

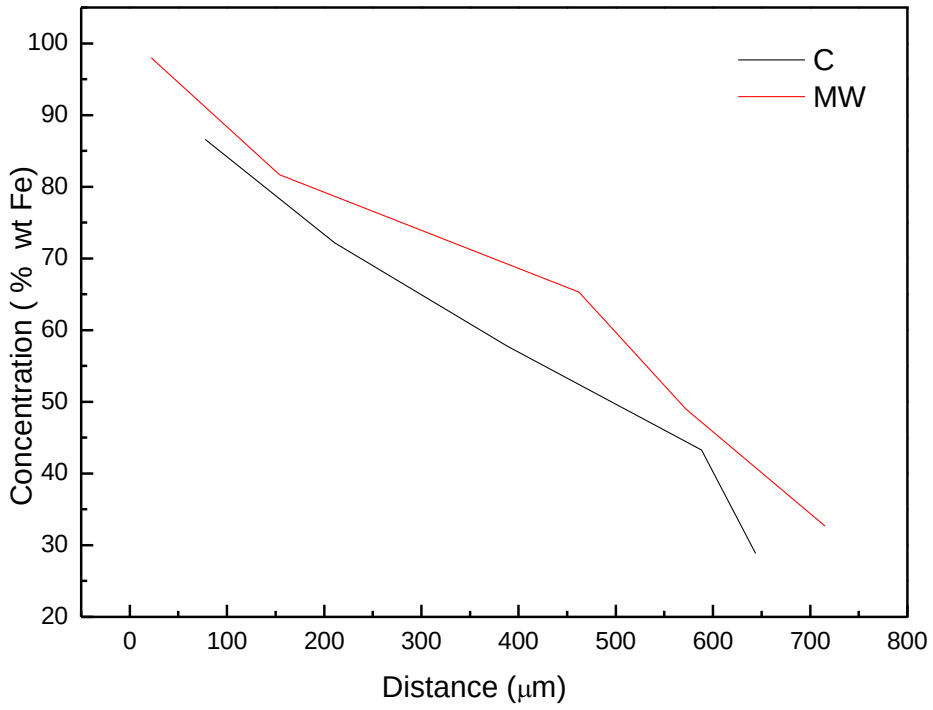

Figure 4.48. Comparative concentration profiles of the diffusion couples microwave (MW) and conventionally sintered at 1050 °C.

In conclusion, the underlying reason behind the advantages encountered via microwave sintering in this study such as enhanced densification, decreased porosity and refined microstructures are thought to be arising from the rapid and volumetric nature of microwave heating in multimode cavities. Powdered metals with uniform, less contaminated and refined microstructures can be obtained in much shorter processing times, and hence with higher energy and time efficiency, using microwave sintering.

CHAPTER 5

CONCLUSION

In this study, microwave and conventional sintering of prealloyed austenitic stainless steels and premixed permalloy powdered compacts are carried out. In this study, microwave and conventional sintering of prealloyed austenitic stainless steel and premixed permalloy powdered compacts were carried out. Effect of microwave sintering on the densification response and microstructural evolution as well as on the mechanical and magnetic properties of powder metallurgical metallic alloys were investigated in comparison to conventional sintering applied under identical conditions. In addition to varying sintering route, various compaction routes and pressures as well as sintering temperatures were employed in the sintering experiments to optimize the sintered compact properties. In the case of microwave heating, in order to avoid arcing and dielectric breakdown of the protective atmosphere leading to uncontrollable temperature increases on the specimen surface, air was used as the sintering atmosphere. It has been found that powder metallurgical metallic alloys displaying superior characteristics as compared to their conventional counterparts can be achieved via microwave sintering route in much shorter processing cycles; resulting in higher process time and energy efficiency.

- Results have shown that for the austenitic stainless steel; microwave sintering resulted in enhanced densification, decreased porosity and grain sizes as well as improved mechanical properties. Despite the higher sintered densities of the microwave sintered stainless steel compacts, the similarity in the dependence of the sintered densities on sintering temperature suggested by the comparable slopes of the density versus temperature graphs of microwave and conventionally sintered samples, the diffusion and densification

mechanisms are thought to be similar for the two sintering routes. The improvement in the densification and mechanical properties are thought to be originating from microstructural refinement associated with rapid and volumetric heating of the microwave sintering route.

- For the permalloy powdered compacts, various sintering experiments were conducted at different sintering temperatures on samples compacted under various pressing pressures and methods . Obtained samples were characterized in terms of densification, microstructural evolution, microhardness and magnetic properties. Results have demonstrated that microwave sintered samples attain higher densities displaying less amount of porosity with smoother pore morphologies along with improved microhardness compared to those of their conventionally sintered counterparts.
- In double-action uniaxially pressed samples, optimum sintered densities were obtained at intermediate compaction pressures such as 100 MPa by microwave heating, and upon a further increase in the compaction pressure, and hence green density, the sintered densities tend to decrease at varying sintering temperatures. However, for conventionally sintered samples, sintered densities were prone to increase with increasing green densities. These differences in the densification response of the microwave and conventionally sintered compacts are thought to arise from the differences in the heating mechanisms of the two routes. Since for the microwave sintering case, penetration of the microwave radiation into the sample body and volumetric heating is of major concern, further increase in green densities causes an increase in the electrical conductivity of the compact resulting in reduced microwave penetration due to the shielding effect.
- For the compacts directly formed by cold isostatic pressing, an optimization in the sintered densities was observed with respect to sintering temperature for both microwave and conventional sintering cases. At elevated temperatures, excessive grain growth and pore coalescence were observed in both microwave and conventionally sintered samples causing a decrease in the interfacial area, and hence hindering further densification. Moreover, only

CIPed samples and only uniaxially compacted samples under 100MPa both attained the same green density, where CIPed samples assumed a rod-like shape with less surface to volume ratio, while uniaxially compacted samples assumed a disc-like shape having a larger surface to volume ratio. As a result, effect of compaction method on the sintered properties for both sintering routes could have been investigated. In the case of conventional sintering, sintered densities of only CIPed and only uniaxially compacted samples reached approximately the same values, whereas CIPed samples attain higher densities than the uniaxially compacted samples in the microwave sintering case. From these results, it has been concluded that sample geometry as well as green density contributes to the sintering efficiency of microwave heating, since heat is generated within the sample and is lost to the surroundings from the external surfaces making the surface to volume ratio of the samples an important parameter. Moreover, average grain size increased in only CIPed compacts for both microwave and conventional sintering cases as compared to uniaxially compacted samples, which was attributed to the increased amount of particle contacts and necking due to the extensive plastic deformation introduced via CIPing.

- Cold isostatic pressing followed by double-action uniaxial pressing under 200 MPa of pressure provided samples with maximum green density, and for the conventional sintering case the sintered densities increased as well. However, the increase in sintered densities accompanied by microstructural coarsening for both microwave and conventional sintering cases is detrimental in terms of the mechanical properties as compared to the only CIPed or double action uniaxially compacted samples.
- Maximum sintered densities in the case of microwave sintering could not exceed 91% of the theoretical density, where further increase in densification could not be achieved by further increasing the sintering temperature due to the extensive grain boundary oxidation. As a result, usage of protective sintering atmospheres in more suitable and better sealed furnaces is expected to overcome this problem.

- When the densification response and microstructural evolution of microwave and conventionally sintered samples were correlated to their mechanical and magnetic properties, it has been observed that mechanical properties of the compacts are mainly controlled by the sintered density of the conventionally and microwave sintered compacts. Therefore, microhardness values of the samples got optimized at maximum sintered densities, and in general, microwave sintered samples exhibited superior microhardness values than their conventionally sintered counterparts. Nevertheless, soft magnetic properties of the samples are more strongly dependent on the grain size and grain boundary oxidation, and because of this fact conventionally sintered samples often displayed higher permeability especially at higher sintering temperatures where excessive grain growth takes place. However, for optimum soft magnetic properties, annealing heat treatment could be applied to obtain grain growth, so the advantage of microwave sintering in providing better densified compacts at much shorter processing cycles can still be exploited.
- Studies on of diffusion couples revealed that concentration profiles of the microwave and conventionally sintered samples are quite similar to each other, suggesting similar mechanisms of diffusion being active for both heating methods. Improved densification behavior of the microwave sintered samples was determined to be arising from the rapid and volumetric heating and consequent microstructural refinement, providing more interfacial area during the soaking period along which diffusion is accelerated and higher sintered densities can be achieved. Since the diffusion coefficients and activation energies could not be determined in this study, due to the complicated Fe-Ni phase diagram and intermetallics involved, this hypotheses cannot be proved in a rock solid manner; however, the findings are in good agreement with the previous studies in the literature claiming that activation energies observed in multimode microwave sintering cavities are similar to the conventional sintering case. On the other hand, main differences in activation energies are observed in samples sintered in single mode microwave cavities. In the single mode cavities, energy is concentrated

around the specimen and intensities of electric and magnetic field components of the microwaves changes with respect to location in the furnace. Therefore local melting and plasma formation occurs owing to the non-uniform electric and magnetic field components deducted from the lowered activation energies nearly as close as to those of the liquid state diffusion.

To sum up, microwave sintering of powder metallurgical metallic alloys resulted in improved densification, refined microstructures and improved mechanical properties than the conventional sintering case in much shorter processing cycles. Soft magnetic properties of the as sintered samples depend strongly on average grain size as well as oxidation of grain boundaries, therefore, microwave sintered samples were inferior to their conventionally sintered counterparts in some cases, yet post-sinter annealing to achieve bigger grain sizes can yield improved soft magnetic properties for microwave sintered samples compared to their conventional counterparts owing to the additional advantage of decreased amount of porosity. Consequently, under optimum conditions powder metallurgical soft magnetic compacts can be produced efficiently with reduced processing time and energy.

REFERENCES

[1] R.M. German, Powder Metallurgy Science, Metal Powder Industries Federation, 1989.
[2] Y.V. Deshmukh, Industrial Heating, Taylor & Francis Group, 2005.
[3] in, NASA.
[4] R. Meredith, in, The Institute of Electrical Engineers, 1998.
[5] A.C. Metaxas, Power Engineering Journal, (1991) 237-247.
[6] E. Gupta M; Wong Wai Leong, Microwaves and Metals, John Wiley & Sons, 2007.
[7] C. Leonelli, P. Veronesi, L. Denti, A. Gatto, L. Iuliano, Journal of Materials Processing Technology, 205 (2008) 489-496.
[8] E.T. Thostenson, T.W. Chou, Composites Part A: Applied Science and Manufacturing, 30 (1999) 1055-1071.
[9] in, 2011.
[10] NASA atmospheric data on earth sciences for teachers and amateurs, retrieved from http://mynasadata.larc.nasa.gov/ElectroMag.html on 05.04.2011
[11] J.W. Walkiewicz, G. Kazonich, S.L. McGill, Minerals and Metallurgical Processing, 5 (1988) 39-42.
[12] K.I. Rybakov, V.E. Semenov, S.V. Egorov, A.G. Eremeev, I.V. Plotnikov, Y.V. Bykov, Journal of Applied Physics, 99 (2006) 1-9.
[13] S. Das, A.K. Mukhopadhyay, S. Datta, D. Basu, Bulletin of Materials Science, 32 (2009) 1-13.
[14] A.G. Whittaker, D.M.P. Mingos, Journal of the Chemical Society, Dalton Transactions, (1995) 2073-2079.
[15] M. Celuch, W. Gwarek, M. Soltysiak, in: 2008 International Conference of Recent Advances in Microwave Theory and Applications, MICROWAVE 2008, 2008, pp. 404-405.
[16] J. Ma, J.F. Diehl, E.J. Johnson, K.R. Martin, N.M. Miskovsky, C.T. Smith, G.J. Weisel, B.L. Weiss, D.T. Zimmerman, Journal of Applied Physics, 101 (2007).
[17] D. Demirskyi, D. Agrawal, A. Ragulya, Scripta Materialia, 62 (2010) 552-555.
[18] D. Demirskyi, D. Agrawal, A. Ragulya, Journal of Alloys and Compounds, 509 (2011) 1790-1795.
[19] K. Saitou, Scripta Materialia, 54 (2006) 875-879.
[20] Retrieved from http://www.duniway.com/images/pdf/pg/paschen-curve.pdf on 05.04.2011
[21] P. Mishra, G. Sethi, A. Upadhyaya, Metallurgical and Materials Transactions B: Process Metallurgy and Materials Processing Science, 37 (2006) 839-845.
[22] S. Takayama, G. Link, M. Sato, M. Thumm, in: AIChE Annual Meeting, Conference Proceedings, 2004, pp. 1485-1486.
[23] R.M. Anklekar, K. Bauer, D. Agrawal, R. Roy, Powder Metallurgy, 48 (2005) 39-46.
[24] S.M.L. Nai, J.V.M. Kuma, M.E. Alam, X.L. Zhong, P. Babaghorbani, M. Gupta, Journal of Materials Engineering and Performance, 19 (2010) 335-341.

[25] S. Nawathe, W.L.E. Wong, M. Gupta, in, 2009, pp. 868-873.
[26] G. Sethi, A. Upadhyaya, D. Agrawal, Science of Sintering, 35 (2003) 49-65.
[27] W.L.E. Wong, M. Gupta, in, 2005, pp. 511-515.
[28] S. Takayama, G. Link, M. Sato, M. Thumm, in: Conference Digest of the 2004 Joint 29th International Conference on Infrared and Millimeter Waves and 12th International Conference on Terahertz Electronics, 2004, pp. 729-730.
[29] R.M. Anklekar, D.K. Agrawal, R. Roy, Powder Metallurgy, 44 (2001) 355-362.
[30] T. Marceloa, J. Mascarenhas, F.A.C. Oliveira, in, 2010, pp. 946-951.
[31] J. Mascarenhas, T. Marcelo, Metal Powder Report, 63 (2008) 12-14,16.
[32] J. Mascarenhas, T. Marcelo, A. Inverno, J. Castanho, T. Vieira, Metal Powder Report, 63 (2008) 12-15.
[33] K. Rajkumar, S. Aravindan, Journal of Materials Processing Technology, 209 (2009) 5601-5605.
[34] W.L.E. Wong, M. Gupta, Composites Science and Technology, 67 (2007) 1541-1552.
[35] D. Demirskyi, D. Agrawal, A. Ragulya, Materials Letters, 64 (2010) 1433-1436.
[36] V.D. Buchelnikov, D.V. Louzguine-Luzgin, A.P. Anzulevich, I.V. Bychkov, N. Yoshikawa, M. Sato, A. Inoue, Physica B: Condensed Matter, 403 (2008) 4053-4058.
[37] R.M. German Powder Metallurgy Science, Metal Powder Industries Federation, 1984.
[38] S. Allan, H. Shulman, M. Fall, R. Sisson, D. Apelian, P. Strickland, Heat Treating Progress, 8 (2008) 39-42.
[39] P. Chhillar, D. Agrawal, J.H. Adair, Powder Metallurgy, 51 (2008) 182-187.
[40] S. Gedevanishvili, D. Agrawal, R. Roy, Journal of Materials Science Letters, 18 (1999) 665-668.
[41] T. Horikawa, K. Miura, M. Itoh, K.I. Machida, IEEE Transactions on Magnetics, 41 (2005) 2064-2070.
[42] M.G. Kutty, S. Bhaduri, J.R. Jokisaari, S.B. Bhaduri, in: Ceramic Engineering and Science Proceedings, 2001, pp. 587-592.
[43] D. Lewis Iii, M.A. Imam, A.W. Fliflet, R.W. Bruce, L.K. Kurihara, A.K. Kinkead, M. Lombardi, S.H. Gold, in: Materials Science Forum, 2007, pp. 3249-3254.
[44] R. Roy, D. Agrawal, J. Cheng, S. Gedevanlshvili, Nature, 399 (1999) 668-670.
[45] S. Takayama, G. Link, M. Thumm, A. Matsubara, M. Sato, S. Sano, Y. Makino, Funtai Oyobi Fummatsu Yakin/Journal of the Japan Society of Powder and Powder Metallurgy, 54 (2007) 590-594.
[46] K.S. Tun, M. Gupta, Composites Science and Technology, 67 (2007) 2657-2664.
[47] W.L.E. Wong, S. Karthik, M. Gupta, Materials Science and Technology, 21 (2005) 1063-1070.
[48] T. Gerdes, M. Willert-Porada, K. Rodiger, in, 1996, pp. 45-50.
[49] K. Rödiger, K. Dreyer, T. Gerdes, M. Willert-Porada, International Journal of Refractory Metals and Hard Materials, 16 (1998) 409-416.
[50] B.R. Sunil, D. Sivaprahasam, R. Subasri, International Journal of Refractory Metals and Hard Materials, 28 (2010) 180-186.
[51] A. Yonetken, A. Erol, M. Erdogan, Metal Powder Report, 65 (2010) 40-43.

[52] G. Prabhu, A. Chakraborty, B. Sarma, International Journal of Refractory Metals and Hard Materials, 27 (2009) 545-548.
[53] S.S. Panda, V. Singh, A. Upadhyaya, D. Agrawal, Scripta Materialia, 54 (2006) 2179-2183.
[54] C. Padmavathi, A. Upadhyaya, D. Agrawal, Scripta Materialia, 57 (2007) 651-654.
[55] S.S. Panda, A. Upadhyaya, D. Agrawal, Journal of Materials Science, 42 (2007) 966-978.
[56] M.G. Kutty, S. Bhaduri, J.R. Jokisaari, S.B. Bhaduri, in, 2001, pp. 587-592.
[57] R.W. Bruce, A.W. Fliflet, H.E. Huey, C. Stephenson, M.A. Imam, in, 2010, pp. 131-140.
[58] S. Luo, C.J. Bettles, M. Yan, G.B. Schaffer, M. Qian, in, 2010, pp. 141-147.
[59] Y.V. Bykov, K.I. Rybakov, V.E. Semenov, Journal of Physics D: Applied Physics, 34 (2001) R55-R75.
[60] N.M. Negari, R. Sarraf-Mamoory, N. Riahi-Noori, Metal Powder Report, 64 (2009) 30-32.

APPENDIX A

MAXWELL EQUATIONS

Behaviour of microwaves is governed by Maxwell's equations; hence, careful analysis of Maxwell's electromagnetic theory is essential to understand interaction of materials with microwaves and the resulting heating phenomenon. Maxwell's equations are basically mathematical expressions of Gauss' law, Faraday's law and Ampere's law together with the following auxiliary equations.

$$\text{div } \mathbf{D} = \rho \tag{1}$$

$$\text{div } \mathbf{B} = 0 \tag{2}$$

$$\text{rot } \mathbf{E} = -\, jw\mathbf{B} \tag{3}$$

$$\text{rot } \mathbf{H} = \mathbf{J} + jw\mathbf{D} \tag{4}$$

$$\mathbf{J} = \sigma\mathbf{E} \tag{5}$$

$$\mathbf{D} = \varepsilon_0 \varepsilon^{'}\mathbf{E} \tag{6}$$

$$\mathbf{B} = \mu_0 \mu^{'}\mathbf{H} \tag{7}$$

In these equationsD is the electric flux density (C/m^2), E is the applied electric field (V/m), B is magnetic flux density (Wb/m^2), H is magnetic field (A/m), J is current density (A/m^2), σ is electrical conductivity(second C^2 s/kgm^3), ρ is charge density (C/m^3), $\varepsilon_0$is permittivity (F/m),$\mu_0$is permeability of the free space (H/m), and $\varepsilon^{'}$and $\mu^{'}$ are relative permittivity and permeability coefficients of the material with boundary conditions being;

$$\mathbf{E}_{tan} = 0 \tag{8}$$

$$\mathbf{H}_{normal} = 0 \tag{9}$$

The first boundary condition is a consequence of the fact that for a perfect conductor, potential difference grazing the surface cannot exist no matter how great a current is flowing through it. Analogously, magnetic field lines cannot be orthogonal to the

conductor’s surface since otherwise the continuity of the magnetic loop cannot be maintained, and there will be a magnetic field in the superfical regions of the conductor associated with the current flowing.

APPENDIX B

IRON NICKEL BINARY PHASE DIAGRAM

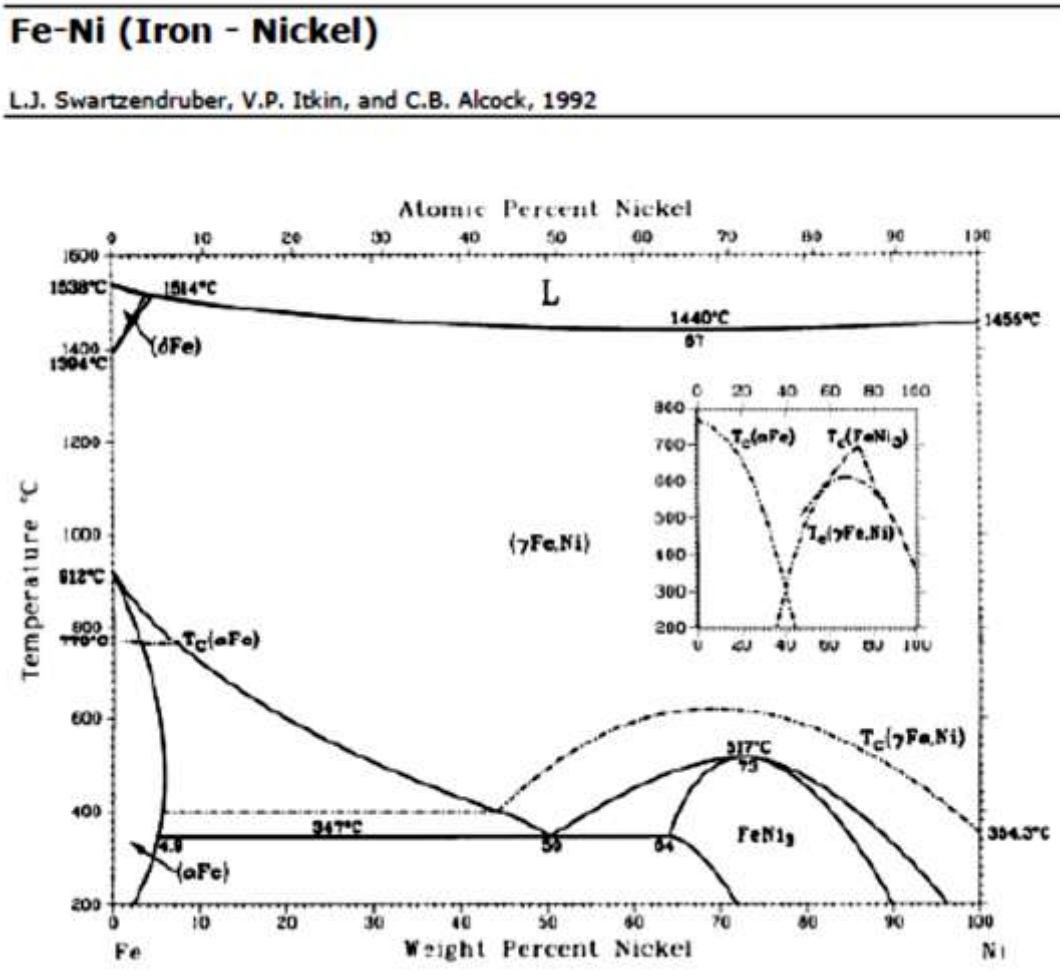

Figure B.1. Iron Nickel Binary Phase Diagram